DTIC
S ELECTE
JUN 2 0 1989
D

**EVALUATION OF THE BISTATIC EQUIVALENCE
THEOREM FOR THE NEAR AND FAR-FIELD
RADAR CROSS SECTION OF COMPLEX TARGETS**

Thesis

Charles G. Walls
Major, USA

AFIT/GE/ENG/89J-1

DEPARTMENT OF THE AIR FORCE

AIR UNIVERSITY

AIR FORCE INSTITUTE OF TECHNOLOGY

Wright-Patterson Air Force Base, Ohio

89   6   19   059

AFIT/GE/ENG/89J-1

DTIC
ELECTE
JUN 20 1989
S
D
D

EVALUATION OF THE BISTATIC EQUIVALENCE
THEOREM FOR THE NEAR AND FAR-FIELD
RADAR CROSS SECTION OF COMPLEX TARGETS

Thesis

Charles G. Walls
Major, USA
AFIT/GE/ENG/89J-1

AFIT/GE/ENG/89J-1

EVALUATION OF THE BISTATIC EQUIVALENCE THEOREM

FOR THE NEAR AND FAR-FIELD RADAR CROSS

SECTION OF COMPLEX TARGETS

THESIS

Presented to the Faculty of the School of Engineering

of the Air Force Institute of Technology

Air University

In Partial Fulfillment of the

Requirements for the Degree of

Master of Science in Electrical Engineering

Charles G. Walls, B.S.

Major, USA

June 1989

Approved for public release; distribution unlimited

Acknowledgments

The purpose of this study was to evaluate the usefulness of the bistatic equivalence theorem with respect to the near and far-field radar cross section of complex targets. Potentially, the Wright Research and Development Center (WRDC), Wright-Patterson AFB, Ohio, could apply the discussed extensions of the bistatic equivalence theorem to reduce RCS measurement time, associated costs, as well as expand their laboratory measurement capabilities.

In performing this study I have received a great deal of help from others. In particular, I would like to thank my sponsor, Mr. Ed Utt, for the insight, technical guidance, and encouragement he provided throughout this effort. I would like to thank my thesis advisor, Dr. Vittal P. Pyati, and the members of my thesis committee, Lt Col William Baker and Maj Harry Barksdale, for their invaluable assistance.

I would also like to thank the other members of the WRDC/SNA office and the staff of Mission Research Corporation and Systems Research Laboratories for their assistance and cooperation during the experimental stages of the thesis. This includes Lt Mike Walker, MSGT Dave Frasher, Jim Common, Richard Porter, Bill Lieper, Chris Clark, and Lee Blanton. A special heartfelt thanks is

extended to Mr. Stan Bashore for the all-encompassing support he rendered on a daily basis.

Most importantly, I express my gratitude and love to my wife, Gloria, for her patience and understanding.

<div align="right">Charles G. Walls</div>

Table of Contents

List of Figures

List of Tables

AFIT/GE/ENG/89J-1

Abstract

This research examined the applicability of the
monostatic-bistatic equivalence theorem (MBET) and
associated extensions in determining the extent to which
correlation exists between monostatic and bistatic data
for both the near and far-field. A secondary objective
was to determine whether reliable bistatic near-field
radar cross section (RCS) data could be collected on a
range originally designed to take monostatic far-field
measurements.

Dr. David Falconer developed two extensions of the
MBET in an effort to estimate the bistatic RCS pattern in
both the near and far-field by measuring the monostatic RCS
pattern at one-half the bistatic angle, at a reduced
frequency, and, for the near-field case, at an adjusted
target-to-receiver separation range. The pattern
representation and accuracy of these two extensions were
examined by measuring the RCS of an ogive, a circular flat
plate, and two circular cylinders of different lengths.
Target selection allowed for the application of the MBET
extensions to targets that provide either a large dynamic
range, support travelling and creeping waves, or have
large specular returns and independent scattering centers.

The variable parameters for the study included the
polarization and target-to-receiver separation range. The
transmit frequency and bistatic angle of interest were 10
GHZ and 30°, respectively.

Results of this study show that Falconer's MBET
extensions have some merit. Application of the far-zone
statement and the resultant monostatic data provided
good representation of the corresponding bistatic
far-field RCS patterns and amplitude levels. Falconer's
near-zone version provided fair representation of the
bistatic near-field RCS patterns and amplitudes. The
accuracy of the RCS amplitude approximations decreased,
though, for targets, such as the 8 in cylinder, that had a
significant higher order effects contribution.

EVALUATION OF THE BISTATIC EQUIVALENCE THEOREM FOR THE NEAR AND FAR-FIELD RADAR CROSS SECTION OF COMPLEX TARGETS

I. Introduction

Background

Efforts had been made as early as 1917 to reduce an aircraft's visibility to enhance its survivability during war. The speed and altitude of aircraft had increased so dramatically by the thirties that unaided visual interception of aircraft by the opposing fighter pilot was virtually impossible. As a result, early-warning radars were introduced (1:7-8).

To counter the radar's capabilities, the Air Force, in 1953, recognized the need and started work towards minimizing an aircraft's detectability by enemy radar. The standard for detectability, devised by radar engineers, to compare and measure a system's peformance was called radar cross section (RCS) (1:14). RCS, denoted by σ, was defined as

$$\sigma = \lim_{R \to \infty} 4\pi R^2 \left| \frac{E_s}{E_i} \right|^2 \tag{1}$$

where E_s is the electric field intensity scattered by the target and observed at a distance R from the target and E_i

is the electric field intensity incident upon the target (2:97-98).

An extensive theoretical and experimental effort has been expended to develop an aircraft possessing a low RCS design. The intent is to minimize the RCS seen by the conventional monostatic radar, defined as a deployment where the transmitter and the receiver are collocated. Emphasis on defeating the capabilities of the monostatic radar stems from the fact that it is more frequently deployed and better suited than the bistatic configuration for most radar applications. The relative ease of information extraction from the received signal and greater scanning ability are its most significant characteristics (3:560). Detection by a monostatic radar becomes more difficult, though, when a potential target has been shaped to deflect incident energy away from the radiation source. Curved surfaces, slanted or tilted leading edges, and minimization of flat surfaces enhance energy deflection, contribute to a lower target RCS, and complicate the detection process for the radar operator. But, by deploying a radar receiver at a predetermined azimuth and range from the transmitter, the deflected energy might be captured depending on such factors as transmit frequency, target size, and the separation angle (4:27). Such a system is referred to as a bistatic radar system. The bistatic radar geometry is shown in Figure 1.
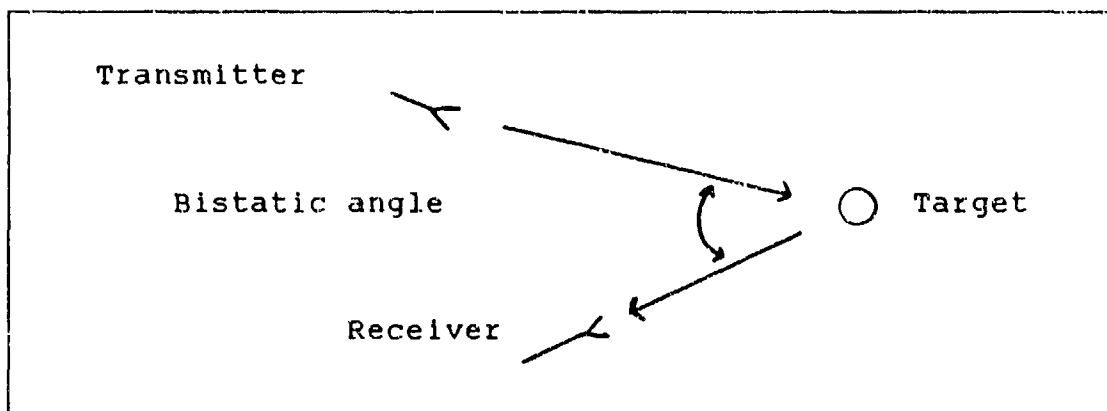
Figure 1. Bistatic Radar Geometry (5:222)

The possibility of bistatic radar being deployed as a countermeasure against low RCS platforms (4:27) has prompted the government and the research community to develop and improve bistatic RCS measurement techniques. The Air Force's 6858th Test Group, for example, recently conducted a bistatic RCS measurement program at the Radar Target Scattering (RATSCAT) facility to determine if targets with a low monostatic RCS are detectable in bistatic conditions. The program was conducted utilizing far-field measurement criteria and techniques (6:1).

Conventional far-field measurement techniques are difficult, costly, or impractical in determining scattering from large targets such as SDI arrays or the B-2 bomber. As a result, near-field measurement techniques are becoming more popular and sometimes indispensable in the study of scattering phenomena (7:1). Elimination of the far-field separation distance criteria

allows for smaller measurement ranges, many of which can be indoors. The potential for cost savings, more accurate results, and control over the test environment has motivated researchers to improve the near-field measurement process (8:743).

Literature Review

Along with improved near-field RCS measurement techniques, work has been accomplished over the years to develop a means of predicting the bistatic RCS of targets without having to deal with the complexities inherent with bistatic scattering. Since monostatic measurements are less complicated, cheaper, and less time consuming to perform than bistatic measurements, researchers began work on investigating the possibility of developing a prediction method for bistatic RCS based on monostatic RCS data.

Crispin, Goodrich, and Siegel Study. This study developed a simple relationship between the monostatic and bistatic cross sections allowing for the determination of the bistatic cross section in terms of the monostatic results. It was presented in the form of a theorem, known as the monostatic-bistatic equivalence theorem (MBET). The theorem simply states that, in the limit of vanishing wavelength, the bistatic cross section is equal to the monostatic cross section taken at one-half the bistatic

4

angle for bodies that are sufficiently smooth (9:11). The
theorem's proof can be found in a subsequent Crispin and
Siegel publication (10:158-160).

Since the development of this theorem is based on
physical optics, it has limited applicability due to
restrictions associated with physical optics theory.
These restrictions (11:2) are:

    1.   The target must be perfectly conducting.

    2.   The target must be significantly larger than
a wavelength.

    3.   The target's RCS must be such that higher
order effects, such as creeping and travelling waves, do
not make a significant contribution.

    4.   A significant portion of the target's
surface should be within approximately $45°$ of the normal
of the bisector of the transmitter and receiver.

    5.   The target must be in the far-field with
respect to the transmitter and receiver.

    6.   Scattering centers must be distinct.

Kell performed a subsequent study in which he
extended the application of the MBET to more general
cases.

Kell's Study. Kell investigated the factors which
govern bistatic scattering and the relation between
bistatic and monostatic scattering in terms of the
combined effect of individual scattering centers on the

target. The study employs the concept of reradiation lobe
patterns from the individual scattering centers to develop
the bistatic pattern in terms of the monostatic pattern
and the bistatic angle (12:983). This development lends
itself to Kell's version of the MBET which states that the
bistatic cross section of aspect angle α and bistatic
angle β is equal to the monostatic cross section measured
on the bisector at a frequency lower by the factor
$\cos(\beta/2)$ (12:987). Kell (12:986-987) indicates that this
MBET statement applies for any chosen aspect angle α if
the following conditions are met:

1. The RCS may be written as the squared sum of
fields from discrete scattering centers:

$$\sigma = \left| \sum_{m=1}^{M} \left[\sigma_m \right]^{1/2} e^{i\phi_m} \right|^2 \tag{2}$$

where

    σ = total RCS

    M = number of discrete scatterers

    σ_m = RCS of mth scatter center

    ϕ_m = phase of field scattered by m^{th} center relative

        to that scattered by 1st center, i.e.,

$$\phi_m = 2k_o z_m \cos(\beta/2) + \xi_m \tag{3}$$

with

$z_m(\alpha)$ = distance between m^{th} and last phase center

ζ_m = residual phase contributions of the mth center

2. The amplitude $\left[\sigma_m\right]^{1/2}$, position z_m, and residual phase ζ_m are insensitive to the bistatic angle β over the range of β considered.

Kell's statement provides for a more general application of the MBET within the restrictive conditions stated above (12:983). In essence, he has added a correction term, $\cos(\beta/2)$, to the frequency of interest as his variation to Crispin and Siegel's version of the MBET. It should be noted that both studies, Crispin, Goodrich, and Siegel as well as Kell's assume a planer incident wavefront.

MacLennan's Study. This study reexamined the mathematical formulation of Kell's far-field extension to the MBET and tested the relationship by comparing computer generated bistatic and monostatic cross sections for simple shapes. Parameters such as bistatic angle, angle of incidence, and surface continuity were varied during testing and analyzed in order to identify any limitations to Kell's method (13:xi).

MacLennan found Kell's far-field relationship to be mathematically correct, limited by physical optic assumptions. With regards to accuracy, it was found to be

dependent upon the interaction of scattering centers with each other as the bistatic angle changed (13:71). Overall, the test results indicated that the relationship had merit for far-field applications. In particular, relatively good agreement (within 3 dB) between the monostatic and bistatic cross sections was found for electrically large flat and singly curved surfaces for angles of incidence up to $30°$ from broadside and for bistatic angles up to $15°$ (13:xi).

The studies reviewed up to this point have been concerned with the far-field application of the MBET. Falconer has investigated the far-field, but also the near-field, viability of the theorem.

Falconer's Study. In his study Falconer provides additional modifications to the monostatic-bistatic equivalence theorem. As he points out, the derivation by Kell was based on two assumptions:

1. The scattering body consists of non-interacting isotropic point scatterers.

2. Its application was restricted to configurations in which the illumination and observation points sit in the far-field with respect to the scattering body (14:4).

But, as cited by Falconer, some studies suggest that, if the illumination and observation angles are within $20°$ of the surface normal at the dominating scattering center,

8

the MBET has some merit in determining the RCS for continuous scatterers (14:4). Another study (14:4-5) was mentioned which showed that the MBET approximation could be applied when operating in the Fresnel portion of the near-field, i.e., when R satisfied the following relationship:

$$(D^3/4\lambda)^{1/2} < R < 2D^2/\lambda \qquad (4)$$

In an effort to expand the applicability of the MBET, Falconer developed formulas for the monostatic and bistatic scattering amplitudes produced by a scattering body with dimensions comparable to the wavelength of the radiating source. The formulas are considered by Falconer to be valid in both the far-field and the Fresnel region of the near-field (14:6).

Falconer's work produced three statements, or extensions, to the MBET. They are (1) tne far-zone, (2) the near-zone, and (3) the time-harmonic statements (14:2). Only the first two will be discussed in this study.

Falconer's far-zone expression states that in the far zone the bistatic scattering amplitude can be estimated by measuring the monostatic scattering amplitude at a reduced frequency, f_r, and at one-half the bistatic angle, provided the appropriate amplitude and phase adjustments are incorporated (14:12). This approximation differs from Kell's derivation in that it calls for a correcting

9

phase factor and an amplitude correction term, (k/k_r), to be applied to the monostatic data (14:12).

The near-zone expression states that the bistatic scattering amplitude can be estimated by measuring the monostatic scattering amplitude at a reduced frequency f_r, a reduced range R_r, and at one-half the bistatic angle (14:13). If the illuminator-to-target (R") and target-to-receiver separation distances are not equal, the monostatic amplitude must be scaled by a factor:

$$sf = (kR'_r)/(k_r R') \qquad (5)$$

where

k = wavenumber = $\left[\dfrac{2\pi}{c}\right] f$ $\qquad (6)$

f = frequency of interest used in taking the bistatic data

k_r = reduced wavenumber = $\left[\dfrac{2\pi}{c}\right] f_r$ $\qquad (7)$

f_r = reduced frequency = $f\left[\cos(\beta/2)\right]$ $\qquad (8)$

R' = target-to-receiver range

R'_r = reduced target-to-receiver range used in monostatic data collection

(14:16)

In discussing the MBET in general, Falconer emphasized the point that the theorem and any version of it, to include his work, do not accurately account for the

10

contribution from creeping and travelling waves (14:19).
A closer look at Falconer's work is in Appendix A.

Problem Statement

A limited amount of data exists for bistatic radar
cross section measurements. Most of the data available
pertains to targets whose radar cross sections were
measured using the traditional monostatic arrangement
under far-field conditions. In particular, availability
of data and corresponding analysis is limited with regards
to monostatic and bistatic near-field RCS measurement
correlation.

Purpose

The purpose of this research was to measure the
monostatic and bistatic near and far-field RCS of four
special shapes and analyze the data to examine the
applicability of the bistatic equivalence theorem and
associated extensions in determining the extent to which
correlation exists between the monostatic and bistatic
data.

Assumptions

The following assumptions will be made for this
effort.

1.   The received-signal power is at least 10 dB above
the noise level of the receiver. This allows for the
noise to be ignored.

2.   For the bistatic case, the incident field striking
the target is a planar wave. The transmitter-to-target
distance (R") will be such that the phase error of the
wave from edge to center will be less than 22.5°. Such a
phase error is not considered detrimental in any analytical
formulation (15:114).

3.   The targets are considered to be perfectly
conducting and smooth, prerequisites for use of the bistatic
equivalence theorem in data analysis (14:4).

4.   Atmospheric attenuation, α, is negligible for the
frequency and ranges of interest since this is an indoor
range (16:2-52).

5.   System losses (L_s) are minimal throughout the
data collection process.

Scope

This effort was confined to measuring the monostatic
and bistatic RCS of an ogive, a circular flat plate, and
two 1-inch diameter, circular cylinders.

Monostatic near and far-field measurements were made
at 9.66 GHZ with vertical and horizontal polarization.
Figure 2 provides the monostatic measurement layout. The
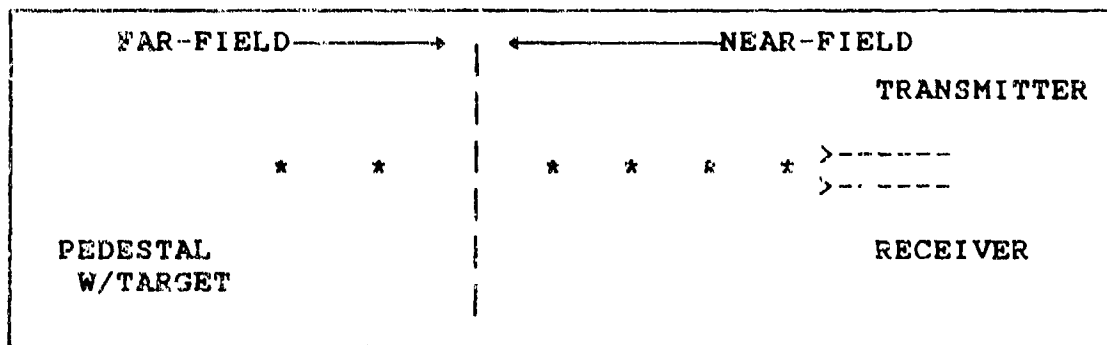asterisks represent various target placement points.

Figure 2.   Monostatic Measurement Layout

Bistatic measurements were conducted at 10 GHZ for both polarizations at a 30° bistatic angle. The transmitter-to-target range (20 feet) always satisfied far-field criteria. The target-to-receiver distance was varied to permit both near and far-field data to be collected.

Figure 3 provides the bistatic measurement layout. The asterisks in this figure represent various receiver placement points. "NF" and "FF" represent the near and far-field zones between the target and receiver.
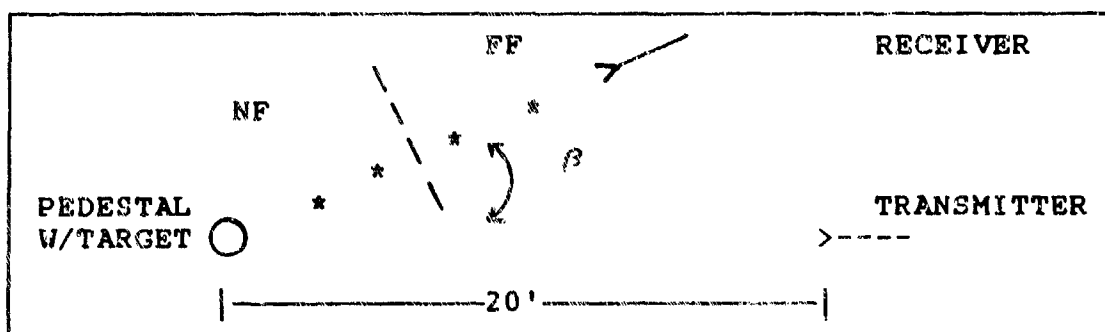

Figure 3.   Bistatic Measurement Layout

Standards

For the bistatic measurements, the target will be
placed in the far-field region with respect to the
transmitter to ensure the incident field on the target is
planar. The transmitter-to-target separation distance R"
must satisfy the following relationship:

$$R" \geq 2D_1 D_2/\lambda \tag{9}$$

where

D_1 = largest dimension of transmitter

D_2 = largest dimension of target

λ = wavelength of interest

Separation distances that are less than the right-hand
side of Equation (9) map the near-field region (2:98).

Approach

This effort applied Falconer's adjustments to the RCS
measurement parameters (frequency and range) in order to
examine the accuracy and limitations of his concept. In
doing so, the Wright Research & Development Center (WRDC)
far-field RCS and antenna measurement range and its
facilities were used to measure, record, and plot the RCS
data obtained from the targets. The project represented
the first attempt to collect bistatic near-field data on
an indoor far-field range (17).

14

Sequence of Presentation

Chapter II will outline the methodology used for data collection. It will address the measurement system, measurement procedures, the test matrix, and the targets utilized for this effort.

Chapter III presents an analysis of the RCS plots contained in Appendix C. Error analysis will also be addressed in this chapter.

Chapter IV contains the conclusions reached from this study as well as recommendations for further research in this area.

II. Methodology

As mentioned in Chapter I, the purpose for this study
was to examine the applicability of the MBET and associated
extensions in determining the extent to which correlation
exists between monostatic and bistatic data for both the
near and far-field. A secondary objective was to determine
whether reliable bistatic near-field RCS could be collected on
a range originally designed to take monostatic far-field
measurements.

In an effort to address the aforementioned issues,
the following approach was taken. First of all, the
planning phase involved configuration and operational
testing of the measurement system, development of data
collection procedures, target selection, and test matrix
formulation. The second phase involved taking far-field
RCS measurements (monostatic and bistatic) of a 6 in
sphere in an effort to develop confidence in system
operability and to evaluate system accuracy by comparing
measured and predicted RCS values. The third phase
involved collecting monostatic far-field RCS data on the
four targets and comparing these values with the
appropriate physical optics RCS approximations. This
served as another check on system operability and the
measurement procedures prior to collecting near-field
data. After the monostatic near-field data was collected,

16

the system was reconfigured to support bistatic data collection. The final phase involved data analysis.

The remaining sections in this chapter address particulars regarding the measurement system, test procedures, targets, and the test matrix.

Measurement System

The radar system utilized in this project was a continuous wave (CW) nulling system. The receiver was a Scientific-Atlanta Phase-Amplitude receiver, Model 1780. The transmitter was a Hewlett-Packard 8340A Synthesized Sweeper.

A Hewlett-Packard 8349B amplifier was inserted between the receive antenna and the CW nulling loop when collecting the bistatic data. The amplifier increased the returned signal level and improved measurement sensitivity (18:34). The system configuration for the monostatic case did not include this amplifier and the resultant monostatic patterns were not as clean, especially in the the noise floor region ($\approx 50-55$ dB).

Standard 22 dB gain, X-band horns were used as the transmit and receive antennas. This type horn was selected because it provides a relatively narrow and controlled beamwidth. This is important in bistatic measurements since direct coupling between transmit and receive horns is a major source of error and must be minimized. The

horn's radiation pattern for both polarizations is contained in Figures 4 and 5.

Test chamber configuration for the monostatic and bistatic cases is shown pictorially in Figures 6 and 7. Figure 8 provides a view of the bistatic receive horn support structure. The structure is made of plywood coated with RAM. A sheet of plywood coated with RAM was incorporated into the design to minimize direct coupling between the horns. The structure was mounted on a wheeled cart to facilitate movement and placement.

Measurement Procedures

The following procedures, as outlined in reference 18, were used to collect the RCS data on each target:

1. Receiver calibration. This step was used to minimize any non-linearities in the receiver's response over its dynamic range. This internal calibration function calibrates the IF channels for both amplitude and phase (18:32).

2. Test channel nulling. The receiver's test channel signal level was reduced to approximately the noise level of the receiver by using a continuous wave nulling procedure. A more in-depth discussion on this procedure can be found in reference 18.
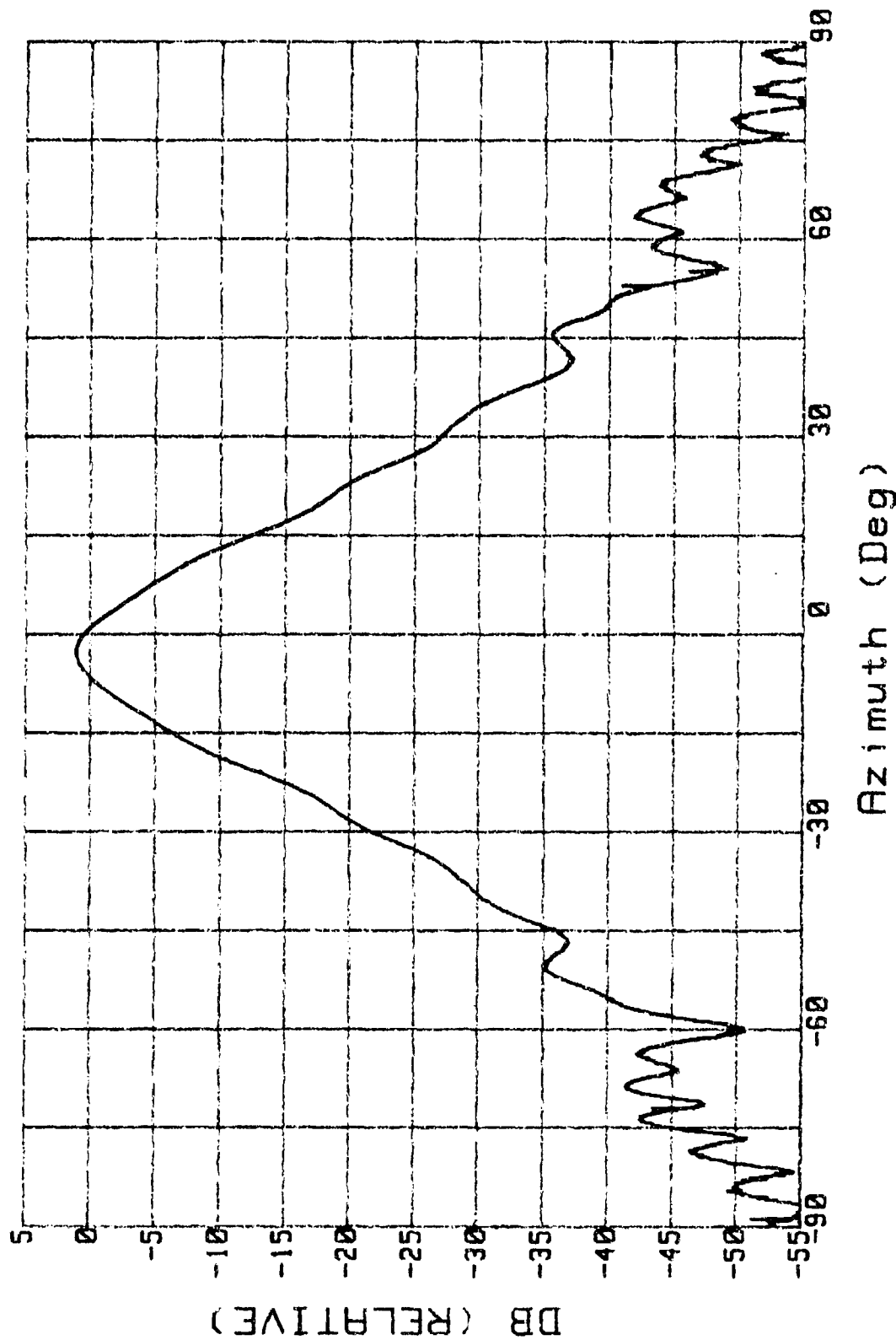
Figure 4. Antenna Radiation Pattern (V Pol)

19
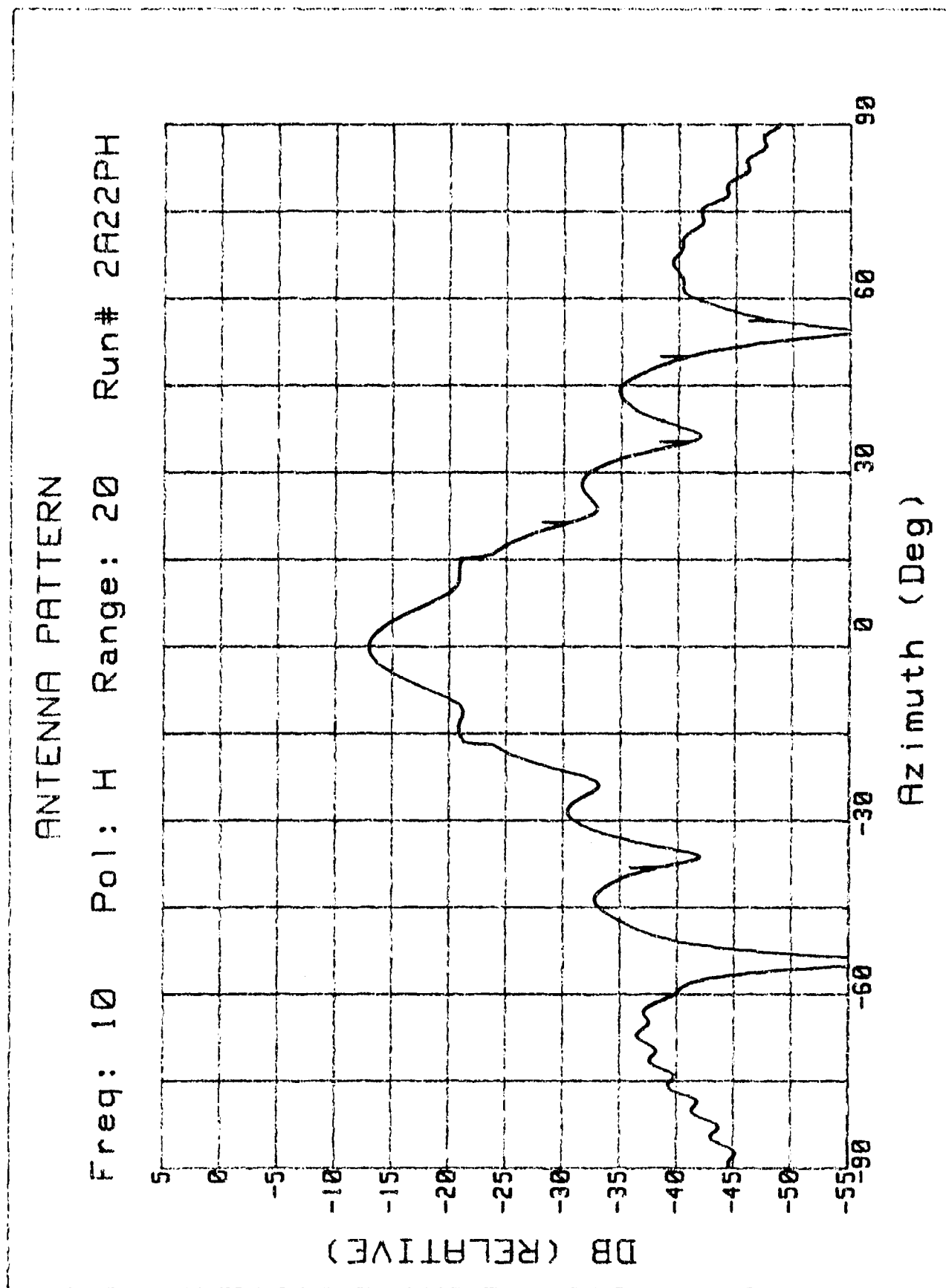
Figure 5. Antenna Radiation Pattern (H Pol)

3. Target placement and measurement. Each target was mounted on the pedestal and rotated through 360°. The return signal was collected and processed and the RCS data was stored by the HP 9836C computer. A code, entitled Range 1 RCS, was utilized to control the data collection process.

4. Calibration. This procedure scaled the target's RCS to the correct magnitude level. Either of two spheres was utilized as a calibration standard since their RCS was easy to predict and independent of aspect angle. The Bistatic Sphere (BISTSPH) code, contained in reference 18, provided the appropriate bistatic RCS values for the spheres. The selection of which sphere to be used as the calibration standard for a given target was based on the expected target RCS and the known sphere RCS. The sphere with a RCS magnitude comparable to that of the target was used as the calibration standard.

5. Data processing. The Range 1 RCS code and the RCS Plot subroutine were used to process the data and create the data plots.

Targets

Four targets were selected for analysis in this effort. They included a circular flat plate, an ogive, and two 1 in diameter circular cylinders of different

21

lengths. These four targets were chosen since, as a group, they provide the following:

      (a)   a large dynamic range (plate).

      (b)   support for travelling and creeping waves (ogive and cylinders).

      (c)   large specular returns and independent scattering centers (cylinders).

With regards to calibration, a 2 in and a 6 in diameter sphere were used as calibration standards.

Target description follows:

1. Circular flat plate (RAM coated on one side):

    Diameter: 8 in

    Thickness: 0.125 in

                    0.1875 in of RAM

2. Ogive:

    Length: 9.6 in

    Circumference: 5.75 in (at center)

3. Circular Cylinder:

    Length: 8 in

    Diameter: 1 in

4. Circular Cylinder:

    Length: 14.25 in

    Diameter: 1 in

A photograph of each target and calibration standard is contained in Appendix B, Figures 9 through 14.

Test Matrix

The test matrix included monostatic and bistatic measurements for both polarizations with varying target-to-receiver separation distances. The bistatic (BSA=30°) measurements were conducted at 10 GHZ while the monostatic data was collected at the reduced frequency of 9.66 GHZ.

Near and far-field data was collected. For the monostatic case, Equation (9) was utilized to determine the different zones. For the bistatic system, the transmitter-to-target range was maintained at 20 feet (far-field) and the target-to- receiver range was varied between the near and far-field. The variables in Equation (9) were redefined to allow for the determination of the different zones. By employing the reciprocity theorem (allowing the target to become the transmitter), D_1 became the maximum target dimension and D_2 the maximum receiver dimension.

Tables 1 and 2 provide a composite summary of the test matrix. Each table specifies the system configuration, polarization, target, and target-to-receiver separation range (R'). Broken lines in the respective columns signify the separation of near and far-field entries for each target. The "VV" or "HH" represent the transmit and receive horn orientation with respect to polarization. In other words, a "VV" entry in a given box signifies that, for a given target and range, a measurement was proposed

23

to be taken with the transmit and receive horns both
oriented to accommodate a vertically polarized wave. The
same rationale applies for the "HH" entry except it is
with regards to horizontal polarization. The first letter
of a given pair represents the transmitter orientation,
the second letter the receive horn orientation.

Table 1. Monostatic Test Matrix

Ogive	Plate	Range (ft)	Cyl (8 in)	Cyl (14.25 in)
VV,HH	VV,HH	10	VV,HH	VV,HH
HH	VV,HH	10.8	VV,HH	HH
VV,HH	VV,HH	12	VV,HH	VV,HH
VV,HH	VV,HH	13	VV,HH	
VV,HH		13.75		VV,HH
VV,HH	VV,HH	15	VV,HH	HH
		16.5		VV,HH
		19		VV,HH
		20		VV,HH

Table 2.   Bistatic Test Matrix

Ogive	Plate	Range (ft)	Cyl (8 in)	Cyl (14.25 in)
VV,HH	VV,HH	7	VV,HH	VV,HH
HH	VV,HH	7.75	VV,HH	HH
VV,HH	VV,HH	9	VV,HH	VV,HH
	VV,HH	10.8	VV,HH	
VV,HH		11		VV,HH
VV,HH	VV,HH	13	VV,HH	HH
VV,HH	VV,HH	15	VV,HH	VV,HH
		19		VV,HH
		20		VV,HH

III. Data Analysis

Falconer's hypothesis can be evaluated by comparing the bistatic data with monostatic data collected at the appropriately adjusted frequency, target-to-receiver range, and aspect angle. Four shapes, as described earlier, were tested to examine the accuracy and limitations of Falconer's MBET statements.

The RCS data was collected over a four month period at WRDC's far-field RCS measurement range. It is a range designed to collect far-field RCS and antenna patterns monostatically. Provisions to accommodate bistatic as well as near-field measurements were not incorporated into the range (17). The measurements were taken with a radar system utilizing a continuous wave nulling loop. A 2 in sphere was used as the calibration standard for the ogive and the 8 in cylinder. A 6 in sphere was used for the other two targets.

Data Tables 3 through 10 can be found in this chapter. They provide peak, or broadside, RCS values for each target. The tables are organized such that the bistatic data and its corresponding monostatic values are listed on the same line for ease in comparison. Each table contains six columns which are defined below:

Column 1: R_r' = target-to-receiver separation distance for the monostatic case

26

Column 2: Mono RCS = peak RCS value for the monostatic case

Column 3: Scale factor (sf). See discussion in Appendix A.

Column 4: R' = target-to-receiver separation distance for the bistatic case

Column 5: Bist RCS = peak RCS value for the bistatic case

Column 6: Diff = |(column 2 + column 3) - column 5|

The dashed lines in columns 1,2,4, and 5 separate near-field (above line) and far-field (below line) ranges and data for the respective system configuration. An asterisk in columns 2 or 5 indicates data was collected and stored, but the plot was not available due to an inability to retrieve the data from storage.

Circular Flat Plate

Vertical Polarization. Figures 15A through 19B provide the RCS patterns, monostatic and bistatic, for the plate subjected to a vertically polarized electric field. The plots indicate that the monostatic patterns do provide a good representation of their bistatic counterpart except in the region $75°$ to $105°$ off of specular (edge-on plate orientation).

Table 3 contains the peak RCS values from the uncoated side of the plate. For the most part, the

27

monostatic and bistatic values are within 1 dBsm of the physical optics approximation of 11.4 dBsm indicating that the measurement system is functioning properly. Column 6 entries indicate that the bistatic far-field RCS amplitude can be approximated (within 1 dBsm) with scaled monostatic data collected at the appropriate frequency, range, and aspect angle. Approximation accuracy decreased as R' decreased, but it remained less than 1.8 dBsm.

Table 3. Peak RCS for Plate (V Pol)

R'_r (ft)	Mono RCS (dBsm)	Scale Factor (dBsm)	R' (ft)	Bist RCS (dBsm)	Diff (dBsm)
10	10.71	1.7	7	10.88	1.53
10.8	10.54	1.59	7.75	10.35	1.78
12	10.15	1.4	9	10.71	0.84
10.8	10.54	0.15	10.8	9.82	0.87
13	10.56	0.15	13	10.49	0.22
15	10.79	0.15	15	11.09	0.15

In summary, it appears that Falconer's far-zone statement holds and provides for a good approximation of the bistatic RCS amplitude for this target and polarization. The near-zone statement and resultant monostatic data appear to produce a fair and less accurate approximation of the bistatic data.

Horizontal Polarization. Figures 20A through 24B
provide the RCS patterns collected when the transmitted
field was horizontally polarized. Once again, the
monostatic patterns are representative of the corresponding
bistatic patterns other than in the region where edge-on
returns are received. It should be noted, though, that the
first level sidelobe null is not symmetric around the
specular return.

Table 4 contains the plate's peak RCS data for
horizontal polarization. The monostatic RCS remained
within 1 dBsm of the physical optics approximation of 11.4
dBsm in both the near and far-field. Bistatic data,
though, decreased in value as R' was decreased. Finally,
the accuracy of the scaled monostatic approximation
decreased as the receiver moved deeper into the near-field.

Table 4. Peak RCS for Plate (H Pol)

R'_r (ft)	Mono RCS (dBsm)	Scale Factor (dBsm)	R' (ft)	Bist RCS (dBsm)	Diff (dBsm)
10	10.76	1.7	7	9.84	2.62
10.8	10.70	1.59	7.75	10.1	2.19
12	10.59	1.4	9	10.1	1.89
10.8	10.70	0.15	10.8	10.26	0.59
13	10.65	0.15	13	10.72	0.08
15	10.53	0.15	15	10.81	0.13

In summary, Falconer's far-zone statement provided
for accurate approximations of the bistatic far-field RCS

amplitudes. The near-zone statement, though, provided only poor to fair representations of the bistatic near-field RCS values. Pattern duplication (not considering amplitude) was good for both the near and far-field.

Ogive

Vertical polarization. Figures 25A through 29B provide the RCS patterns under review in this section. The monostatic patterns do provide a good representation of the corresponding bistatic plot except in the region $45°$ to $135°$ from broadside. The monostatic plots are not "clean" in this region due to noise. The achievable noise floor for this chamber was usually around -55 dB. Target returns of such magnitude, though, were "lost" within the noise. For the bistatic case, an amplifier was employed to enhance the signal-to-noise ratio. The result was a clean, discernable pattern.

Table 5 provides the peak RCS values. Column 6 values indicate that the scaled monostatic data provides a very good approximation of the corresponding bistatic data in both the near and far-field cases.

Horizontal polarization. Figures 30A through 35B contain the RCS patterns for the ogive subjected to a horizontally polarized wave. Comparisons show that the monostatic patterns are not good representations of the

Table 5. Peak RCS for Ogive (V Pol)

R'_r (ft)	Mono RCS (dBsm)	Scale Factor (dBsm)	R' (ft)	Bist RCS (dBsm)	Diff (dBsm)
10	-15.68	1.7	7	-14.51	0.53
12	-15.79	1.4	9	-14.6	0.21
13.75	-14.99	1.12	11	-14.32	0.45
13	-14.64	-	13	-14.21	0.43
15	-14.67	-	15	-14.05	0.62

corresponding bistatic patterns. The monostatic patterns for aspect angles up to $30°$ from either side of the ogive's tip are out of phase with the same region in the corresponding bistatic patterns. In other words, the monostatic patterns show peaks/nulls at aspect angles for which the bistatic returns have nulls/peaks. This phenomena probably can be attributable to the presence of travelling waves running the length of the target.

Table 6 provides the peak RCS values. As shown by the data in column 6, the scaled monostatic values are good approximations of the bistatic far-field data. In the bistatic near-field, the monostatic approximations are poor and the accuracy (> 2dB) gets worse as R' is decreased.

31

Table 6. Peak RCS for Ogive (H Pol)

R'_r (ft)	Mono RCS (dBsm)	Scale Factor (dBsm)	R' (ft)	Bist RCS (dBsm)	Diff (dBsm)
10	-16.07	1.7	7	-17.12	2.75
10.8	-16.06	1.59	7.75	-17.09	2.62
12	-15.92	1.4	9	-17.06	2.54
13.75	-15.96	1.12	11	-16.97	2.13
13	-15.91	-	13	-16.61	0.7
15	-15.51	-	15	-16.31	0.8

Circular Cylinder (8 in)

Vertical polarization. Figures 36 through 40B are
analyzed here. Examination of the plots reveals that the
monostatic patterns for this target and polarization
provide very good representations of their corresponding
bistatic patterns.

Table 7 shows that, for the far-field case, the scaled
monostatic data represent good bistatic RCS amplitude
approximations. In the near-field, the approximations are
good until $R'=7$ feet. At this point, accuracy begins to
significantly decrease and this trend would be expected to
continue as R' became smaller. This is because the
unscaled monostatic and corresponding bistatic RCS
differential remains constant ($\approx 0.6-0.8$ dBsm) as R' is
varied. The scaling factor, though, will continue to

32

increase as R' decreases, resulting in a poorer approximation. For this target and polarization, it appears that a scaling factor is not needed.

Table 7. Peak RCS for 8 in Cylinder (V Pol)

R'_r (ft)	Mono RCS (dBsm)	Scale Factor (dBsm)	R' (ft)	Bist RCS (dBsm)	Diff (dBsm)
10	-10.36	1.7	7	-10.02	1.36
10.8	-10.6	1.59	7.75	- 9.78	0.77
12	-10.4	1.4	9	- 9.69	0.69
10.8	-10.6	0.08	10.8	-10.12	0.4
13	-10.56	0.08	13	- 9.81	0.67
15	-10.62*	0.08	15	- 9.65	0.89

<u>Horizontal polarization.</u> Figures 41A through 45B show that the monostatic patterns provide a good, consistent representation of the corresponding bistatic patterns except for the amplitude.

Table 8 provides the peak RCS values for the referenced plots. The accuracy of the scaled monostatic data could be considered fair to very poor and decreases as R' decreases. Travelling wave contributions to the RCS are adversely impacting on the accuracy of the amplitude approximations.

Table 8. Peak RCS for 8 in Cylinder (H Pol)

R'$_r$ (ft)	Mono RCS (dBsm)	Scale Factor (dBsm)	R' (ft)	Bist RCS (dBsm)	Diff (dBsm)
10	- 9.74	1.7	7	-11.3	3.26
10.8	- 9.52	1.59	7.75	-11.05	3.12
12	- 9.56	1.4	9	-10.89	2.73
10.8	- 9.52	0.08	10.8	-11.41	1.97
13	- 9.55	0.08	13	-11.15	1.68
15	- 9.35	0.08	15	-10.79	1.52

Circular Cylinder (14.25 in)

Vertical polarization. Figures 46A through 51B indicate that there is good correlation between the monostatic and bistatic patterns.

Table 9 shows that the accuracy (< 0.9 dBsm) of the amplitude approximations is very good in both the near and far-field. It should also be noted that the monostatic and bistatic peak RCS values decrease as R' transitions from the far-field through the near-field.

Horizontal polarization. Figures 52A through 59B show that the RCS pattern correlation is good except in the region that represents the cylinder's end-on return. The monostatic patterns do not produce the "dip" found in the bistatic patterns at end-on (105° and -75°).

Table 9. Peak RCS for 14.25 in Cylinder (V Pol)

R'_r (ft)	Mono RCS (dBsm)	Scale Factor (dBsm)	R' (ft)	Bist RCS (dBsm)	Diff (dBsm)
10	-8.73	1.7	7	-7.75	0.72
12	-7.98	1.4	9	-7.4	0.82
13.75	-7.76	1.12	11	-7.16	0.52
16.5	-7.13	0.56	15	-6.89	0.32
19	-7.1	0.08	19	-6.43	0.59
20	-7.02	0.08	20	-6.32	0.62

Table 10 shows that the accuracy of the amplitude approximations was very good in the far-field. The accuracy became worse, though, as R' was decreased. It should be noted that if the scale factor was not applied, the peak amplitude correlation would have been very good (< 0.6 dBsm) throughout the near and far-field.

Summary. Table 11 summarizes the merit of the MBET and Falconer's statements with respect to pattern representation and the accuracy of the RCS amplitude approximations for each target and polarization. The "FF" and "NF" in column 4 signify far and near-field.

35

Table 10.   Peak RCS for 14.25 in Cylinder (H Pol)

R'_r (ft)	Mono RCS (dBsm)	Scale Factor (dBsm)	R' (ft)	Bist RCS (dBsm)	Diff (dBsm)
10	-6.72	1.7	7	-6.65	1.63
10.8	-6.33	1.59	7.75	-5.95	1.21
12	-6.4	1.4	9	-5.81	0.81
13.75	-5.95	1.12	11	-5.79	0.96
15	-5.86	0.83	13	-5.95	0.92
16.5	-5.68	0.56	15	-5.57	0.45
19	-5.36*	0.08	19	-5.29	0.01
20	-4.93	0.08	20	-5.42	0.57

Subjective evaluations of the approximation accuracy are based on the following:

	Difference (D) (dBsm)
good	D < 1.0
fair	1.0 < D < 2.0
poor	2.0 < D

where the Difference (D) represents the values from column 6 of Tables 3 through 10.

Error Analysis

Diffraction, target placement, calibration error, and antenna coupling were potential sources of error.

Table 11.   Summary of Data Analysis

Target	Polarization	Pattern Representation	Accuracy of Amplitude Approximation
Plate	V	good	(FF) - good (NF) - fair
	H	good	(FF) - very good (NF) - poor to fair
Ogive	V	good	(FF) - very good (NF) - very good
	H	poor	(FF) - good (NF) - poor
Cylinder (8 in)	V	very good	(FF) - good (NF) - fair to good
	H	very good	(FF) - fair (NF) - very poor
Cylinder (14.25 in)	V	good	(FF) - very good (NF) - good to very good
	H	good	(FF) - very good (NF) - fair to good

Diffraction from the front tip of the target support
structure and from the leading edge of the bistatic receiver
support structure potentially affected the incident
wavefront (disrupted its planar characteristic) and the
resultant RCS value.   The extent to which the diffracted
waves affected the incident wavefront was not evaluated.

Improper target alignment on the pedestal mount resulted in several non-symmetrical RCS patterns and inaccurate RCS returns. In particular, the ogive was sometimes positioned slightly off horizontal which resulted in the target's broadside pattern to be canted (see Figure 32A). Alignment of the flat plate surface perpendicular to the incident wavefront was difficult. Any offset from the perpendicular introduced some error into the RCS data.

As discussed by McCool in reference 18, precise placement of the bistatic receive antenna at the desired bistatic angle is imperative in minimizing calibration error. A determined effort was made to ensure that the receive horn was centered on the 30° bistatic angle reference line. By maintaining the antenna within $\pm 1^\circ$ of the desired bistatic angle, the maximum calibration error introduced was less than 0.1 dbsm. This error bound is based on analysis of bistatic RCS values computed for the calibration spheres using the Bistatic Sphere code.

For the bistatic measurements, direct coupling between the horns was a concern. In an attempt to minimize this coupling, the receive horn was shielded from the transmitter with RAM coated plywood. Even though the effectiveness of this shielding technique was not quantified, it is felt that the antenna coupling error was significantly reduced.

IV. Conclusions and Recommendations

Conclusions

The following conclusions are drawn from this research effort.

1. Near-field monostatic and bistatic data can be collected on WRDC's indoor, far-field RCS measurement range

2. The monostatic-bistatic equivalence theorem, as modified by Dr. Falconer's far-zone statement, provides good RCS predictions of bistatic _far-field_ RCS patterns and amplitudes at a bistatic angle of 30° and a transmitting frequency of 10 GHZ.

3. Falconer's near-zone version of the MBET provides fair RCS predictions of the bistatic _near-field_ RCS patterns and amplitudes for those targets that have no higher order effects contributing to the RCS.

4. The MBET, even when modified by Falconer's statements, does not account for the effect travelling and creeping waves have on the RCS patterns.

Recommendations

Further study is warranted to quantitatively determine the limits of Falconer's method. In particular, the effect of varying parameters such as frequency, shape complexity, and target-to-receiver separation range (near

vs. far-field) should be examined more extensively. The additional effort should address the following:

1. **Bistatic Angle Variance**. An analysis addressing the accuracy and limitations of Falconer's method as the bistatic angle is varied from $30°$ to $90°$ is needed. Falconer's modifications to the MBET and the data collection process, i.e., amplitude and phase correction terms and the introduction of the reduced range concept, may extend the range of bistatic angles for which accurate correlation exists between the monostatic and bistatic data.

2. **Variance of Target Dimension(s)**. As shown by this effort, the applicability and accuracy of Falconer's MBET concept appeared to be a function of the target dimension in the plane of the electric field. Varying target dimension(s) in an effort to determine target size that will support a significant creeping and/or travelling wave contribution to the RCS could be examined. As mentioned earlier, the MBET and its extensions do not account for these higher order effects and, therefore, its usage in data analysis would not be appropriate.

3. **Phase Analysis**. A study examining the applicability of Falconer's MBET statements regarding phase correlation between the monostatic and bistatic measurements would be worthwhile.

With regards to the far-field measurement range, the following recommendatio s are provided:

40

1. Incorporate a pulse gating measurement system to minimize nulling errors and provide for more accurate data.

2. Develop a platform that will provide improved user access to the support pedestal during target placement. The current target placement procedure is time-consuming and lends itself to target alignment errors.

3. Enhance the understanding and capabilities of the Range 1 RCS code. First of all, development of a user's guide to document the capabilities and operating procedures associated with the code would be very useful. Secondly, a subroutine that computes Falconer's scaling factors should be developed and incorporated into the main code. The subroutine should possess the capability to provide plots and data printouts of the scaled monostatic values. Finally, the RCS Plot code should be incorporated within the Range 1 RCS code.

4. Investigate the possibility of developing a low RCS, target support pylon dedicated to bistatic RCS work. The pylon should provide a low RCS return, possess maneuverability to provide the desired target orientations, and be positioned within the test chamber such that it is an integral part of a referencing system developed to ensure proper alignment of the transmit and receive horns with the target.

5. Design a bistatic receive horn support structure that will minimize direct coupling between the horns. The design

should also consider minimizing the effect of diffracted waves from the structure's edges on the incident wavefront.

Appendix A: Overview of Falconer's Statements

As mentioned in Chapter I, Falconer developed two
modifications to the monostatic-bistatic equivalence theorem.
They are referred to as the far-zone and near-zone statements
of the MBET and they are summarized in this appendix.

43

Far-Zone Statement

As mentioned in Chapter I, the far-zone statement of
the MBET states that in the far-zone one can estimate the
bistatic scattering amplitude by measuring the monostatic
scattering amplitude at a reduced requency f_r, a target-to-
receiver separation range R', and at one-half the bistatic
angle, providing that amplitude and phase adjustments are
made. The mathematical expression showing the relationship
between the monostatic and bistatic scattered electric
fields is

$$E_b(f,R',\beta) \approx (f/f_r) \exp\left[i(4\pi/c)(f-f_r)R'\right]E_m(f_r,R',\beta/2) \qquad (10)$$

For this study

$$\beta = 30^\circ$$

$$f = 10 \text{ GHZ}$$

$$f_r = 9.66 \text{ GHZ}$$

$$R' = \text{Column 4 entries (below dashed line)}$$
$$\text{of Tables 3 through 10.}$$

Approximation (10) contains two correction terms.
The exponential term is a correcting phase factor which
becomes important when measuring scattered phase in
anechoic chambers (14:12). The term (f/f_r) represents a
modifying amplitude factor, or scaling factor, which is
applied to E_m when the scattering surface looks planar
relative to the incident wavelength λ, as is the case with
the plate. If the radius of curvature of the scattering

44

surface is less than λ in either direction at the
scattering center, as with the cylinders, the scaling
factor would be $\left[f/f_r\right]^{1/2}$. If both radii are less than
λ, as with the ogive, the factor would be dropped from the
approximation (14:12). These scaling factors have been
computed and converted to dBsm for inclusion in column 3
of Tables 3 through 10.

Near-Zone Statement

To reiterate, Falconer's near-zone statement of the
MBET says that the near-field bistatic scattering
amplitude can be estimated by measuring the monostatic
amplitude at a reduced frequency f_r, at an adjusted range
R'_r, and at one-half the bistatic angle providing that the
indicated amplitude and phase adjustments are made
(14:13,16). This statement applies to the situation where
the target-to-receiver range (R') is not equal to the
transmitter-to-target range (R''). The mathematical
expression showing this relationship is

$$E_b(f,R',\beta) \approx (fR'_r/f_r R') \exp\left[i(2\pi f/c)(R' + R'')\right.$$
$$\left. - i(2\pi f_r/c)(R'_r+R''_r)\right] E_m(f_r,R'_r,\beta/2) \qquad (11)$$

The exponential term in approximation (11) represents the
correcting phase factor. The term $(fR'_r/f_r R')$ represents
the amplitude correction term, or scaling factor. The
near-field scaling factor, a function of the R'_r and R'

45

entries in columns 1 and 4 of Tables 3 through 10, can be found in column 3 of the data tables.

The reduced, or adjusted range, used for the monostatic measurements must satisfy the following relationship (14:16):

$$(k_r/R_r') + (k_r/R_r'') = (k/R') + (k/R'') \qquad (12)$$

Factoring out $(2\pi/c)$ and rearranging terms yields

$$(f_r/f) \left[(1/R_r') + (1/R_r'')\right] = \left[(1/R') + (1/R'')\right] \qquad (13)$$

Using Equation (8) and knowing that $R_r' = R_r''$ for the monostatic case, Equation (13) becomes

$$\cos(\beta/2) \left[2/R_r'\right] = \left[(1/R') + (1/R'')\right] \qquad (14)$$

Rearranging terms yields the following expression for R_r'

$$R_r' = 2\left[(R'R'')/(R' + R'')\right] \cos(\beta/2) \qquad (15)$$

For this study the transmitter-to-target range (R″) was 20 feet. This reduces Equation (15) to

$$R_r' = 40 \left[R'/(R'+20)\right] \cos(\beta/2) \qquad (16)$$

with $\beta=30°$. The R_r' values are listed in column 1 of Tables 3 through 10. Those ranges were computed based on the corresponding near-field values of R′ which are listed above the dashed line in Column 4 of the tables.

Appendix B: Target and Chamber Photographs

This appendix contains photographs of the test chamber in both its monostatic and bistatic configurations. A view of the bistatic receive horn support structure is included. Pictures of each target and the calibration standards have also been provided.

47
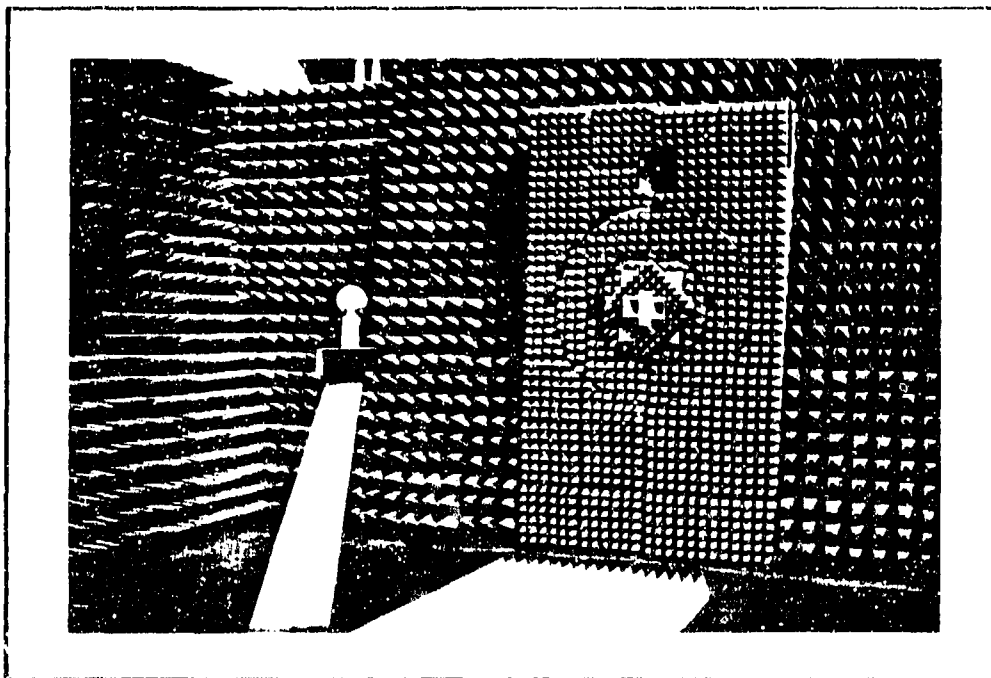
Figure 6. Monostatic Configuration of Test Chamber
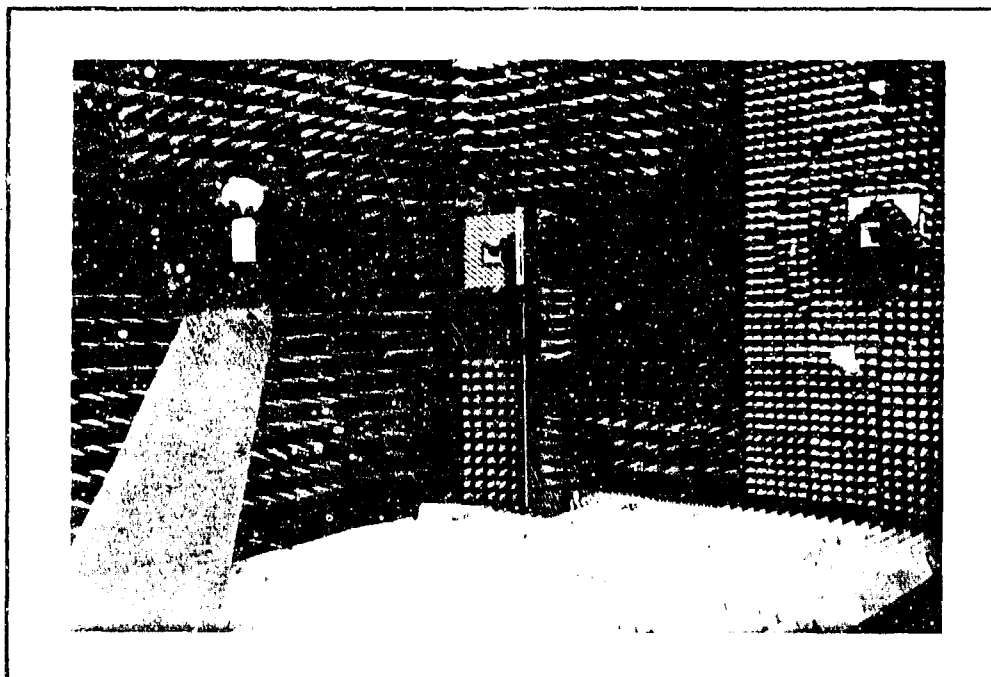
Figure 7. Bistatic Configuration of Test Chamber

48
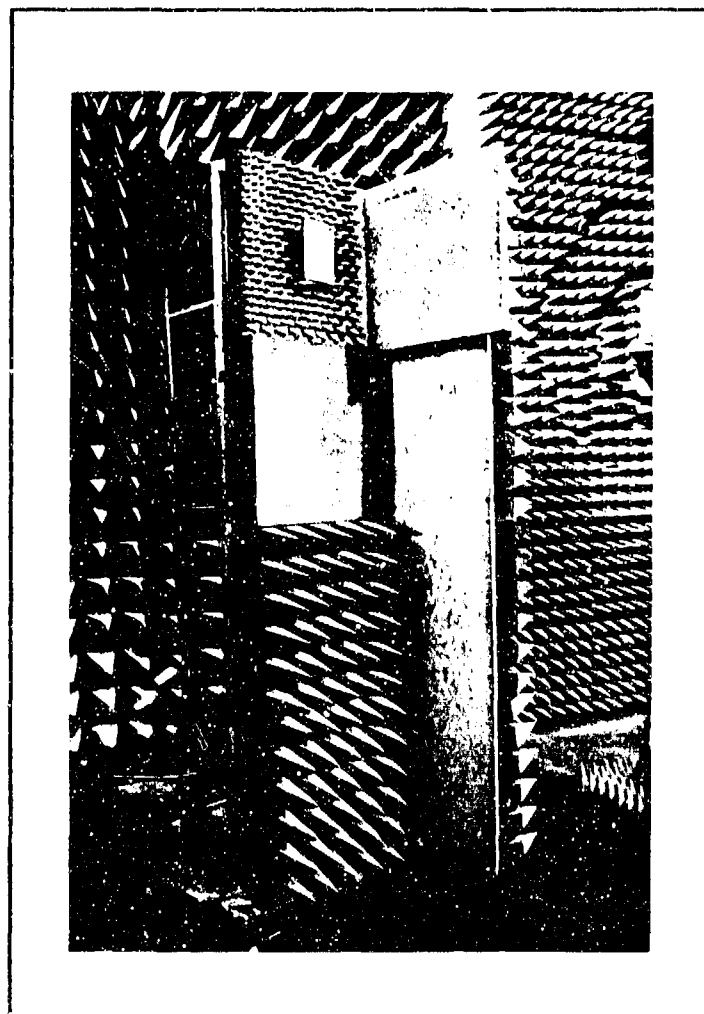
Figure 8. Bistatic Receive Horn Support Structure

49
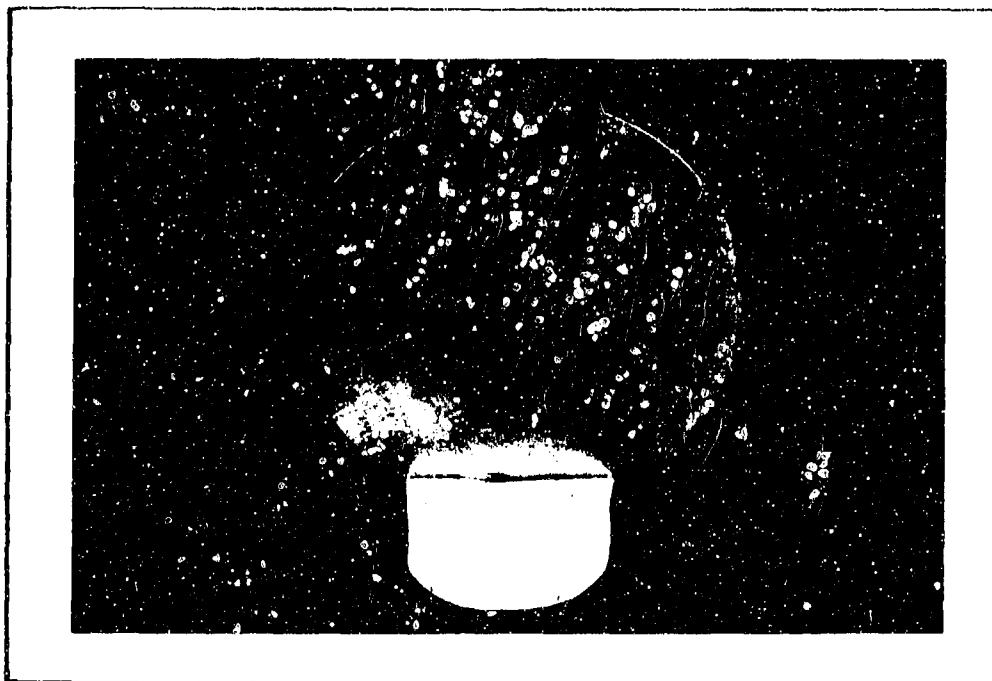
Figure 9.   Circular Flat Plate
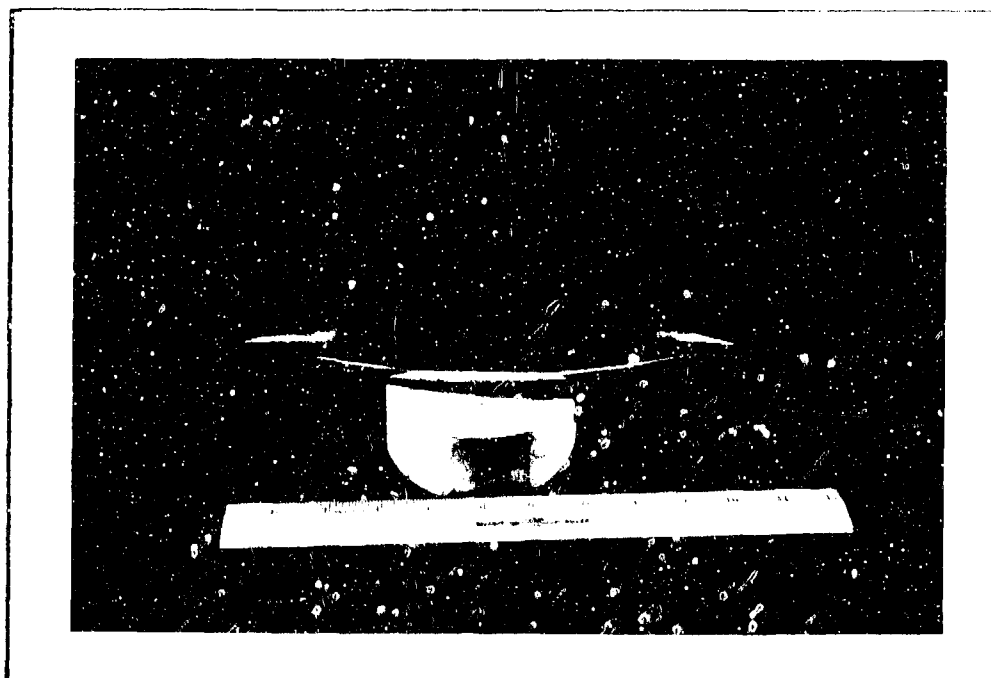
Figure 10.   Ogive

Figure 11. Circular Cylinder (8 in)

Figure 12. Circular Cylinder (14.25 in)
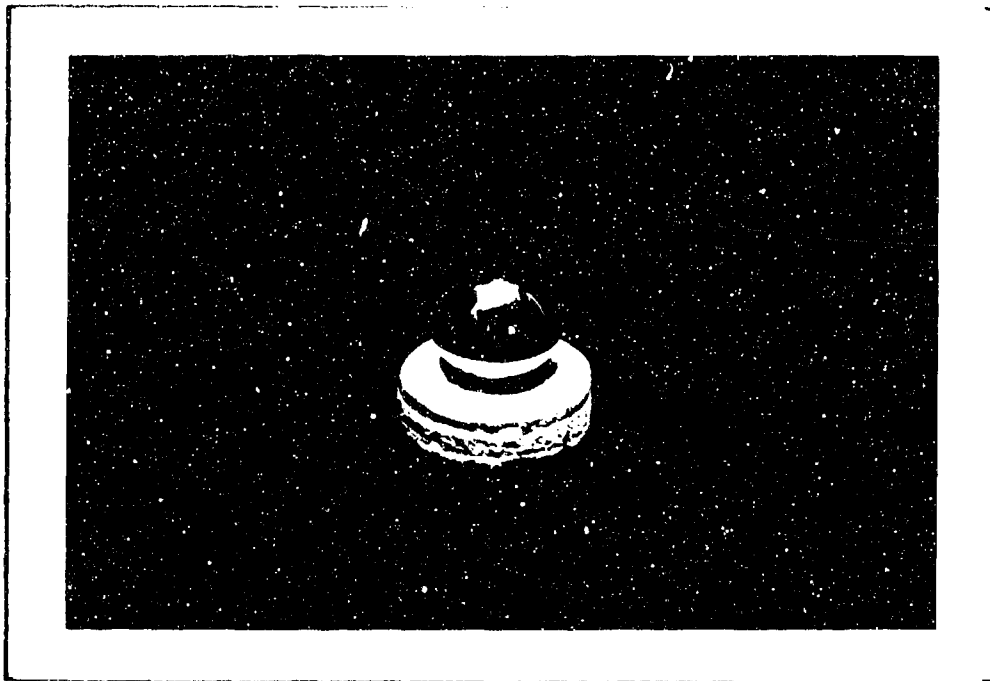
Figure 13.   Sphere (2 in)
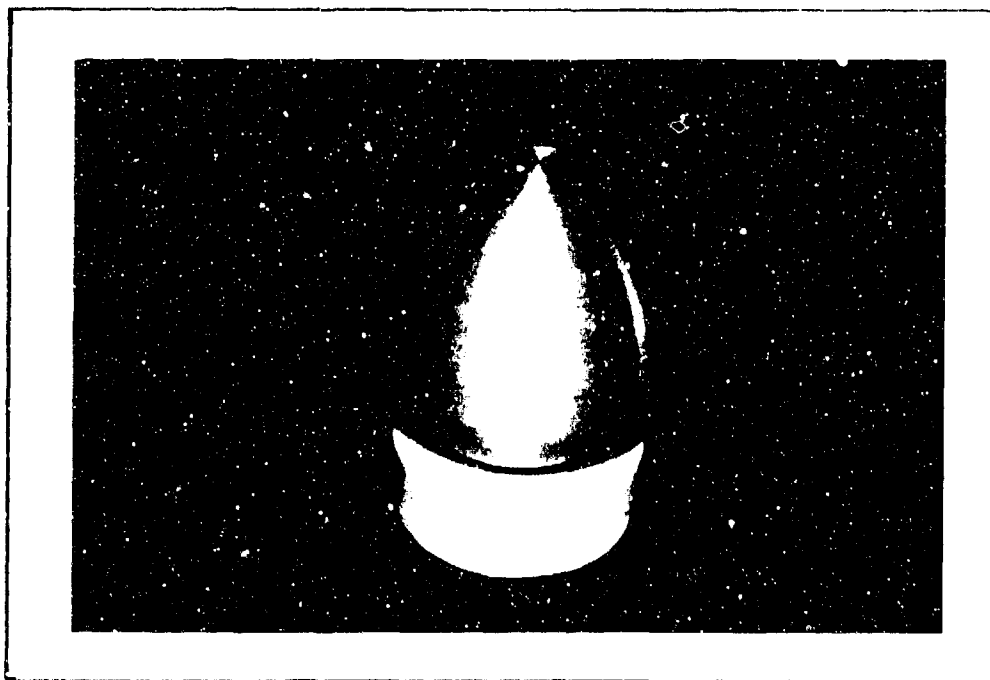
Figure 14.   Sphere (6 in)

52

Appendix C: RCS Data Plots

The monostatic and bistatic RCS data plots are included in this appendix. The plots are sequenced such that the bistatic plot for a given target-to-receiver separation range and polarization is followed by its corresponding monostatic (BSA=0°) plot taken at the adjusted range and/or reduced frequency as called for by Falconer. Monostatic/bistatic plot pairs are referenced by the same figure number. The letter designation provides identification for a particular plot. With regards to measurement parameters, the frequency values are given in GHZ, range in feet, and the bistatic angle (BSA) in degrees.

It should be noted that the monostatic plots do not include the amplitude correction factor. Also, several additional bistatic measurements were taken to increase the data base. The bistatic plots are included, but corresponding monostatic plots are not available.

Figure 15A. RCS: Circ Flat Plate, V Pol, BSA=30, Range=15

54

Figure 15B. RCS: Circ Flat Plate, V Pol, BSA=0, Range=15

Figure 16A. RCS: Circ Flat Plate, V Pol, BSA=30, Range=13

Figure 16B. RCS: Circ Flat Plate, V Pol, BSA=0, Range=13

CIRC FLAT PLATE (8 IN DIA)   BSA=30

Freq: 10   Pol: V   Range: 10.8   Run# 2
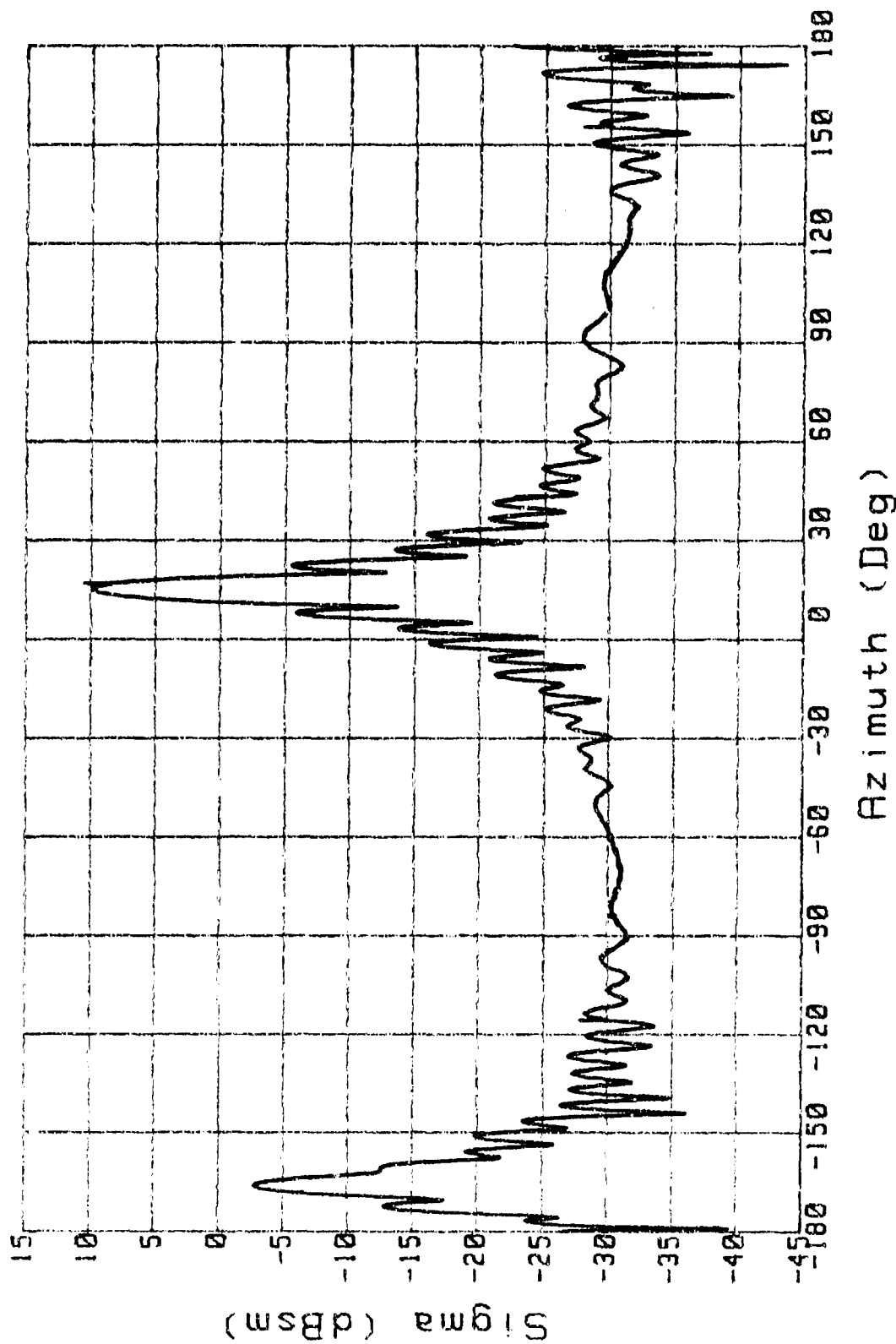
Figure 17A.   RCS: Circ Flat Plate, V Pol, BSA=30, Range=10.8
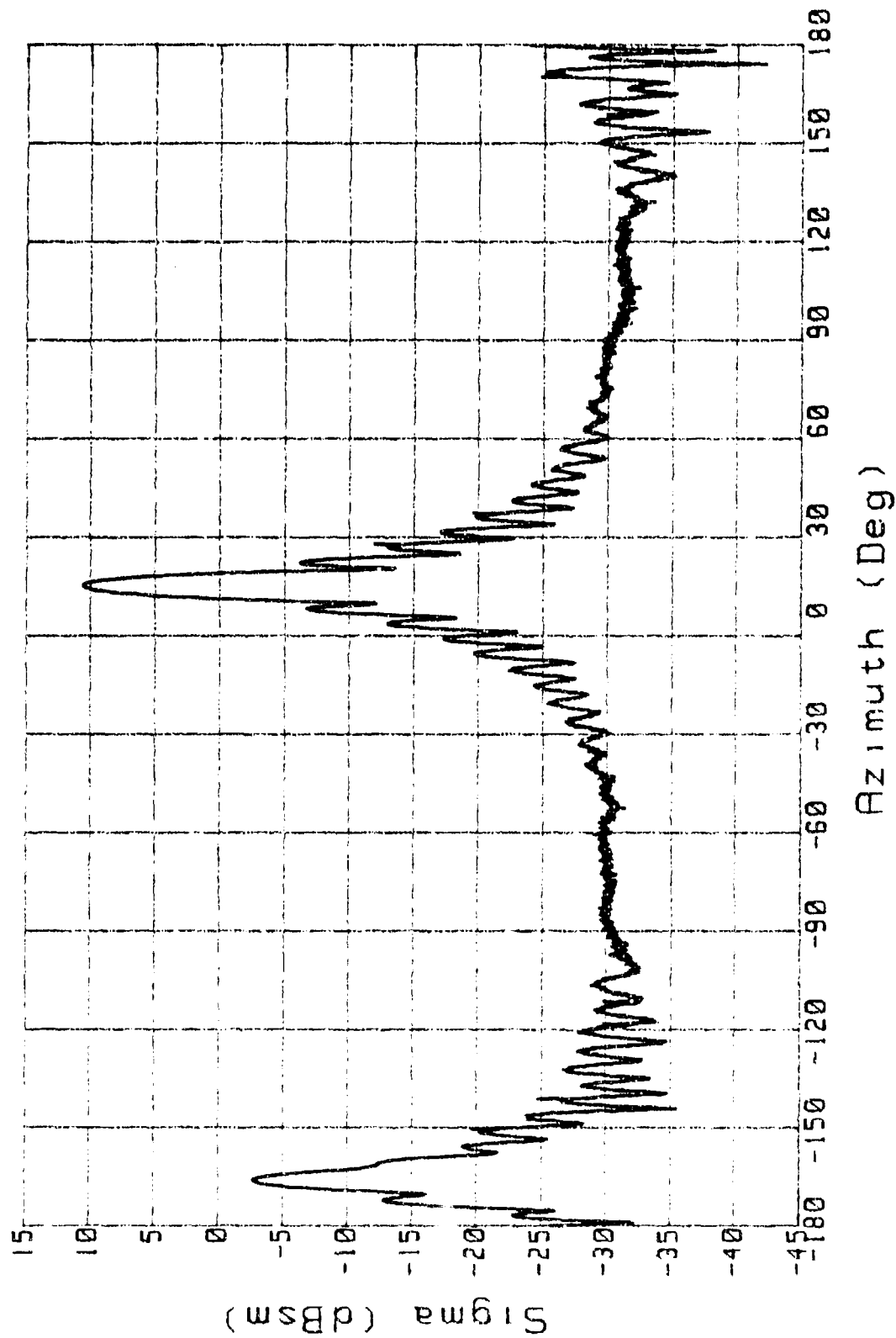
Figure 17B. RCS: Circ Flat Plate, V Pol, BSA=0, Range=10.8
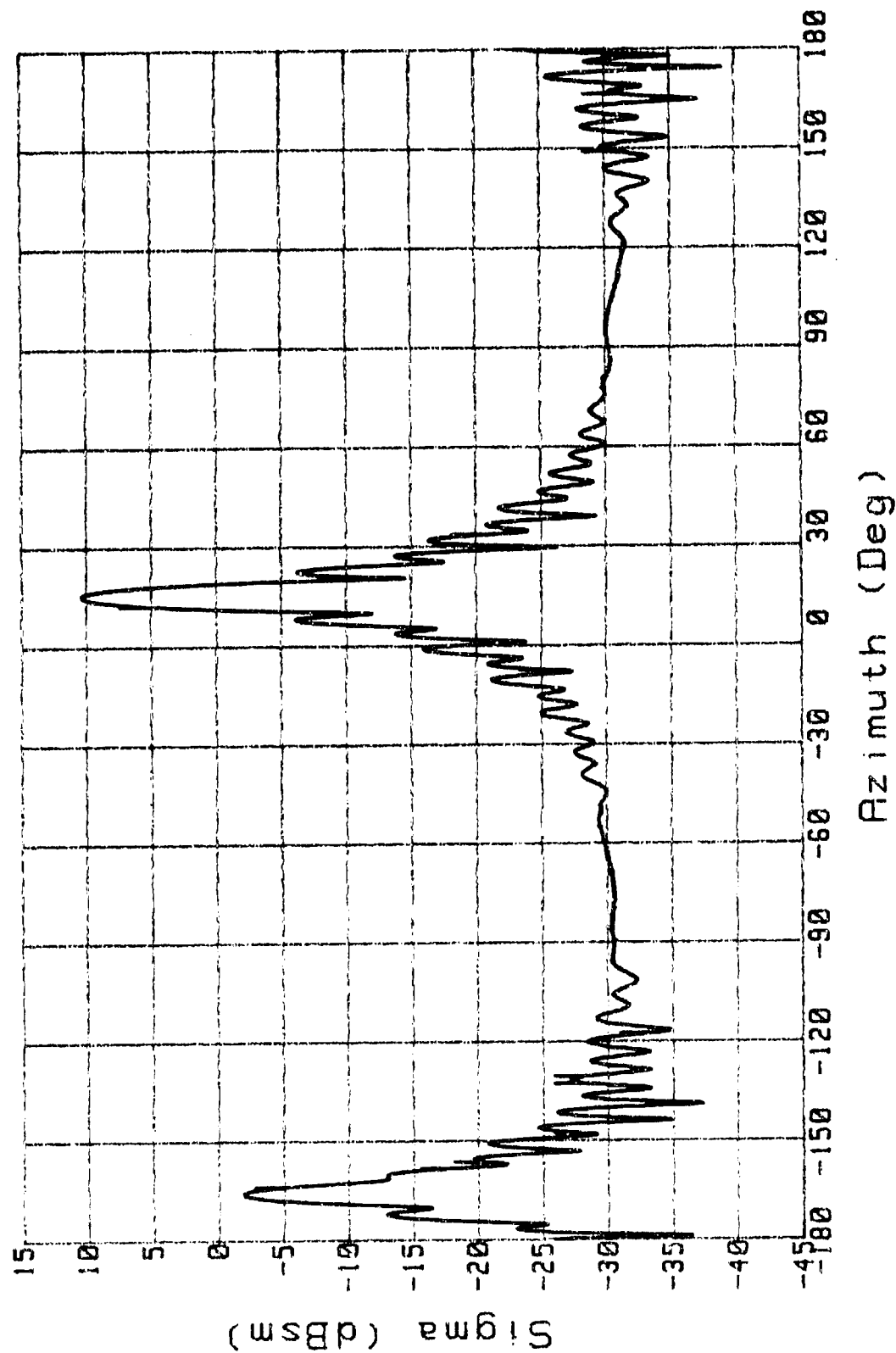
Figure 17C. RCS: Circ Flat Plate, V Pol, BSA=30, Range=7.75

60
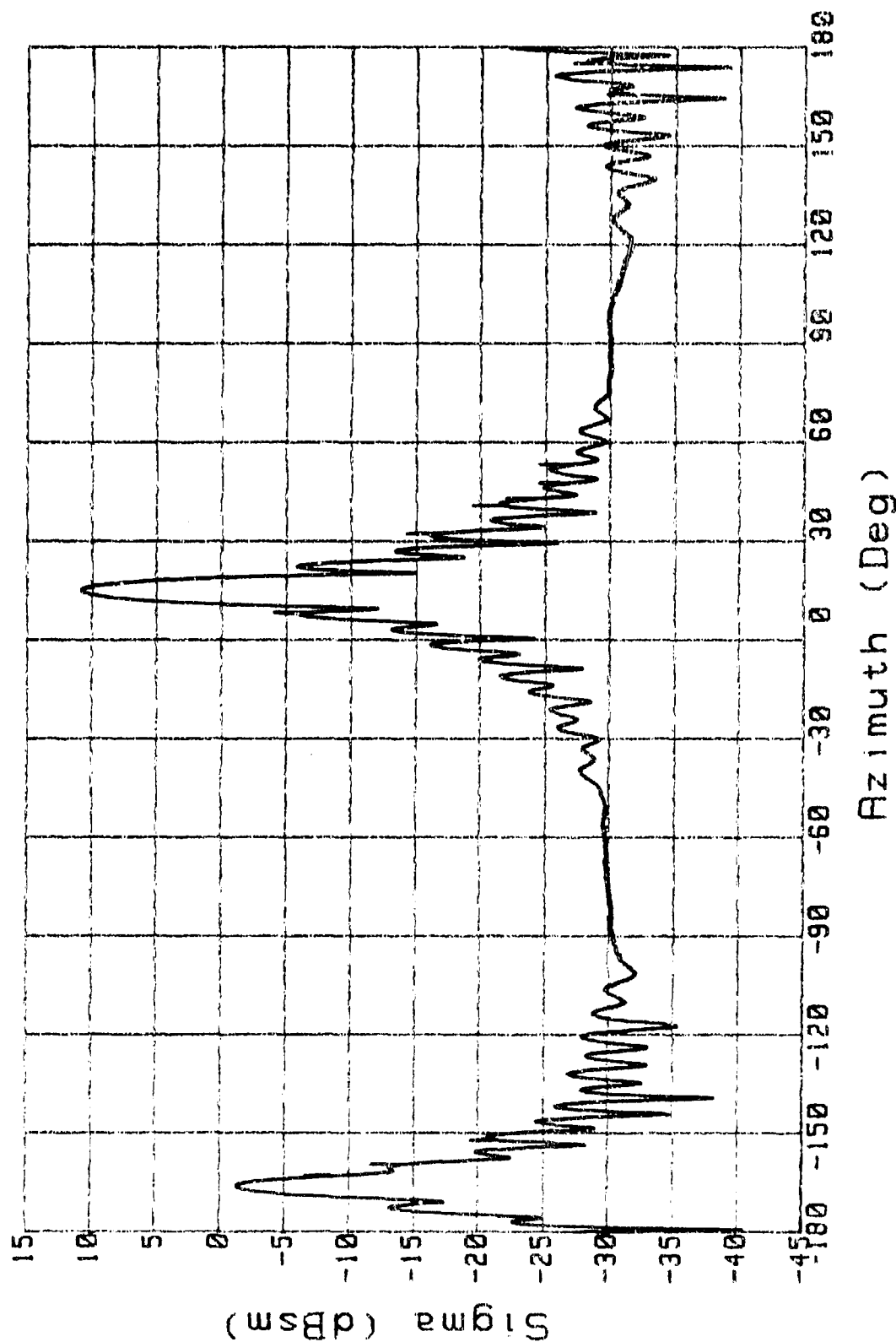
Figure 18A. RCS: Circ Flat Plate, V Pol, BSA=30, Range=9

61

Figure 18B. RCS: Circ Flat Plate, V Pol, BSA=0, Range=12

62

Figure 19A.   PCS: Circ Flat Plate, V Pol, BSA=30, Range=7

Figure 19B.   RCS: Circ Flat Plate, V Pol, BSA=0, Range=10
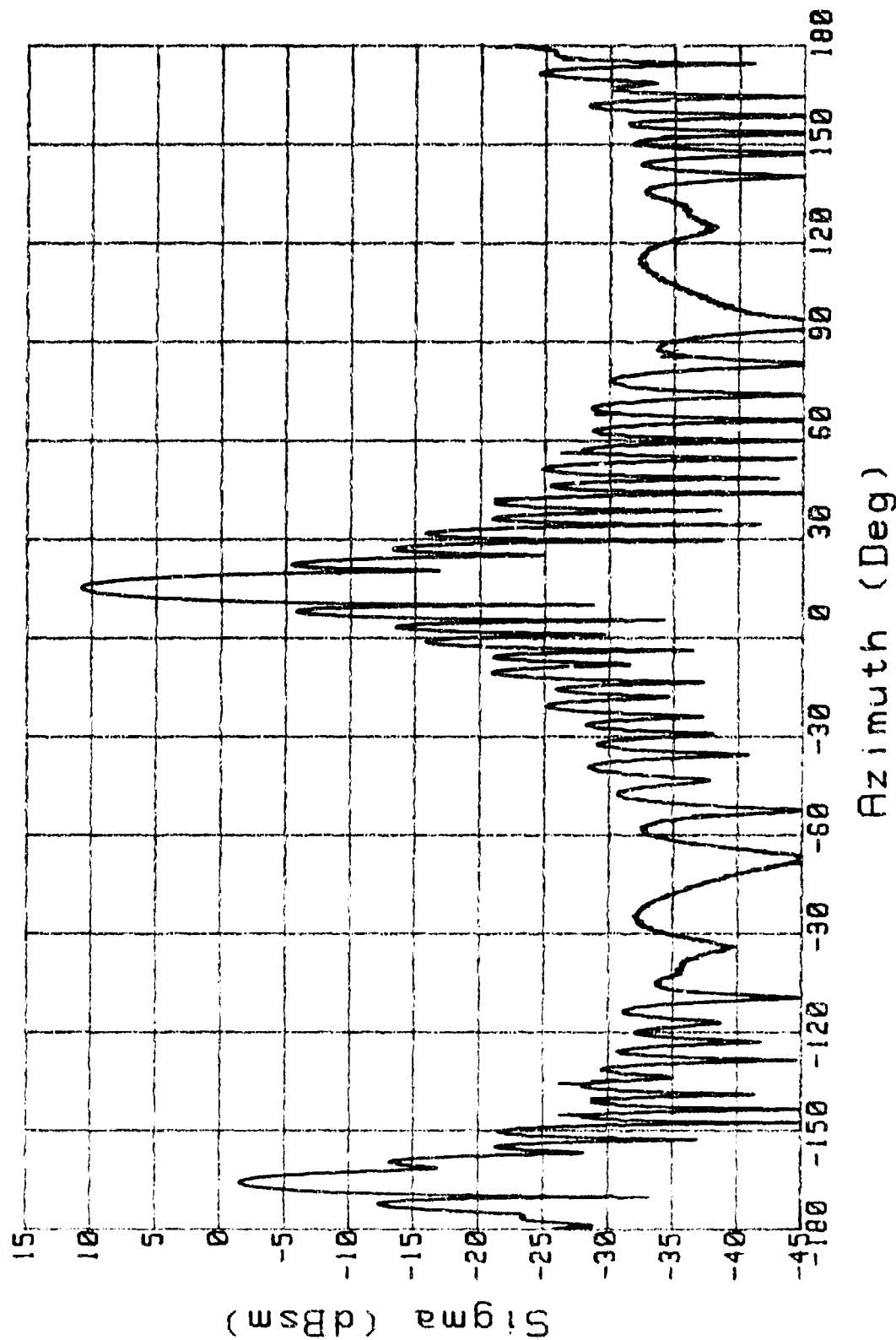
Figure 20A. RCS: Circ Flat Plate, H Pol, BSA=30, Range=15
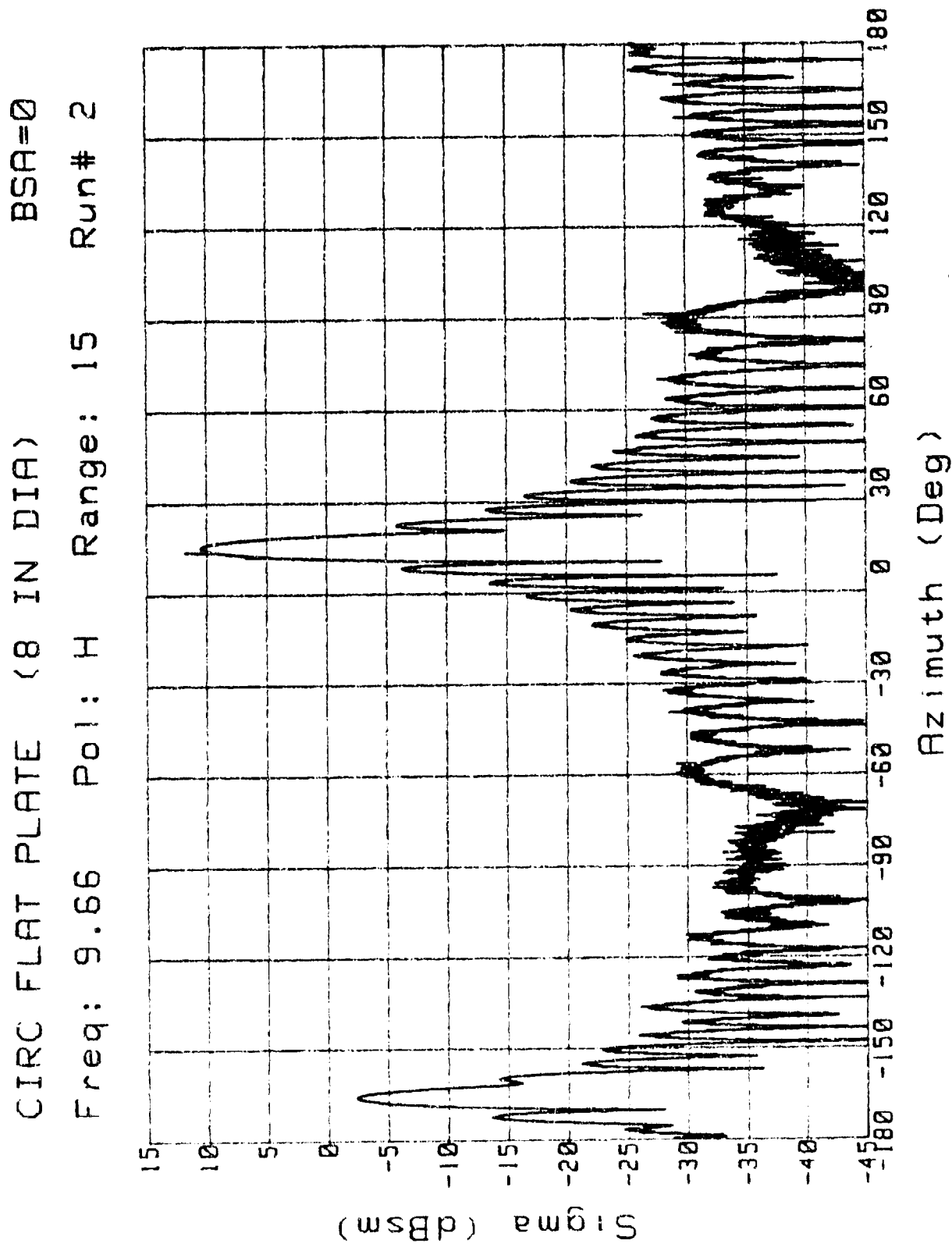
Figure 20B. RCS: Circ Flat Plate, H pol, BSA=0, Range=15
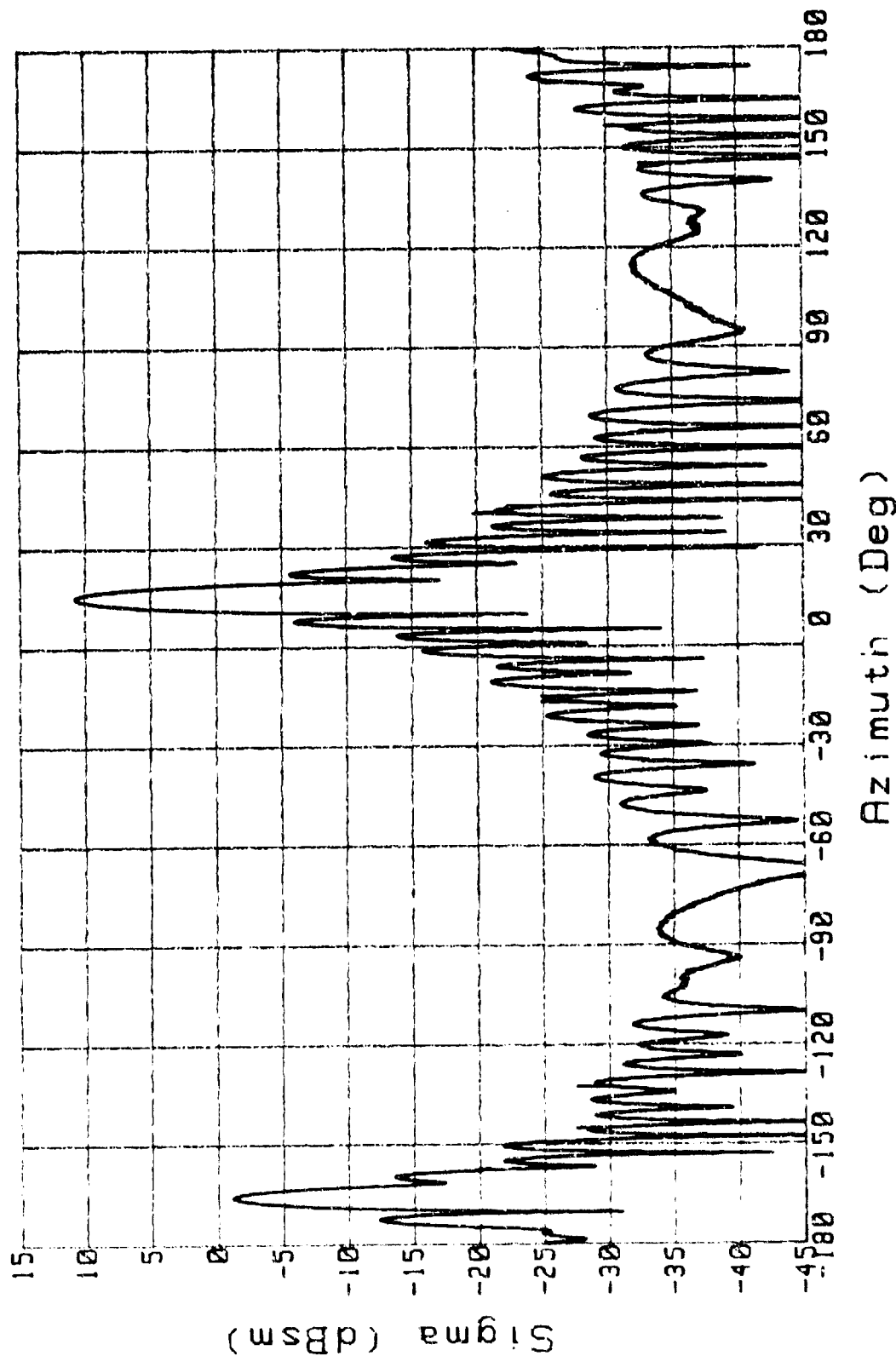
Figure 21A. RCS: Circ Flat Plate, H Pol, BSA=30, Range=13

Figure 21B. RCS: Circ Flat Plate, H Pol, BSA=0, Range=13

Figure 22A. RCS: Circ Flat Plate, H Pol, BSA=30, Range=10.8

Figure 22B. RCS: Circ Flat Plate, H Pol, BSA=0, Range=10.8

Figure 22C.   RCS: Circ Flat Plate, H Pol, BSA=30, Range=7.75

Figure 23A. RCS: Circ Flat Plate, H Pol, BSA=30, Range=9

Figure 23B. RCS: Circ Flat Plate, H Pol, BSA=0, Range=12

73

Figure 24A. RCS: Circ Flat Plate, H Pol, BSA=30, Range=7

74

Figure 24B. RCS: Circ Flat Plate, H Pol, BSA=0, Range=10

Figure 25A. RCS: Ogive, V Pol, BSA=30, Range=15

76

Figure 25B. RCS: Ogive, V Pol, BSA=0, Range=15

77

OGIVE

BSA=30

Freq: 10   Pol: V   Range: 13   Run# 2
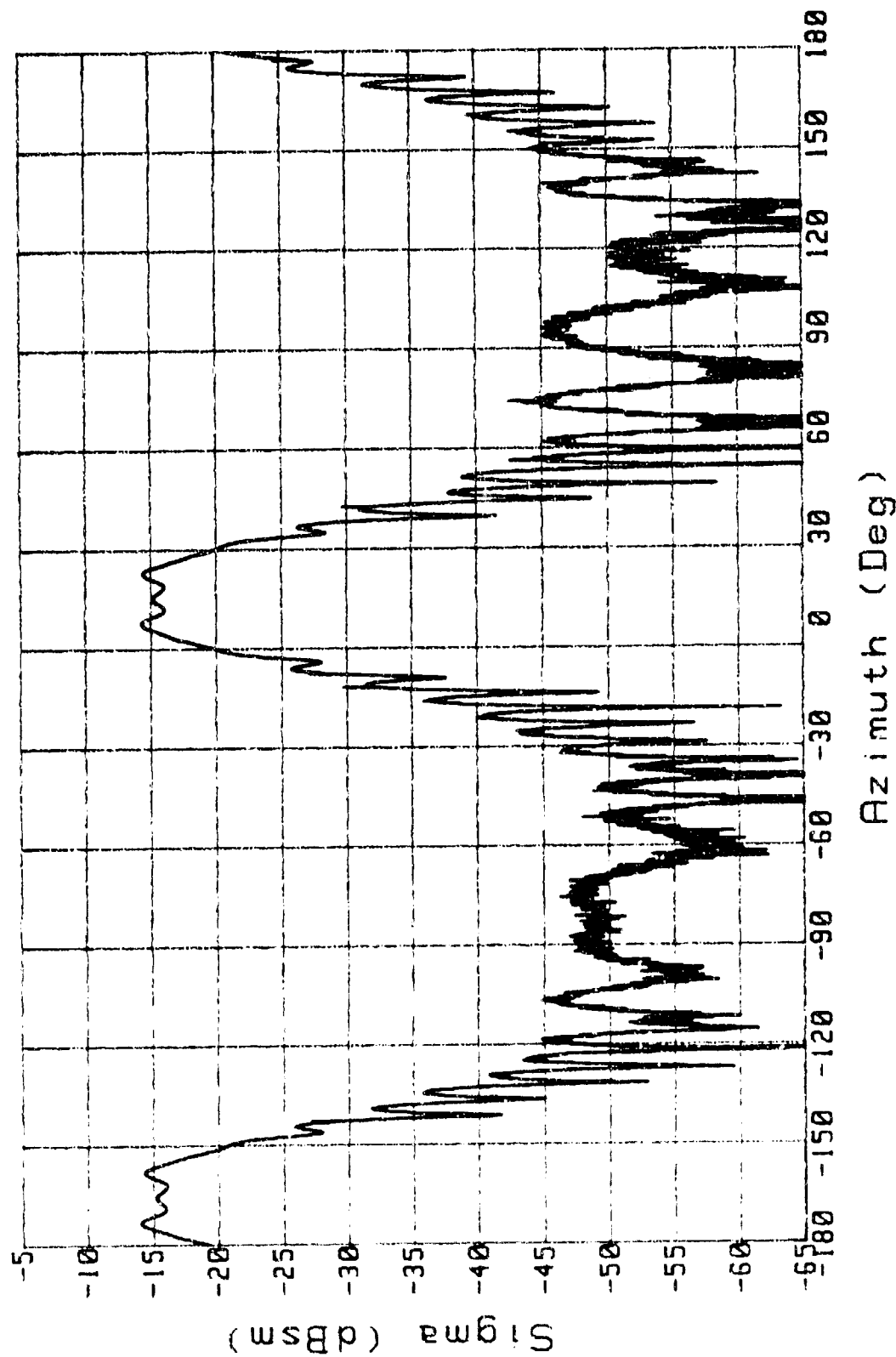
Figure 26A.   RCS: Ogive, V Pol, BSA=30, Range=13

78

OGIVE BSA=0

Freq: 9.66   Pol: V   Range: 13   Run# 3
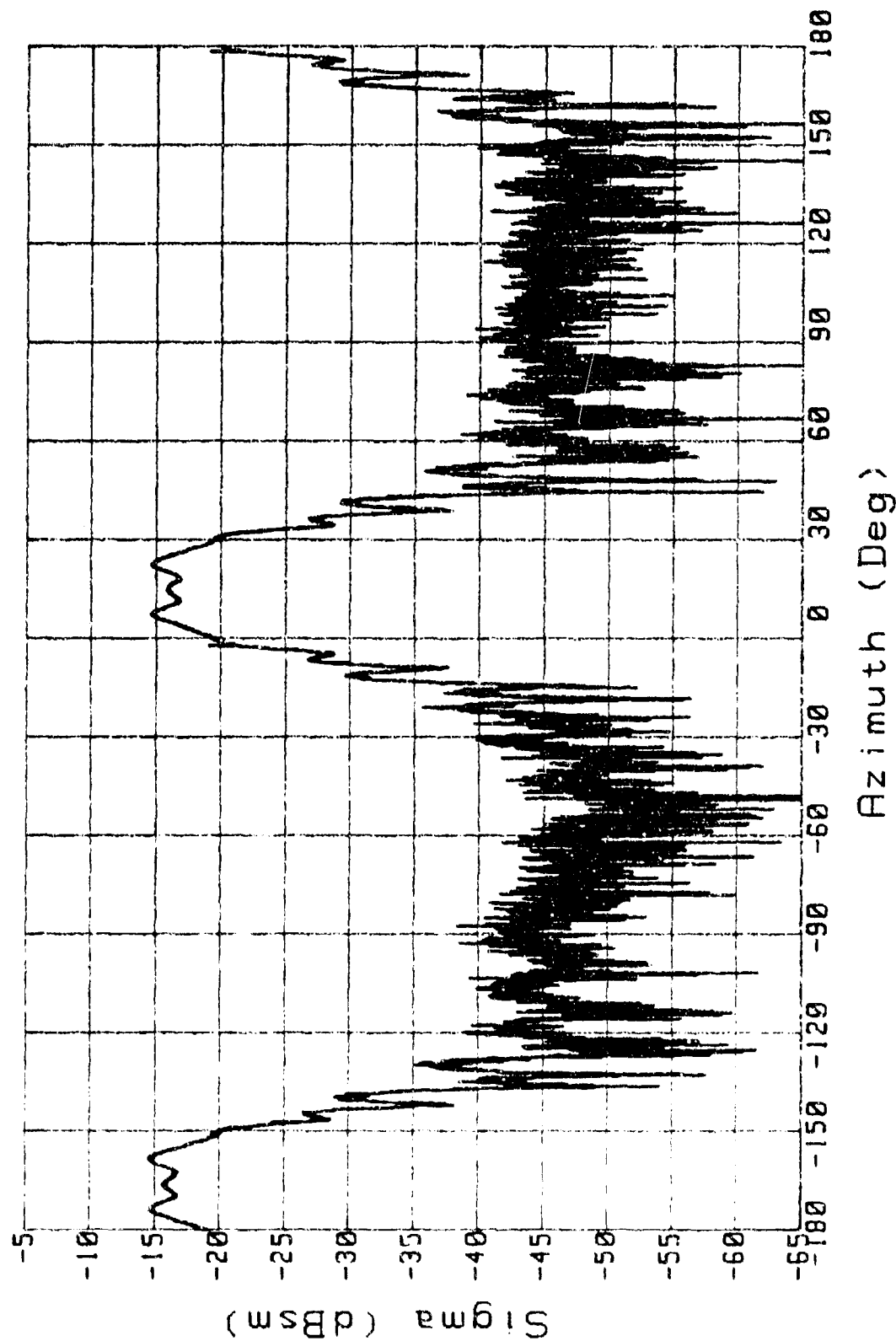
Figure 26B.   RCS: Ogive, V Pol, BSA=0, Range=13

79
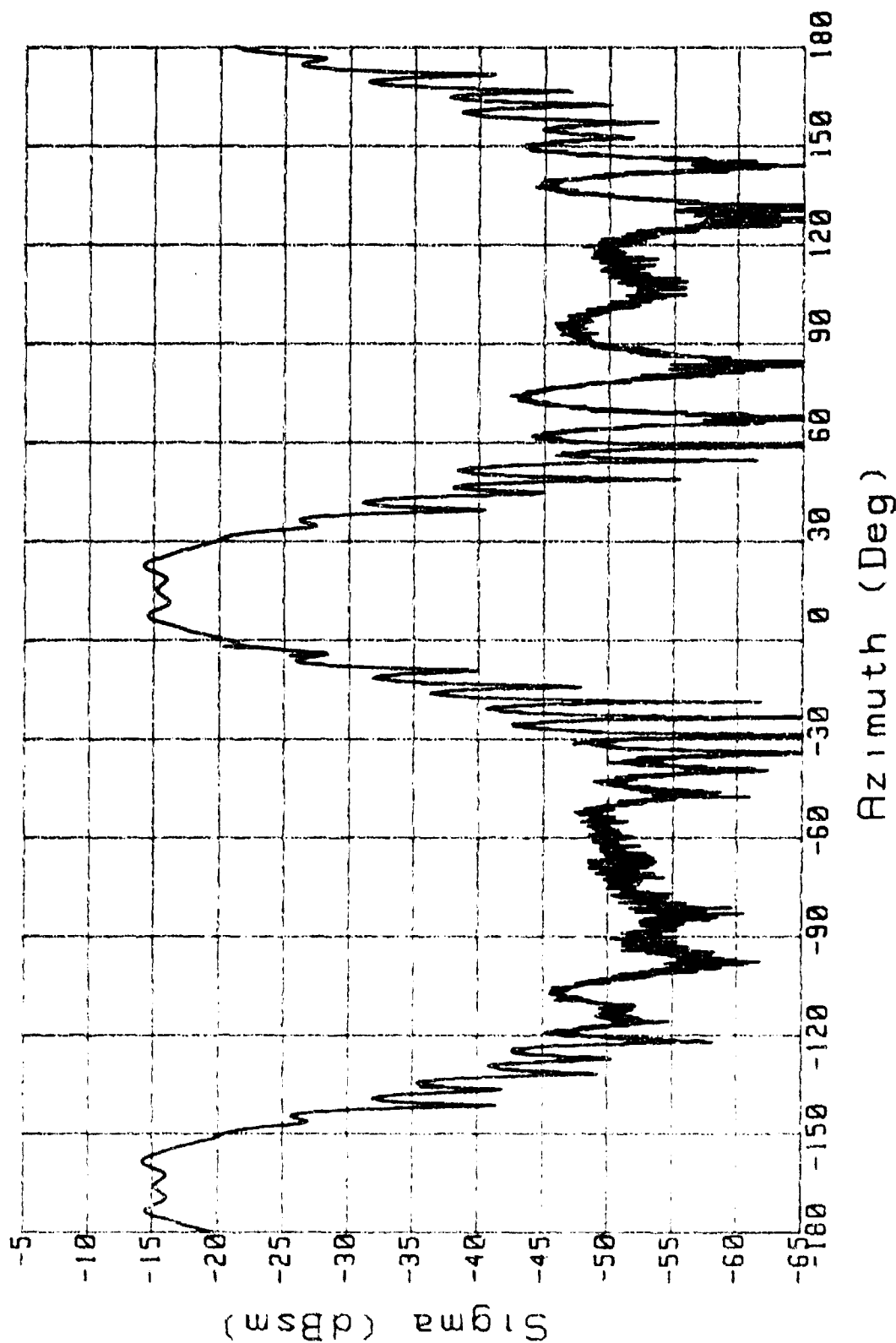
Figure 27A. RCS: Ogive, V Pol, BSA=30, Range=11
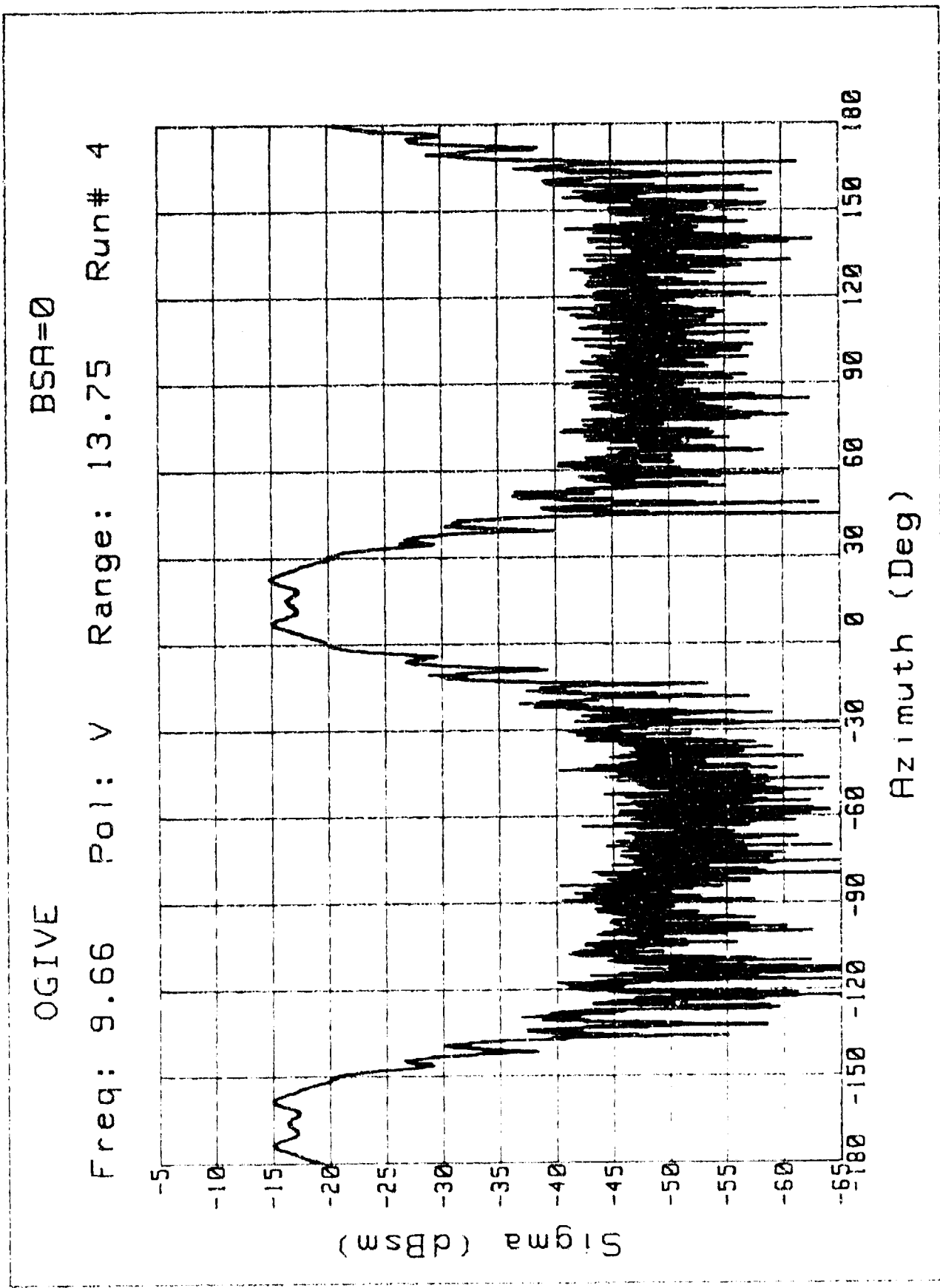
Figure 27B. RCS: Ogive, V Pol, BSA=0, Range=13.75

31
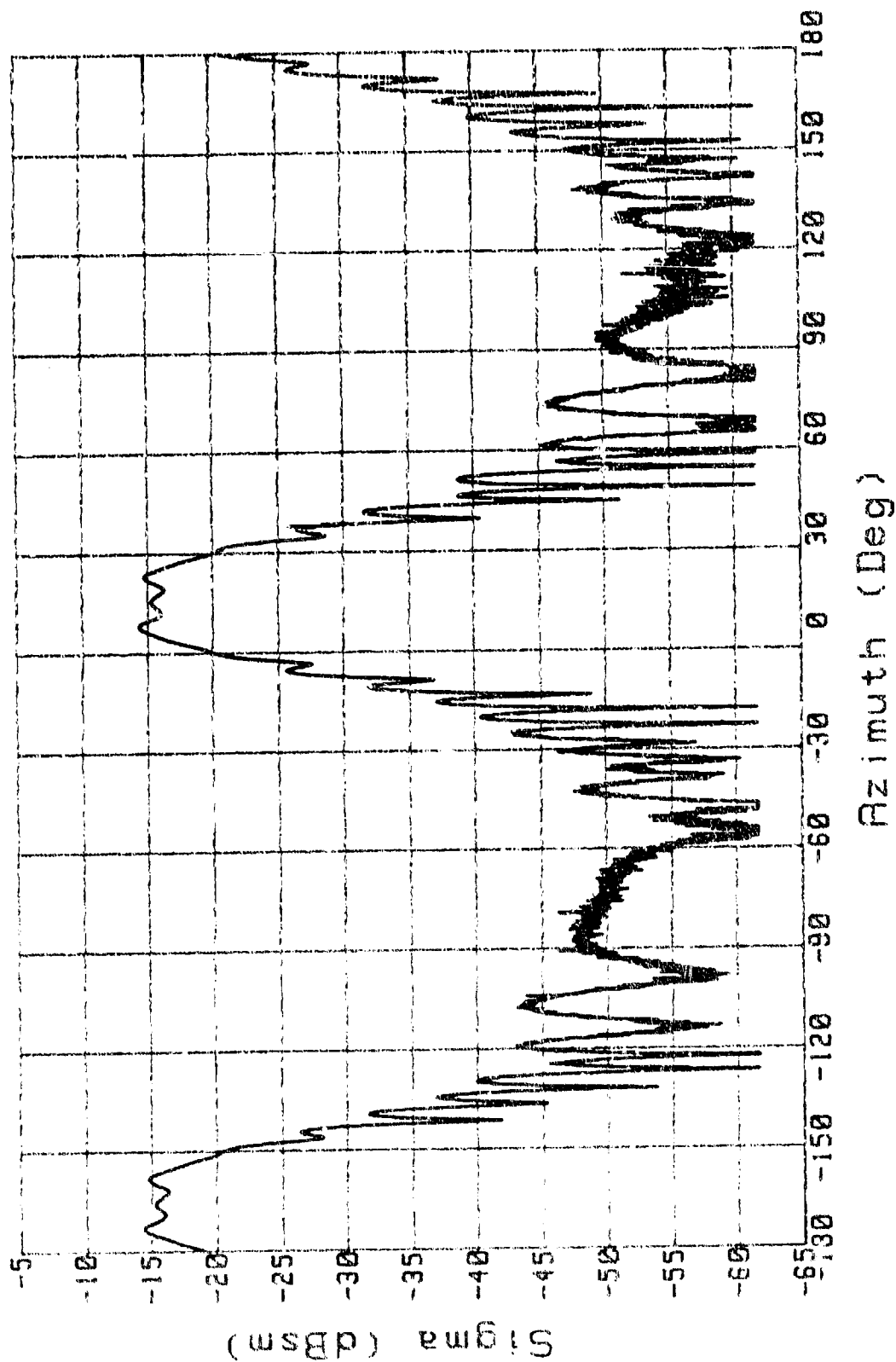
Figure 28A. RCS: Ogive, v Pol, BSA=30, Range=9
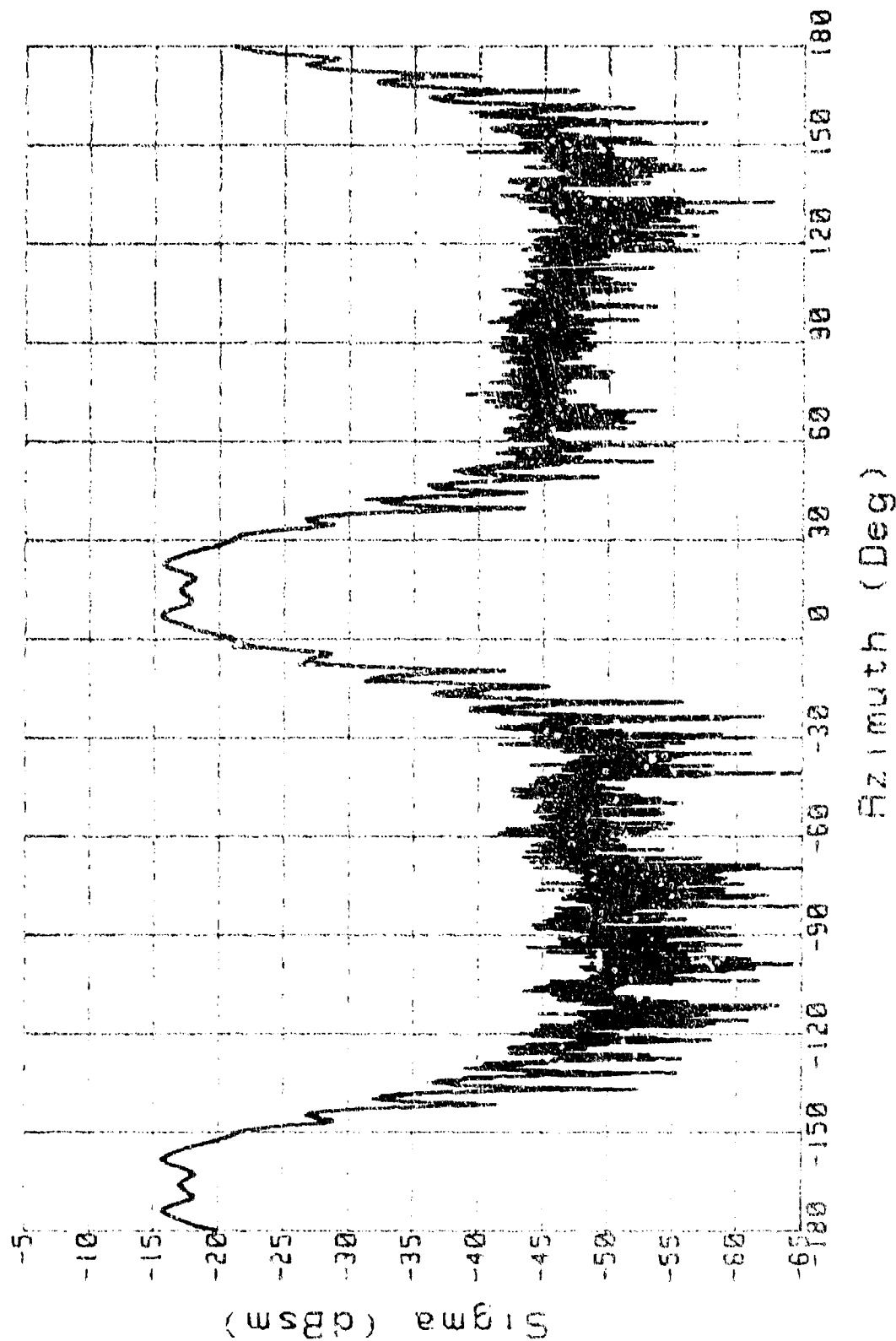
Figure 28B. RCS: Ogive, V Pol, BSA=0, Range=12
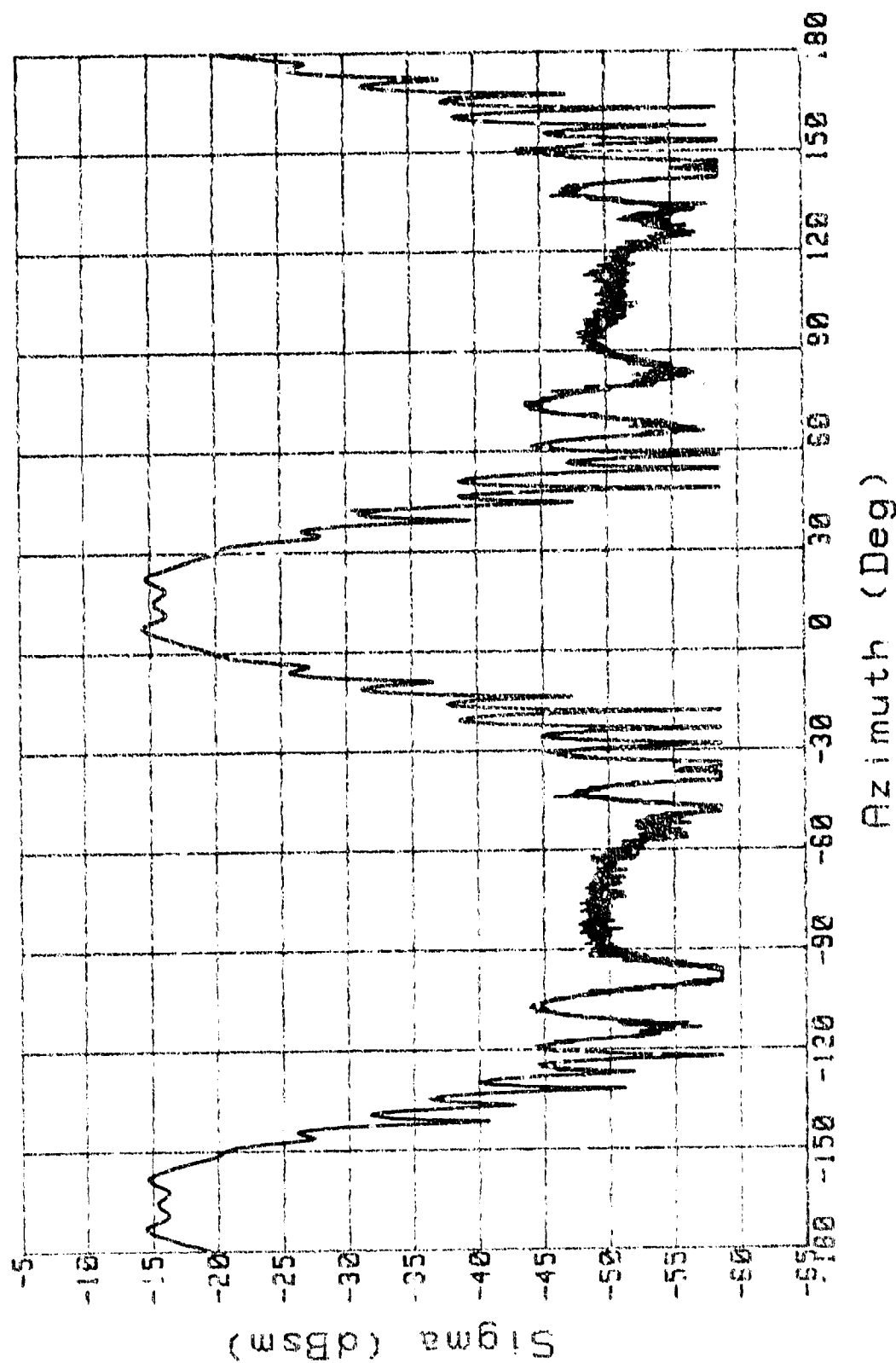
Figure 29A.   RCS: Ogive, V Pol, BSA=30, Range=7
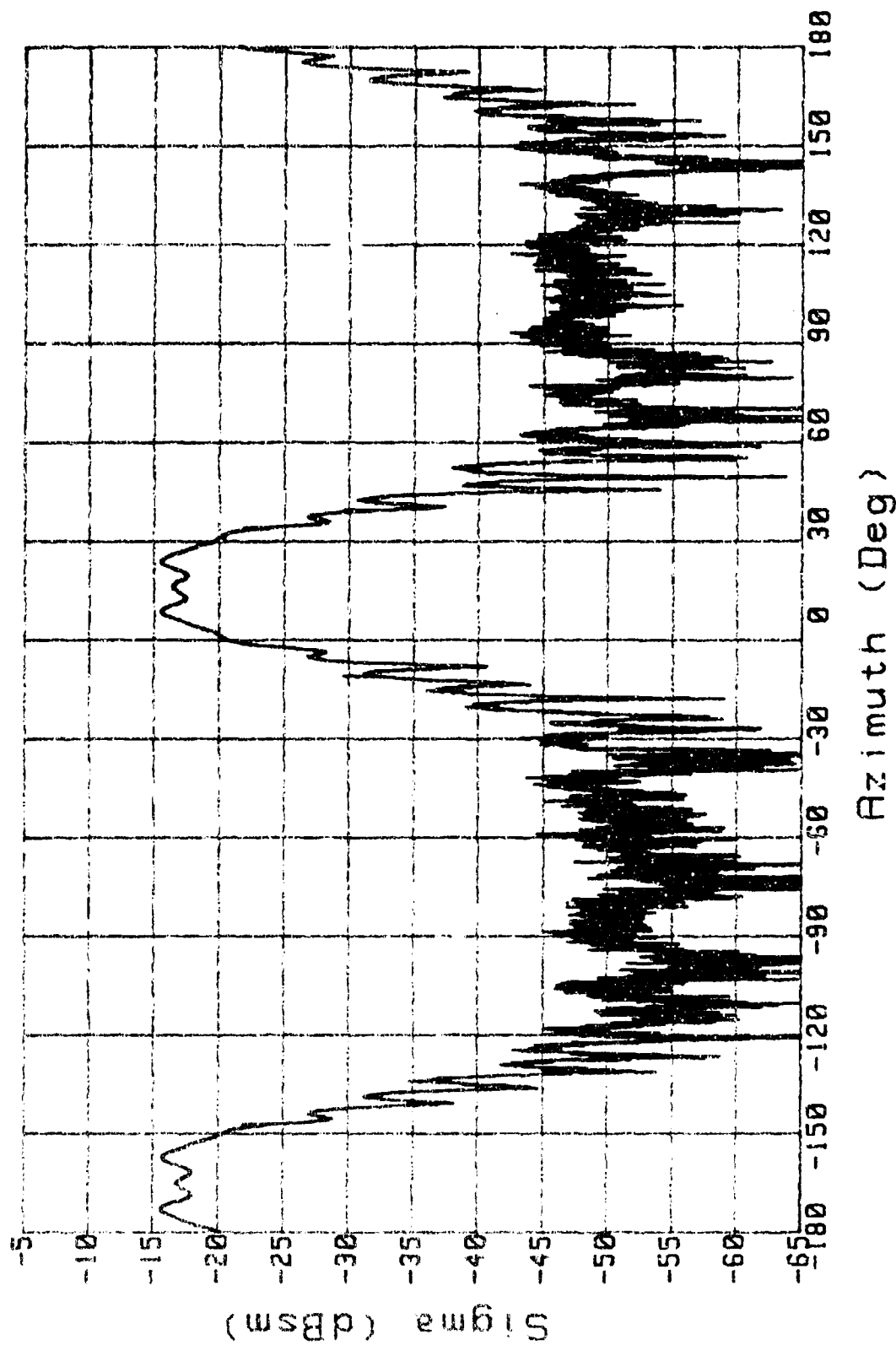
Figure 29B. RCS: Ogive, V Pol, BSA=0, Range=10
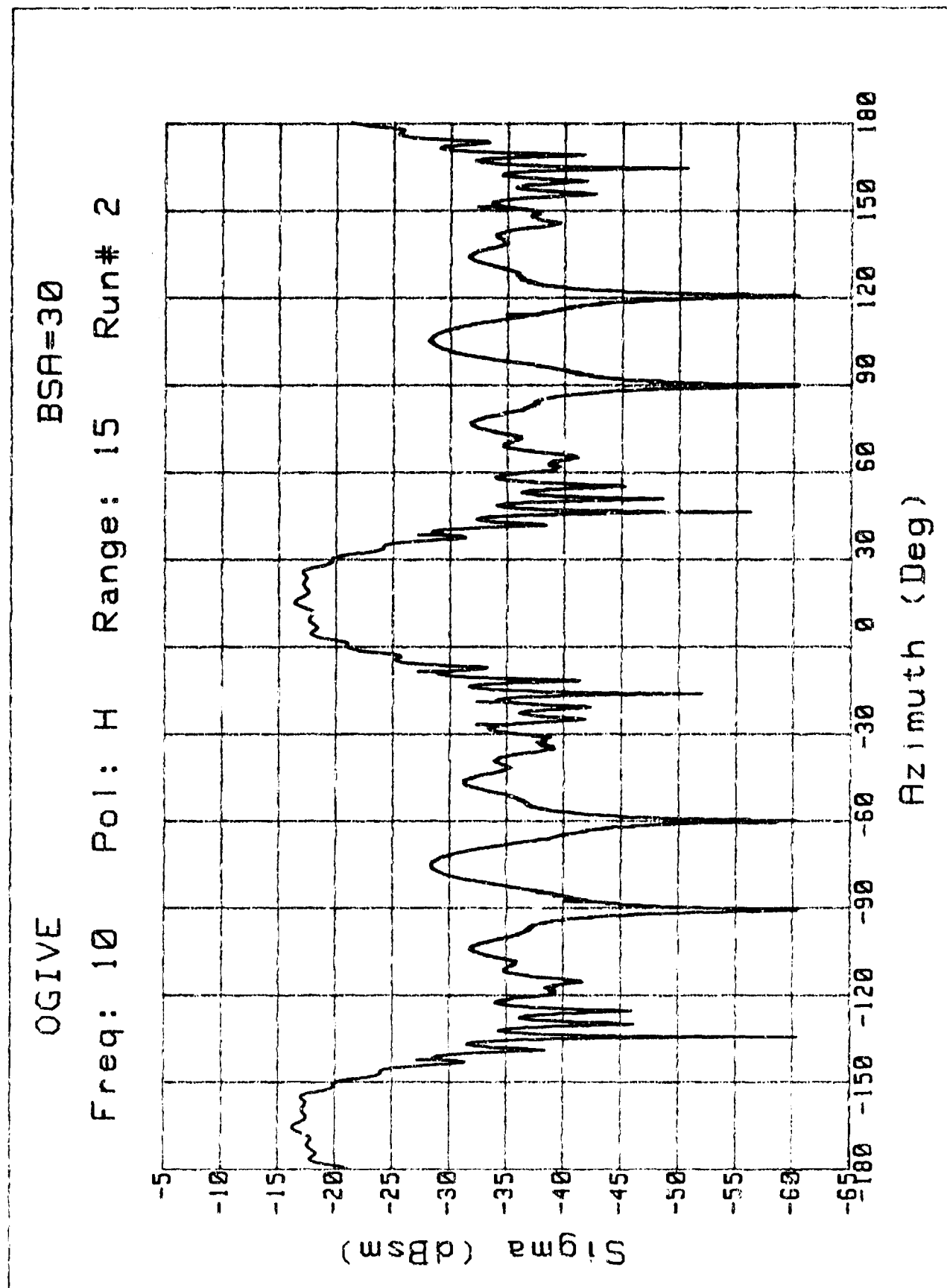
Figure 30A. RCS: Ogive, H Pol, BSA=30, Range=15
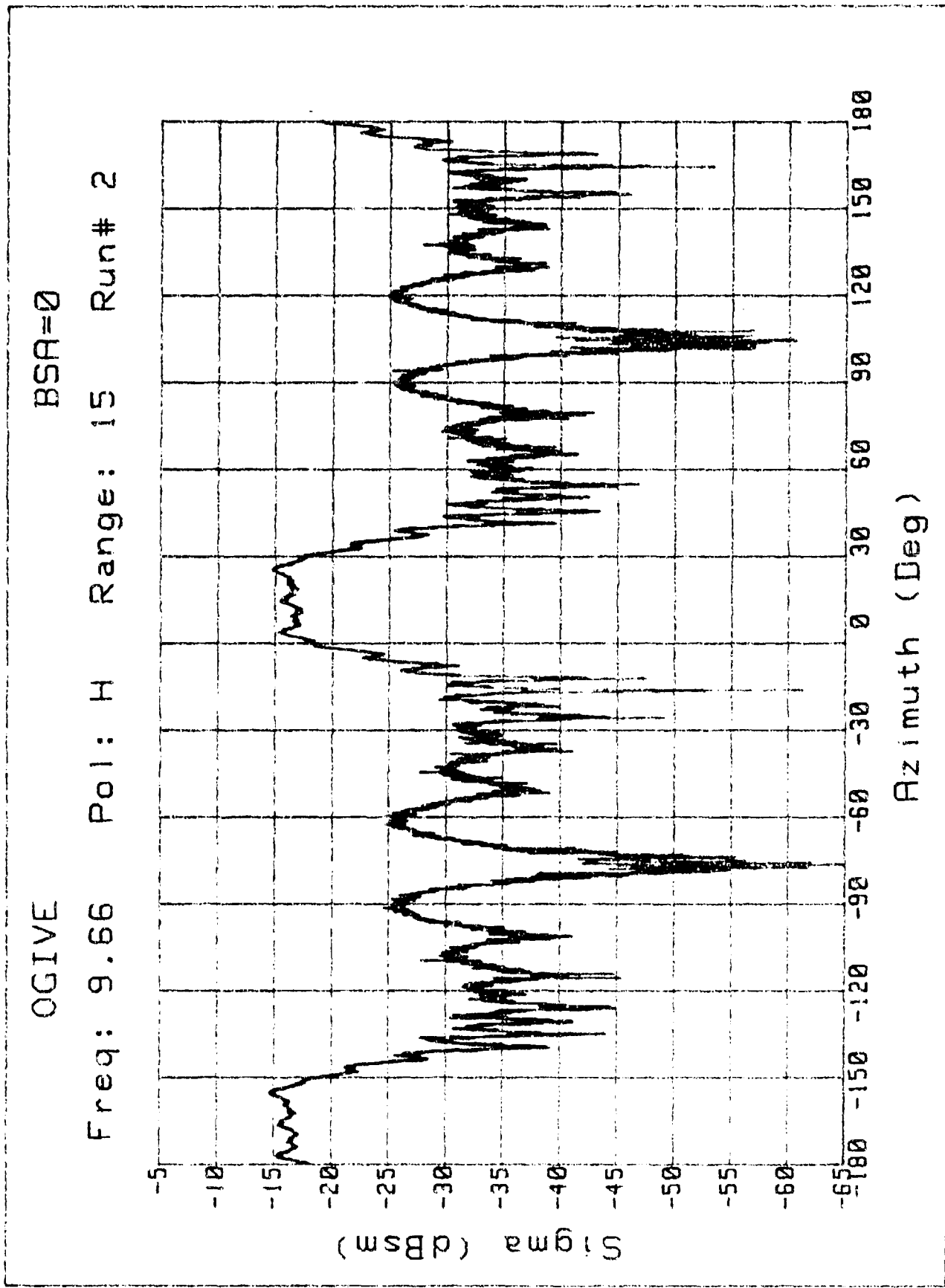
Figure 30B. RCS: Ogive, H Pol, BSA=0, Range=15
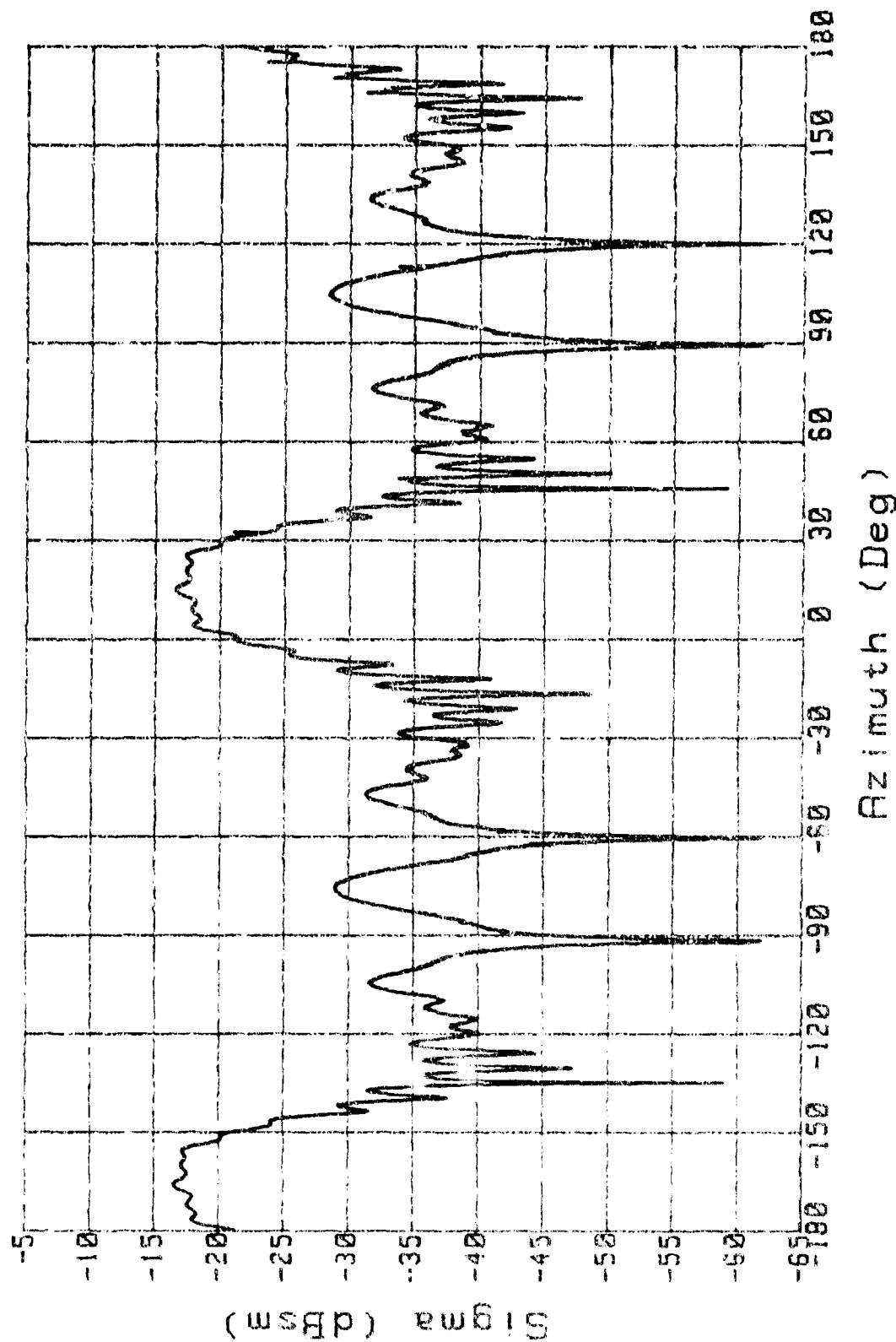
Figure 31A. RCS: Ogive, H Pol, BSA=30, Range=13
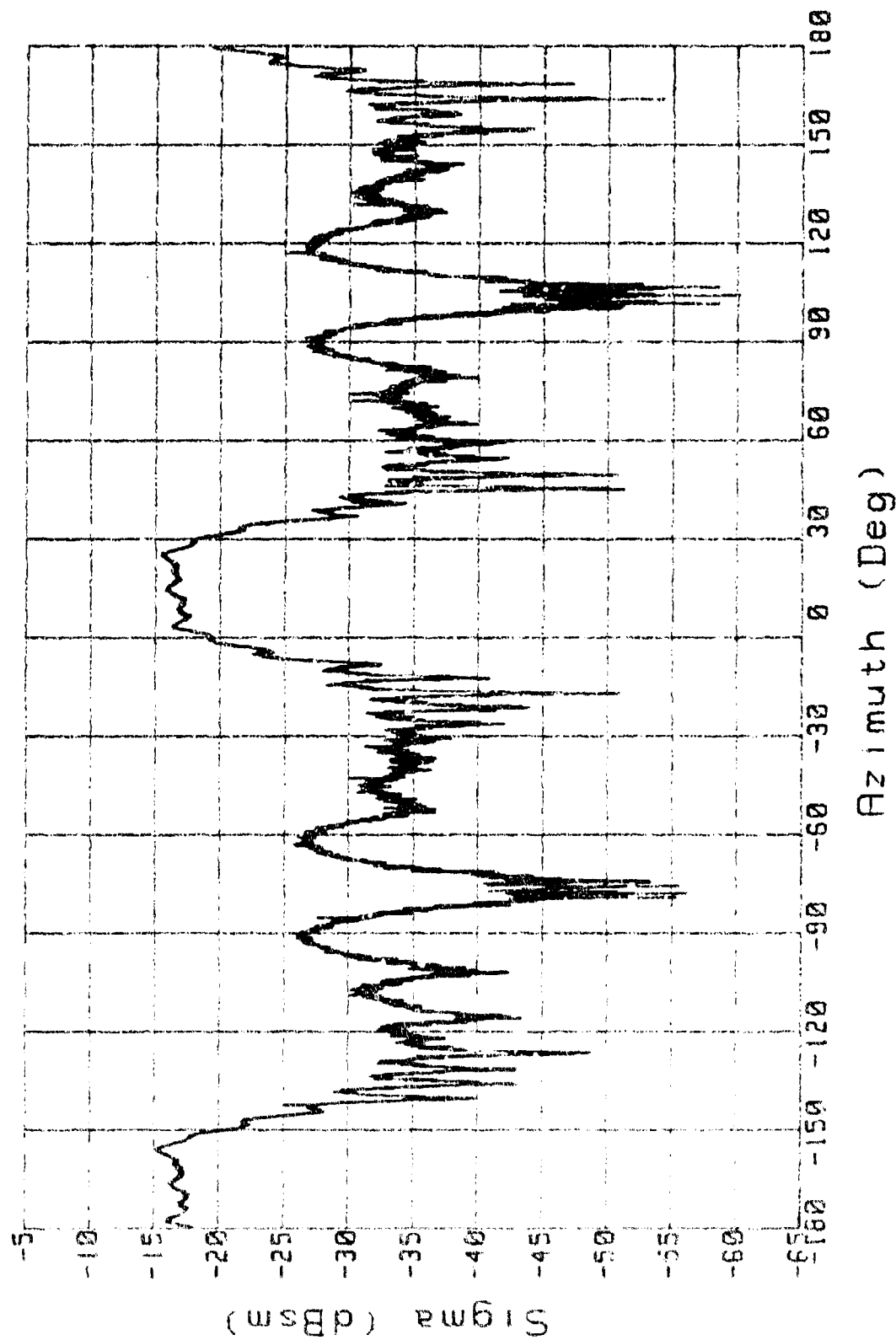
Figure 31B. RCS: Ogive, H Pol, BSA=0, Range=13
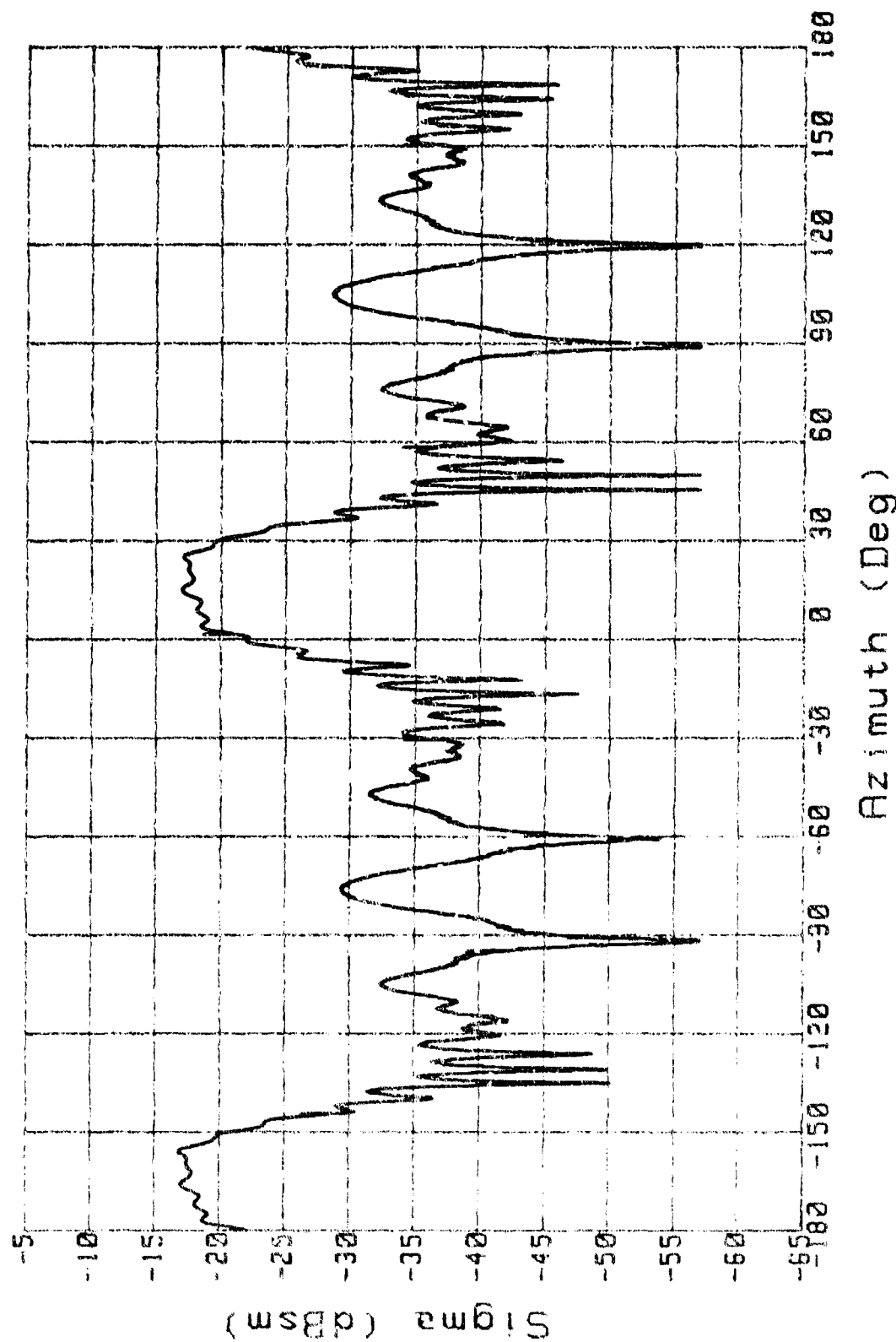
Figure 32A. RCS: Ogive, H Pol, BSA=30, Range=11
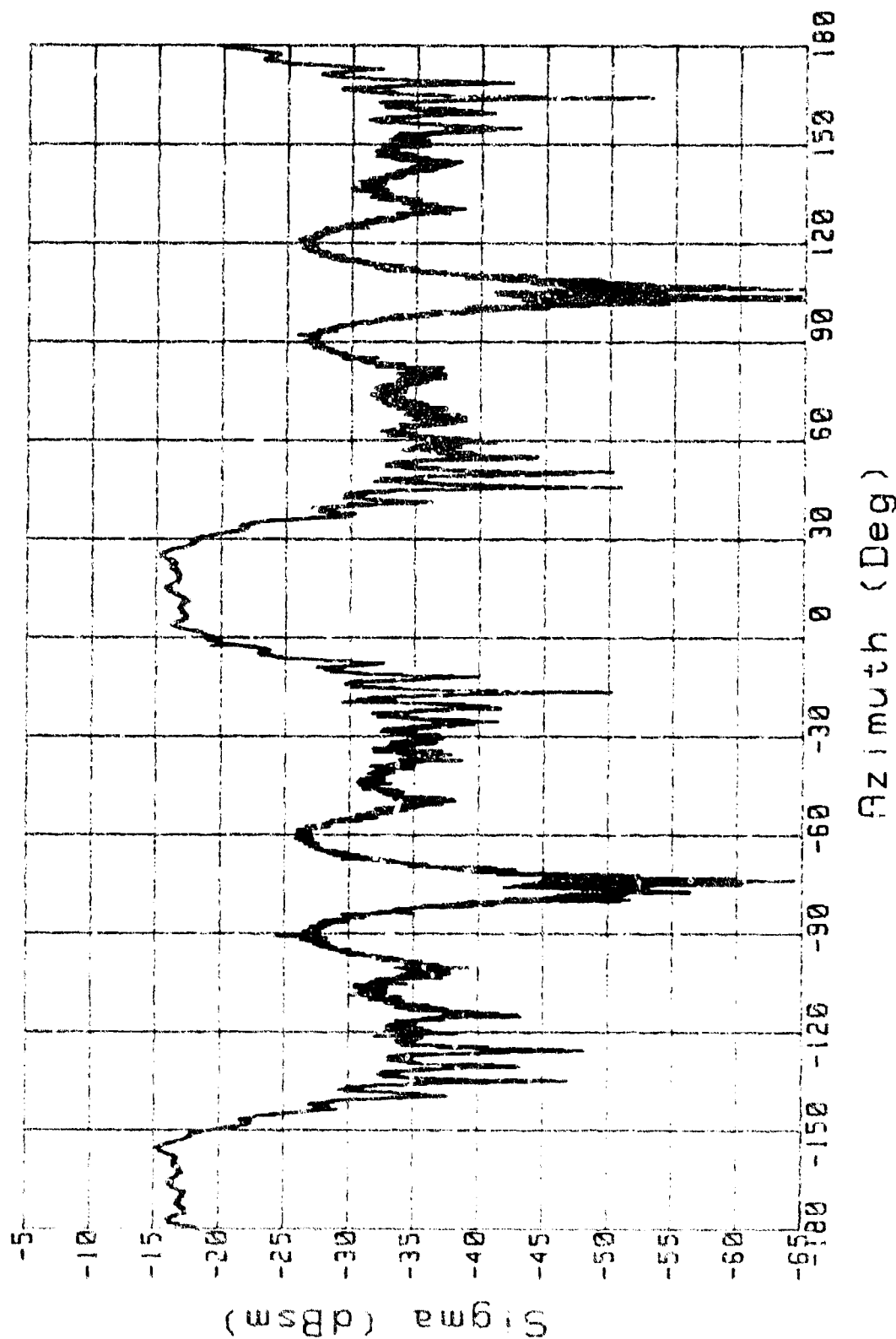
Figure 32B. RCS: Ogive. H Pol, BSA=0, Range=13.75

Figure 33A. RCS: Ogive, H Pol, BSA=30, Range=9
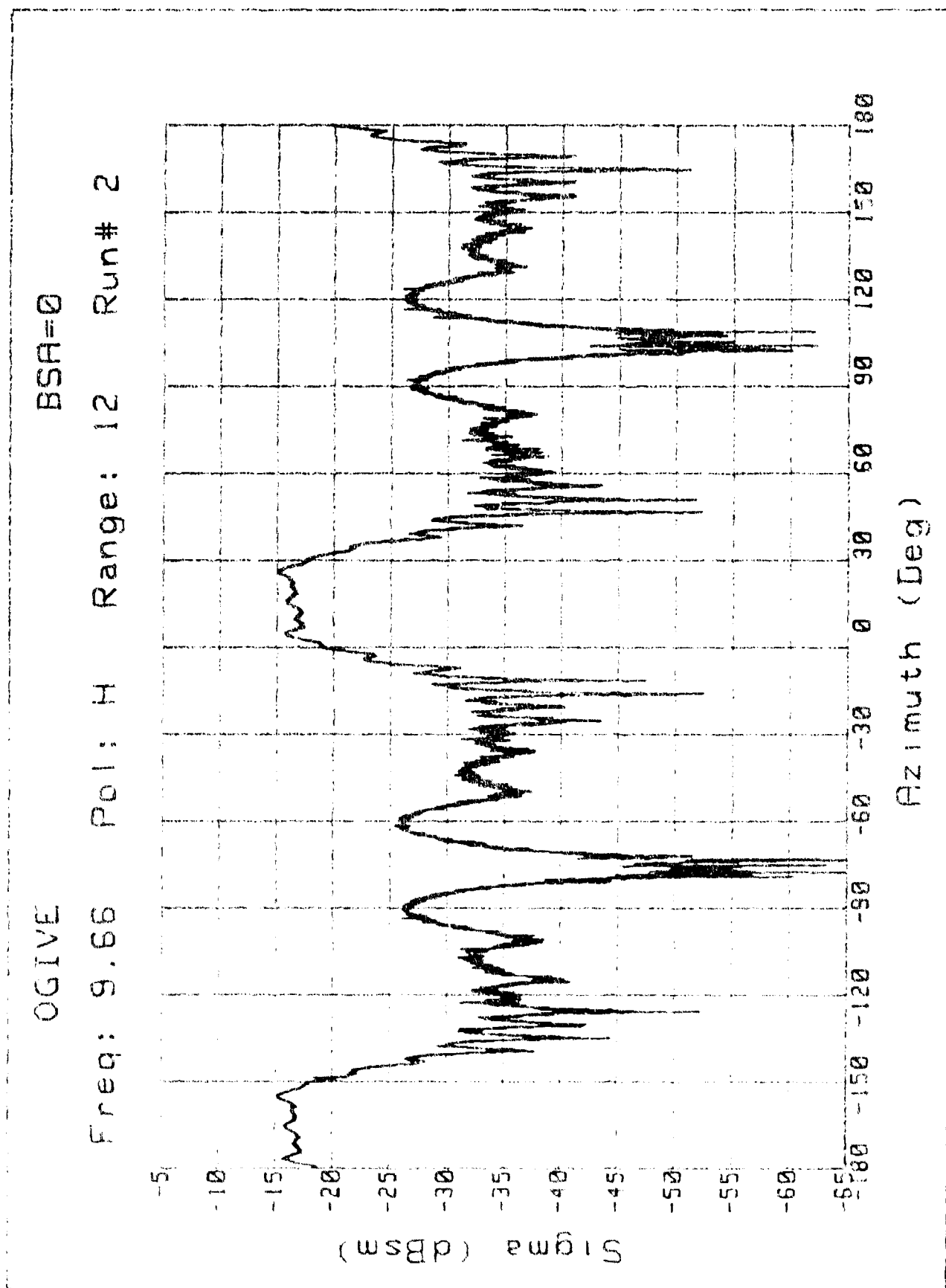
Figure 33B. RCS: Ogive, H Pol, BSA=0, Range=12

Figure 34A. RCS: Ogive, H Pol, BSA=30, Range=7.75
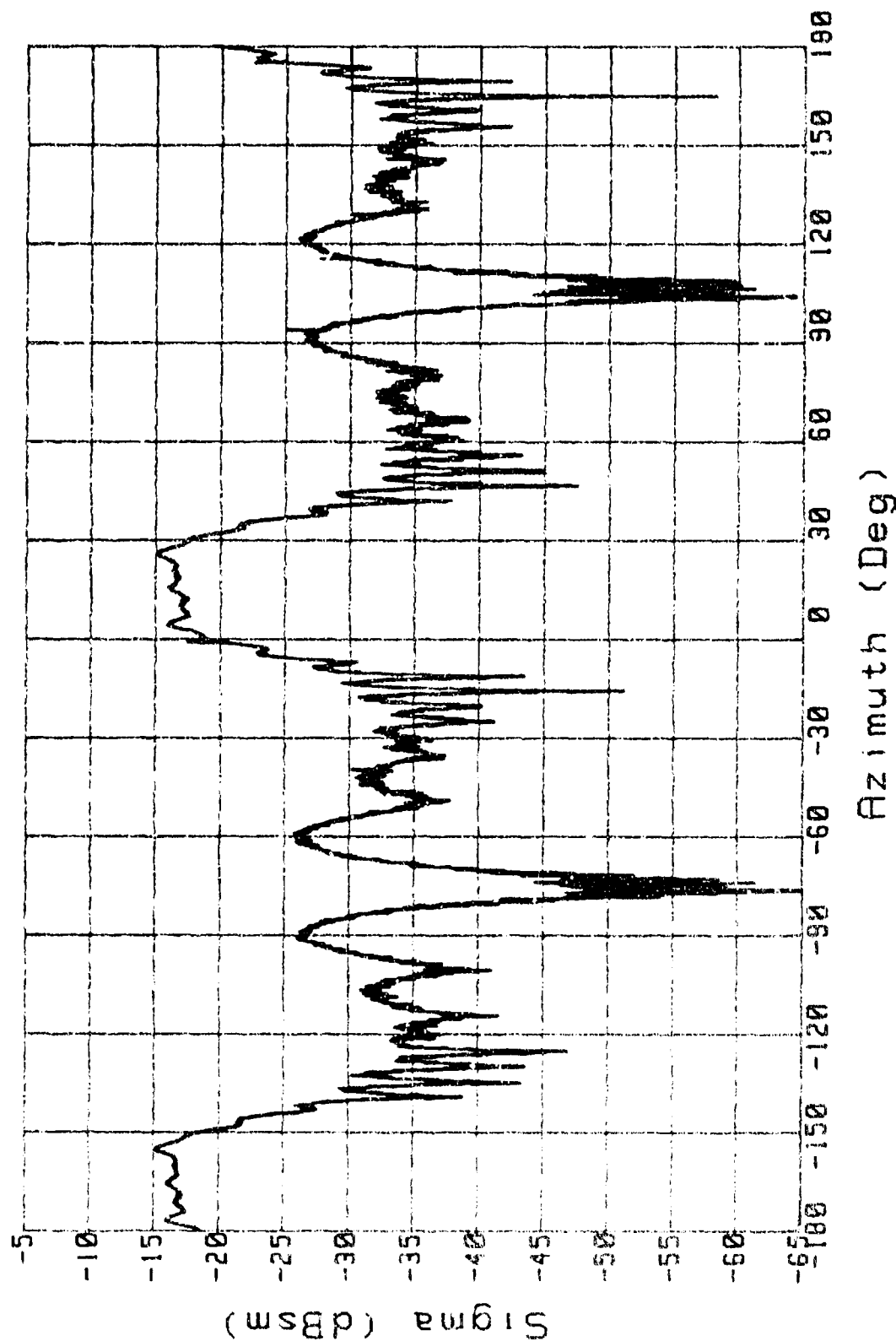
Figure 34B. RCS: Ogive, H Pol, BSA=0, Range=10.8

OGIVE   BSA=30

Freq: 10   Pol: H   Range: 7   Run# 2
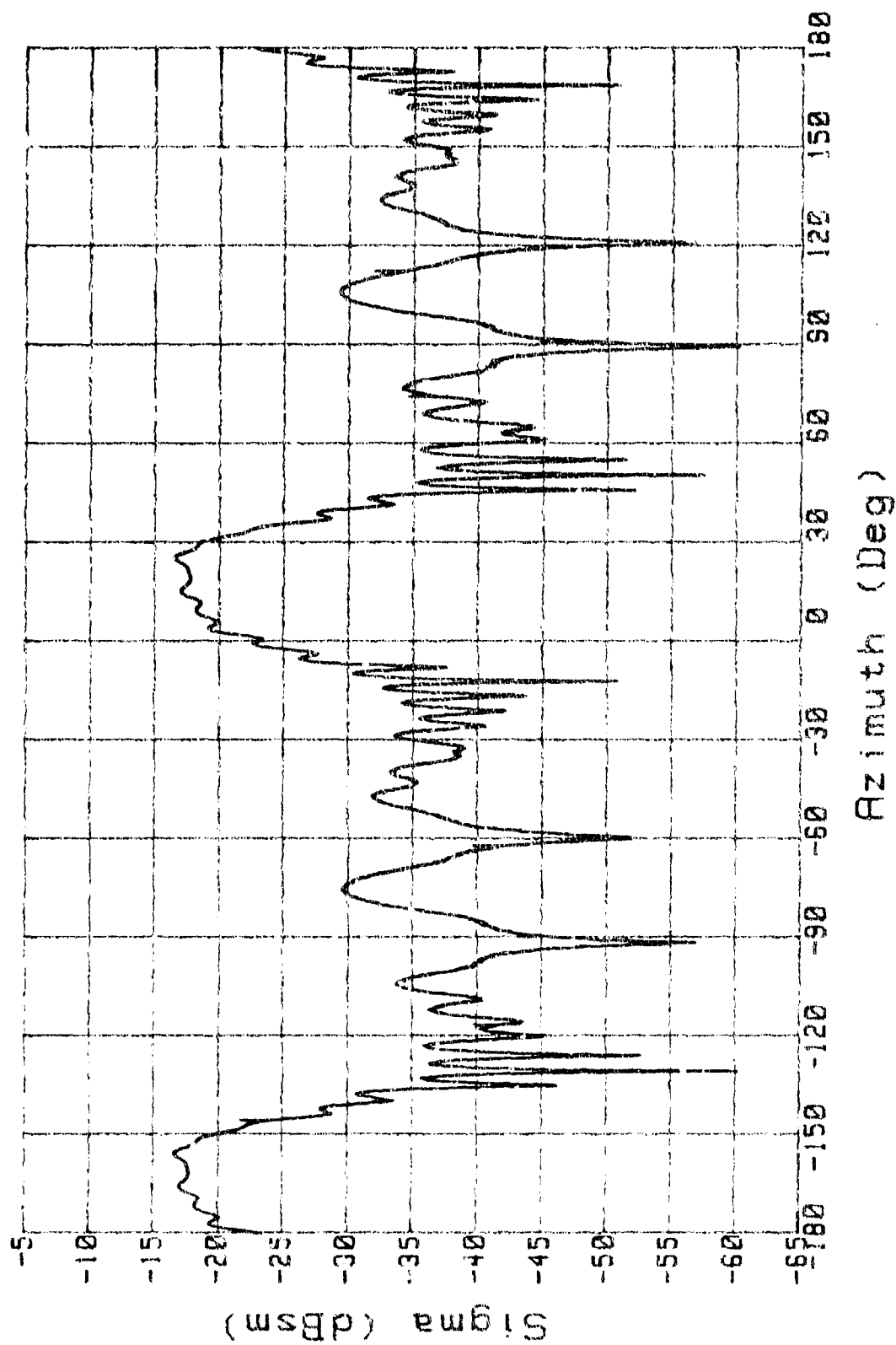
Figure 35A. RCS: Ogive, H Pol, BSA=30, Range=7
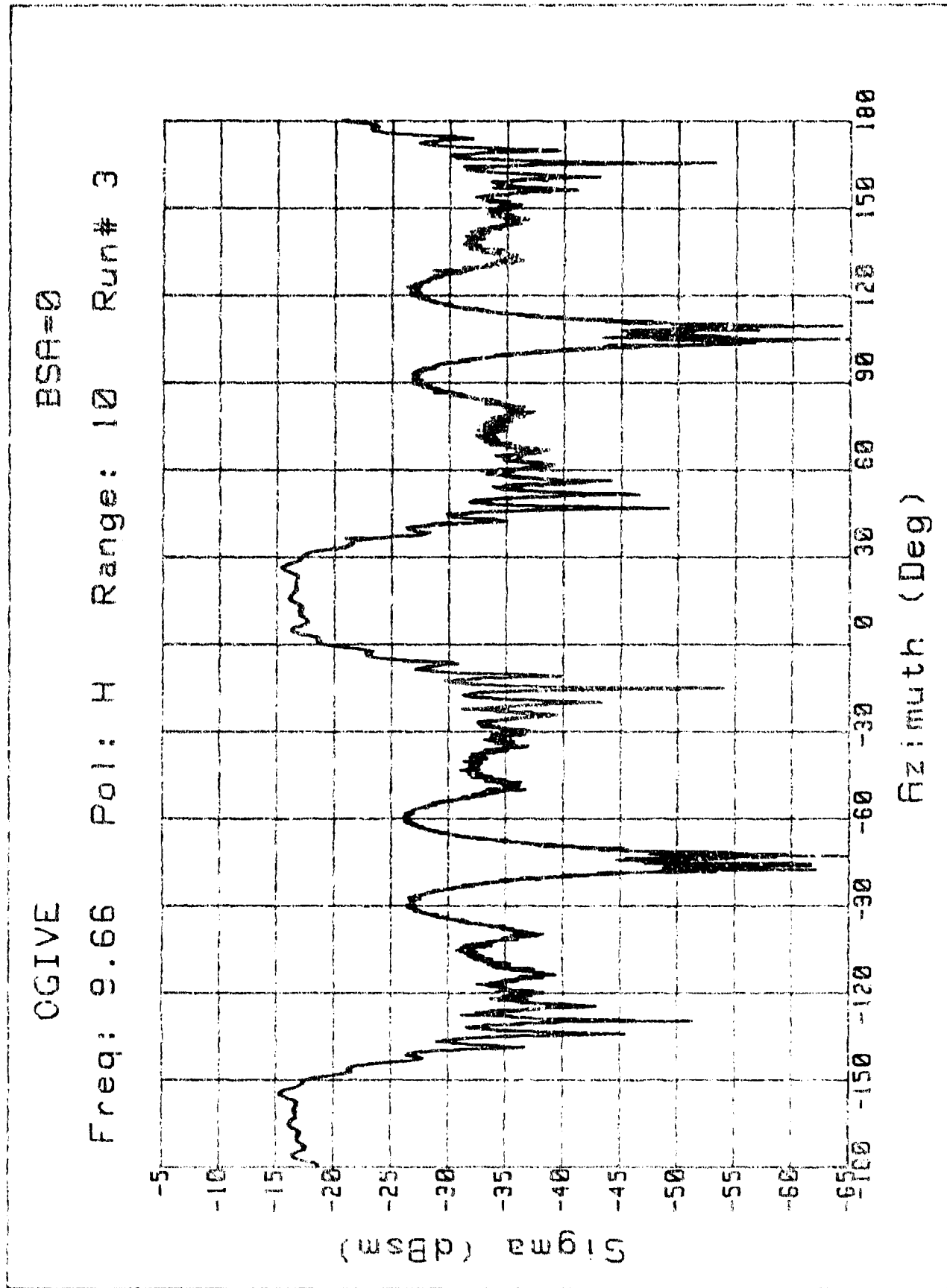
Figure 35B. RCS: Ogive, H Pol, BSA=0, Range=10
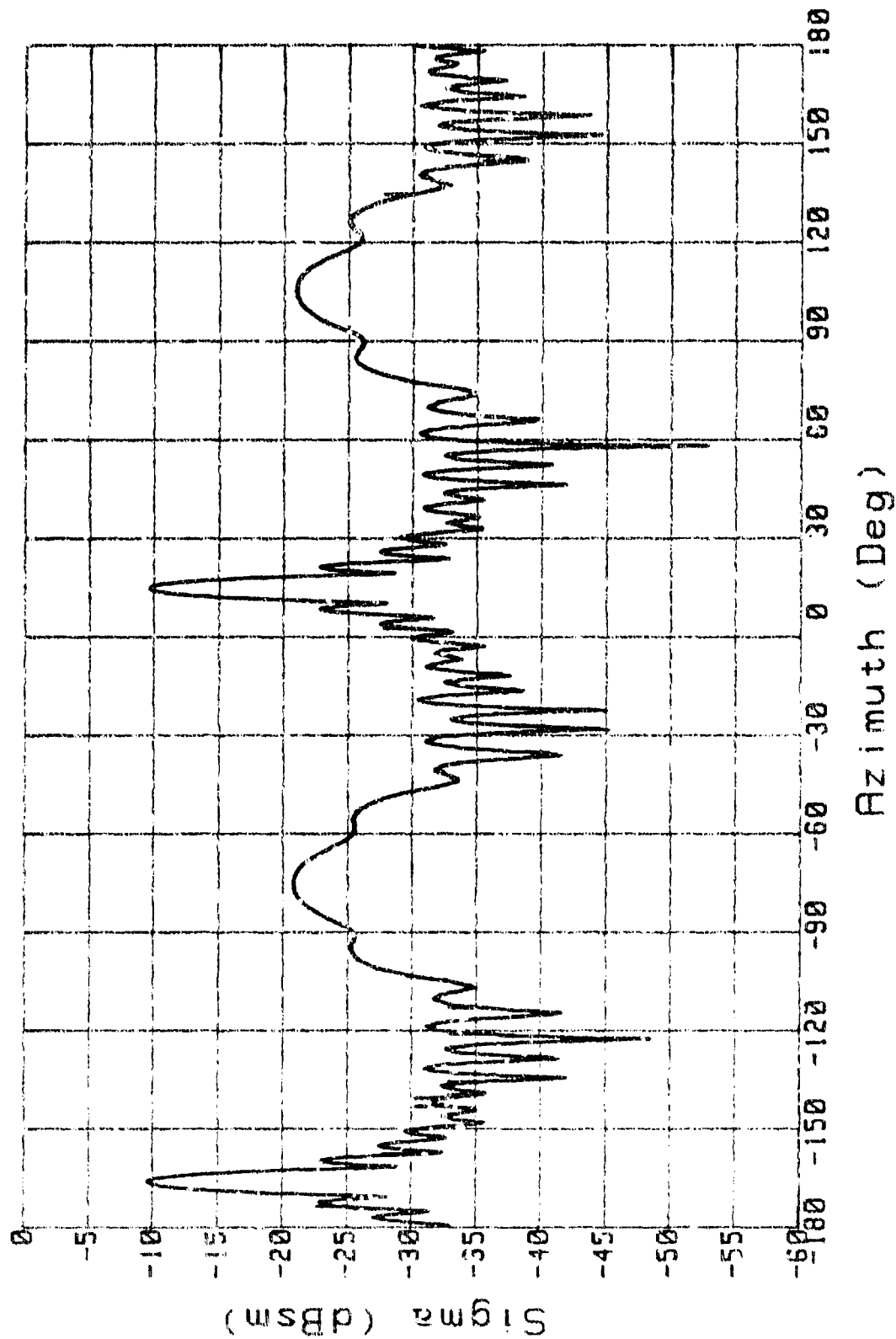
Figure 36. RCS: Cylinder (8 in), V Pol, BSA=30, Range=15
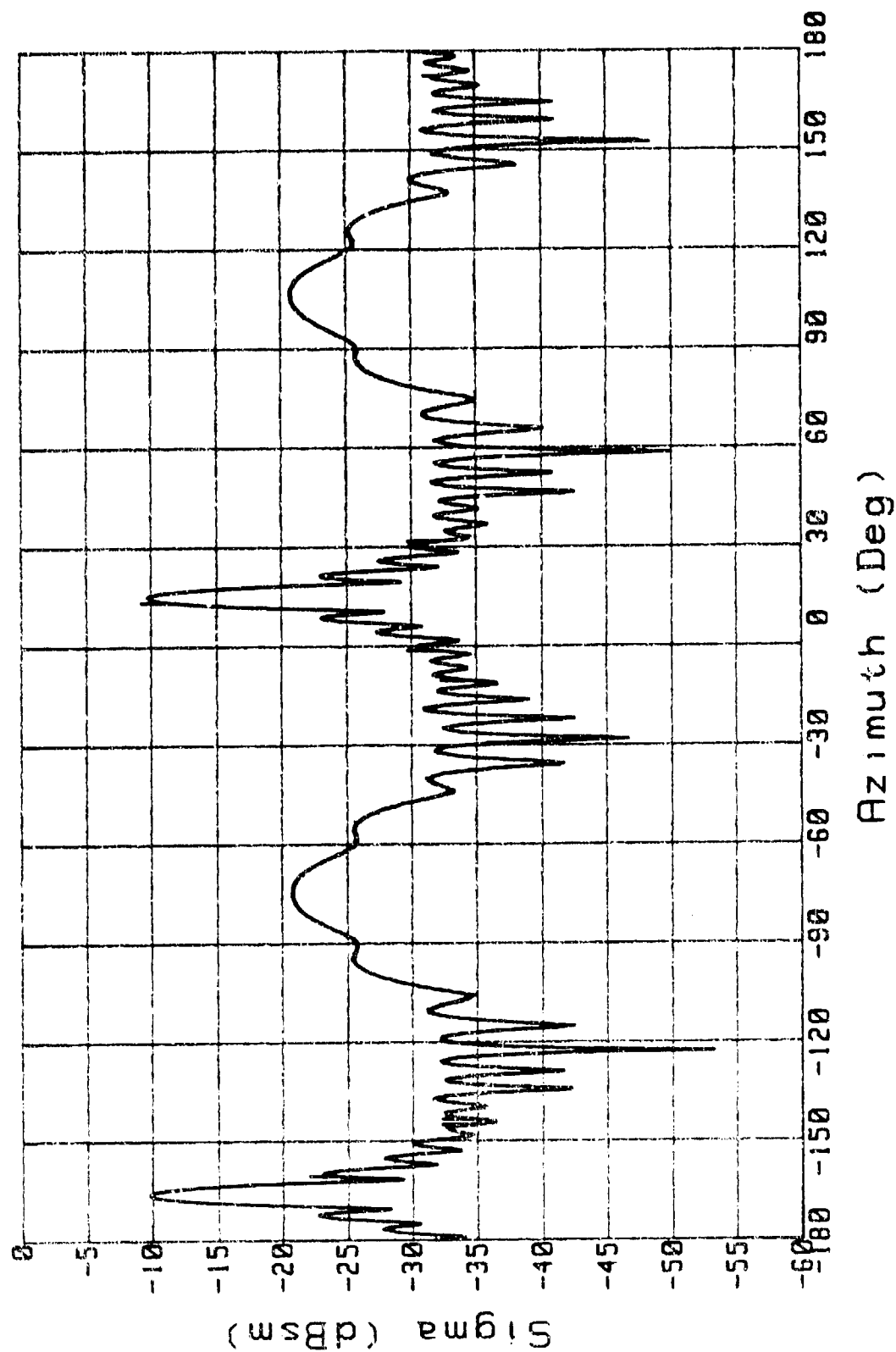
Figure 37A. RCS: Cylinder (8 in), V Pol, BSA=30, Range=13

Figure 37B. RCS: Cylinder (8 in), V Pol, BSA=0, Range=13
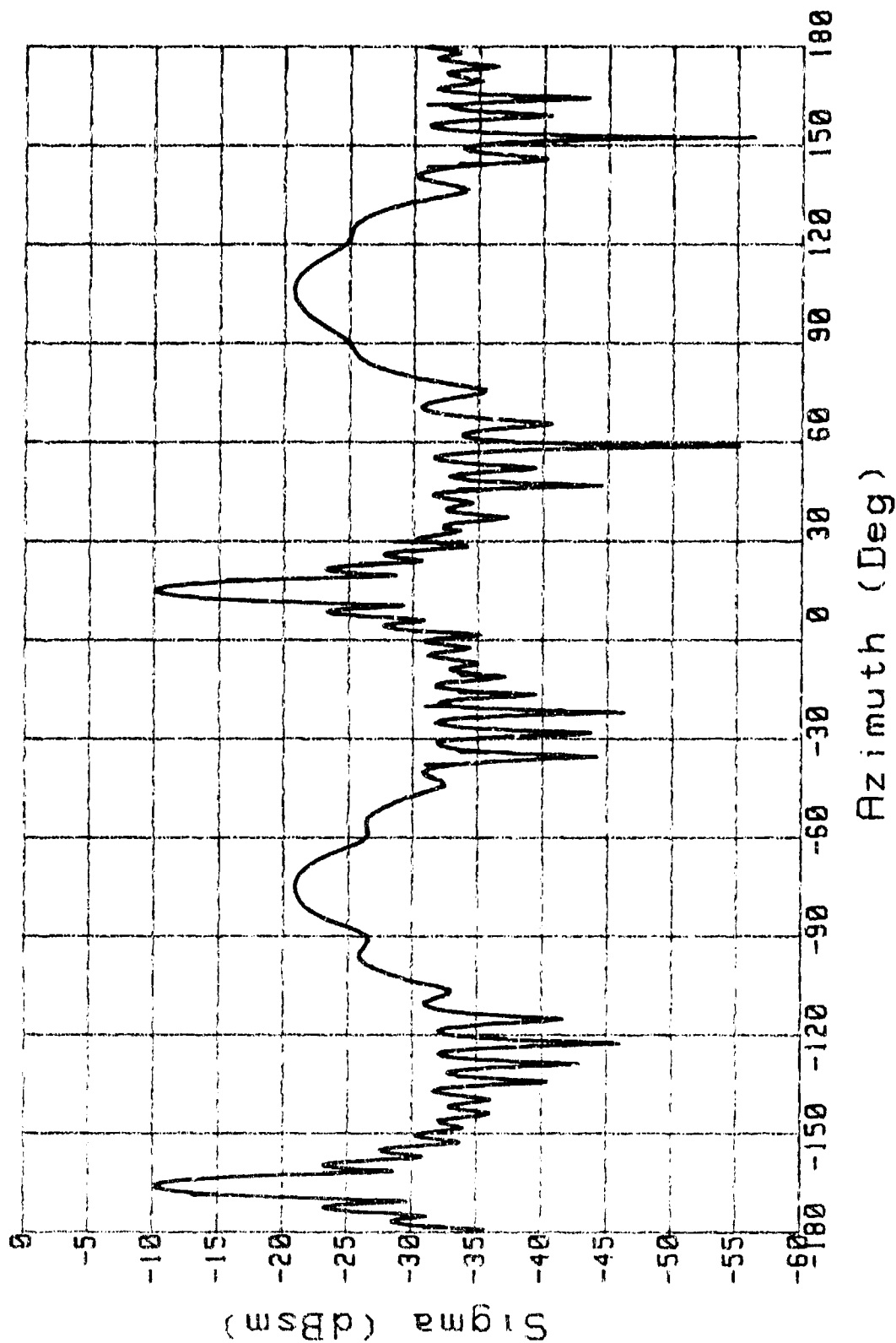
Figure 38A. RCS: Cylinder (8 in), V Pol, BSA=30, Range=10.8

Figure 38B. RCS: Cylinder (8 in), V Pol, BSA=0, Range=10.8
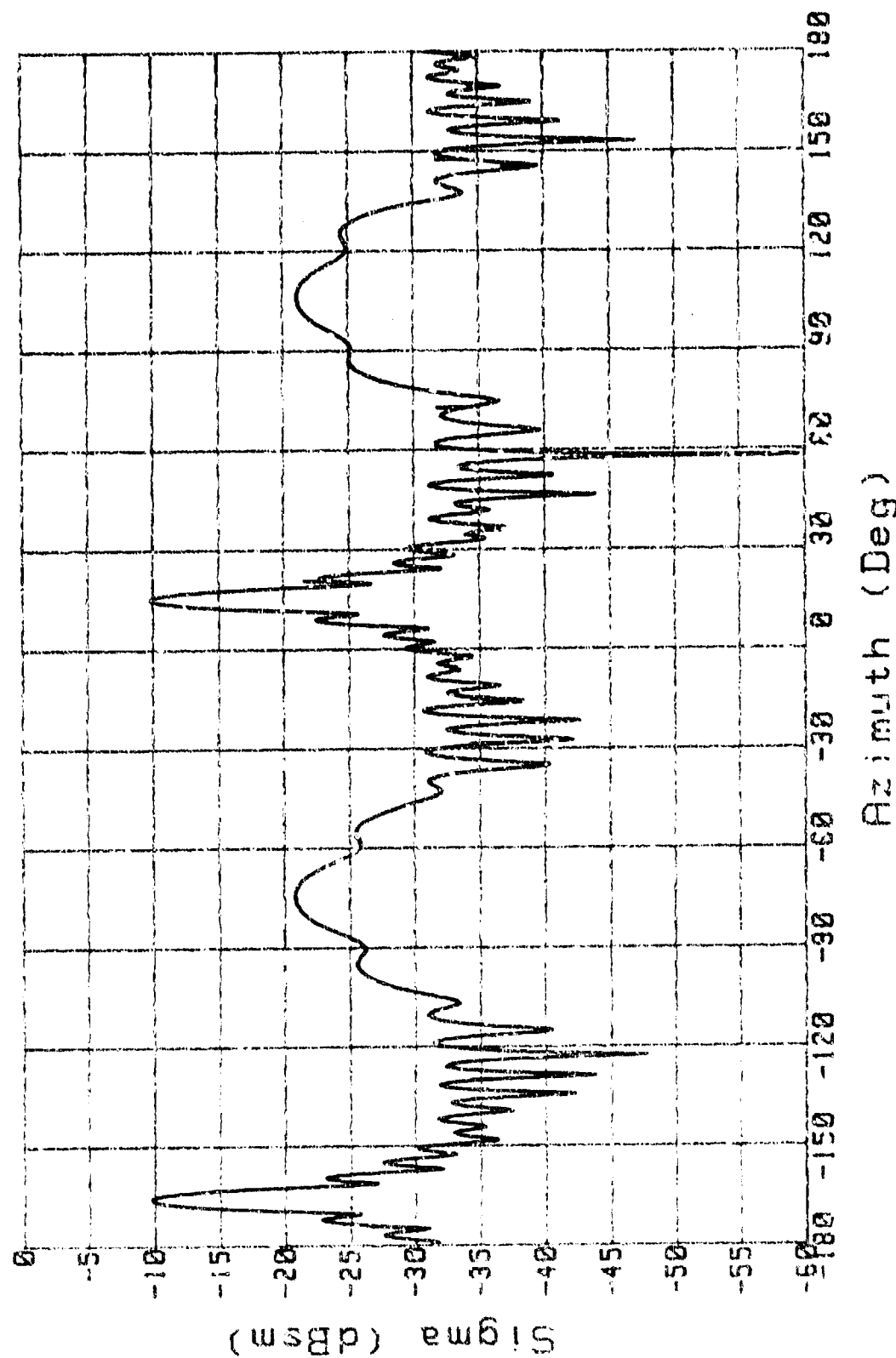
Figure 38C. RCS: Cylinder (3 in), V Pol, BSA=30, Range=7.75
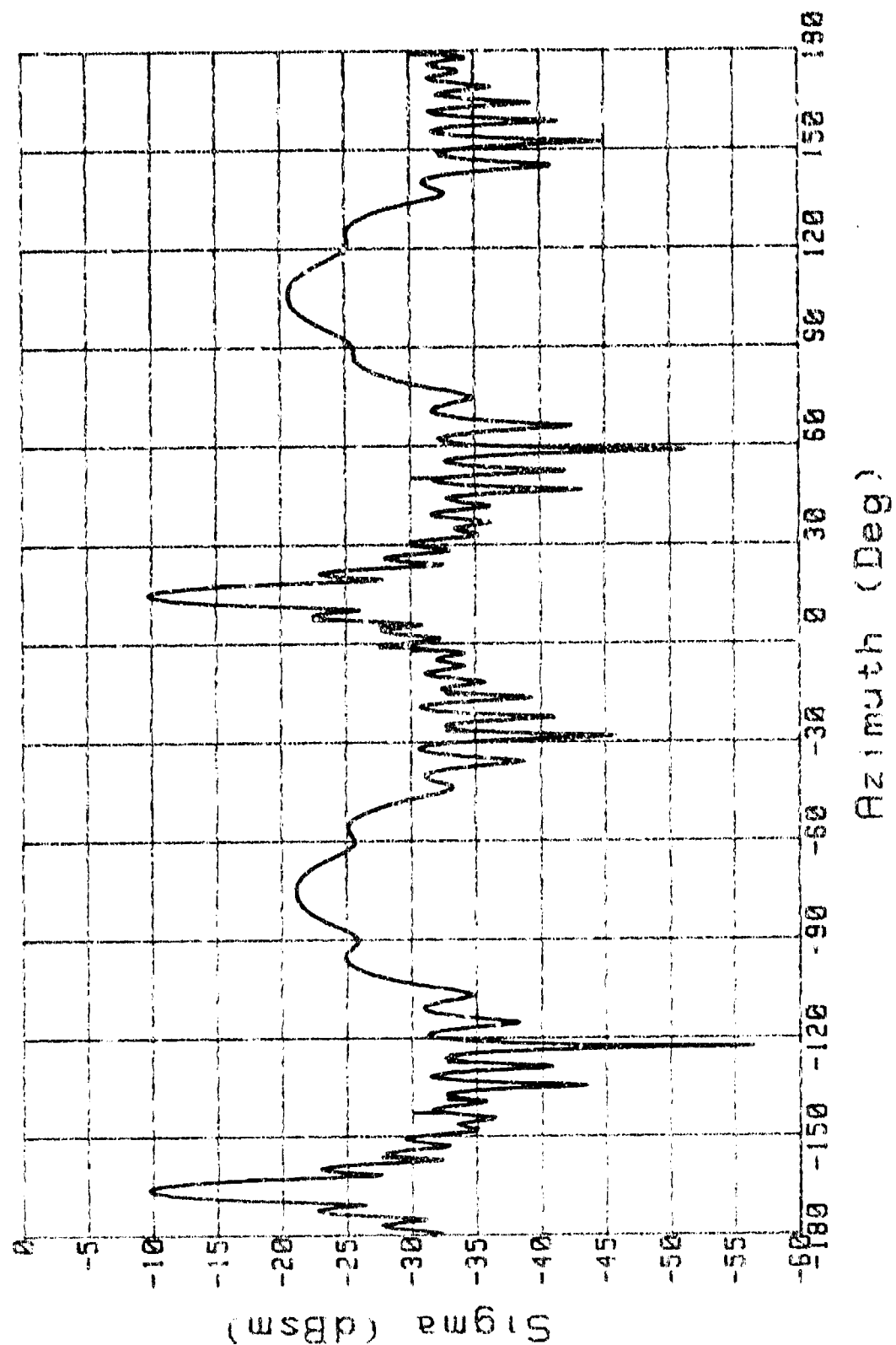
Figure 39A. RCS: Cylinder (8 in), V Pol, BSA=30, Range=9

104

Figure 396. RCS: Cylinder (8 in), V Pol, BSA=0, Range=12

105

Figure 40A. RCS: Cylinder (8 in), V Pol, BSA=30, Range=7
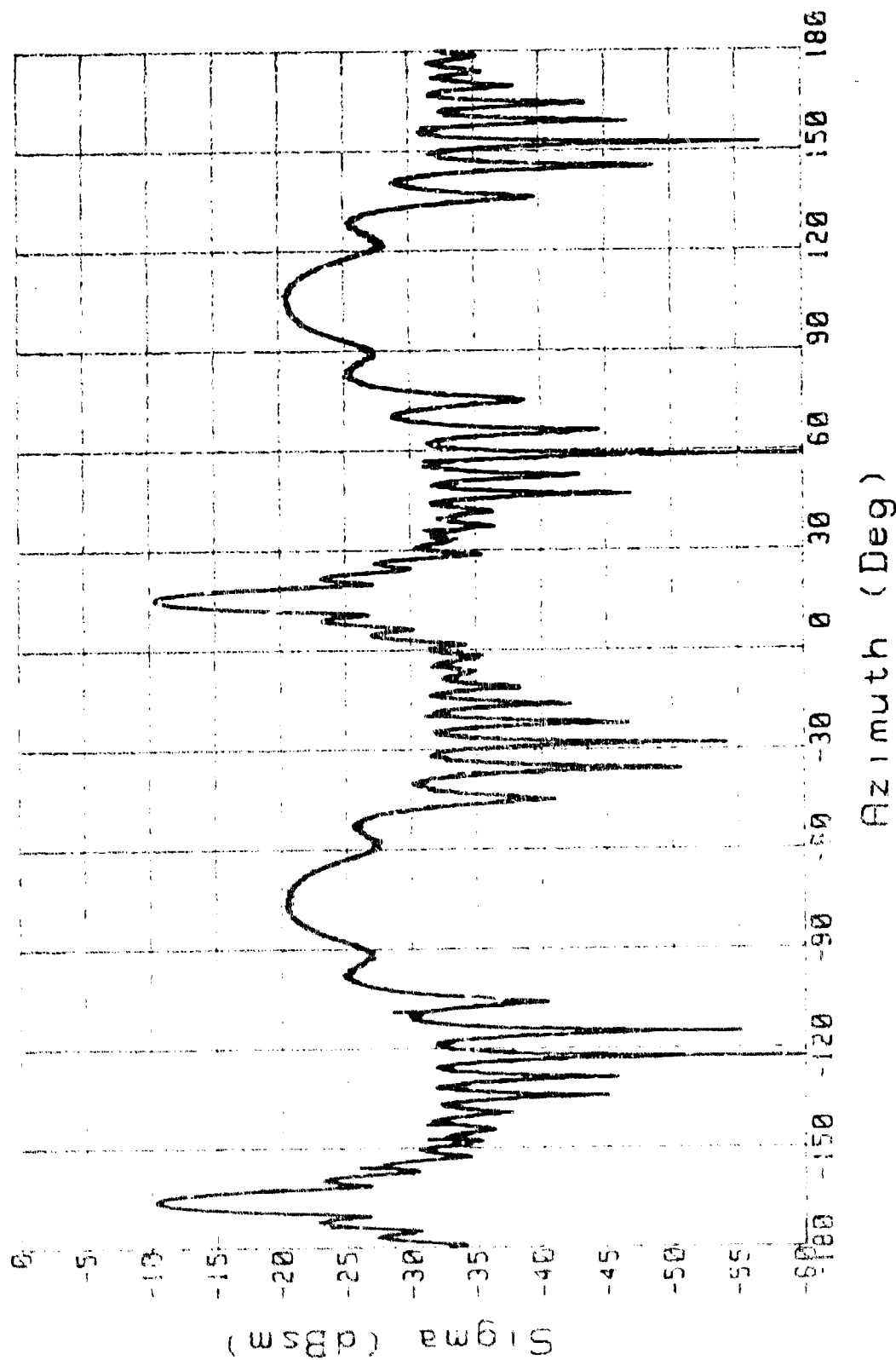
Figure 40B. RCS: Cylinder (8 in), V Pol, BSA=0, Range=10
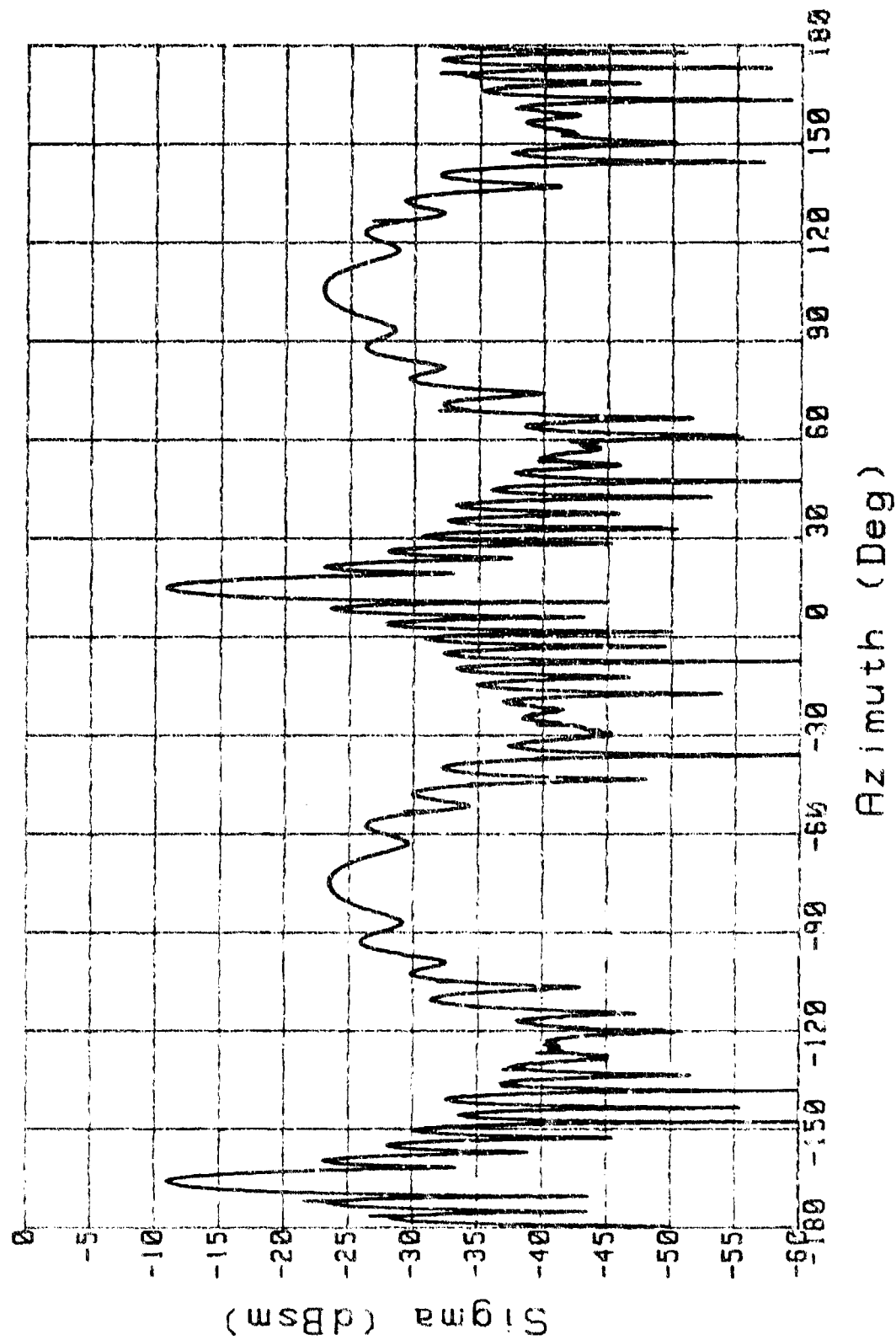
Figure 41A. RCS: Cylinder (8 in), H Pol, BSA=30, Range=15
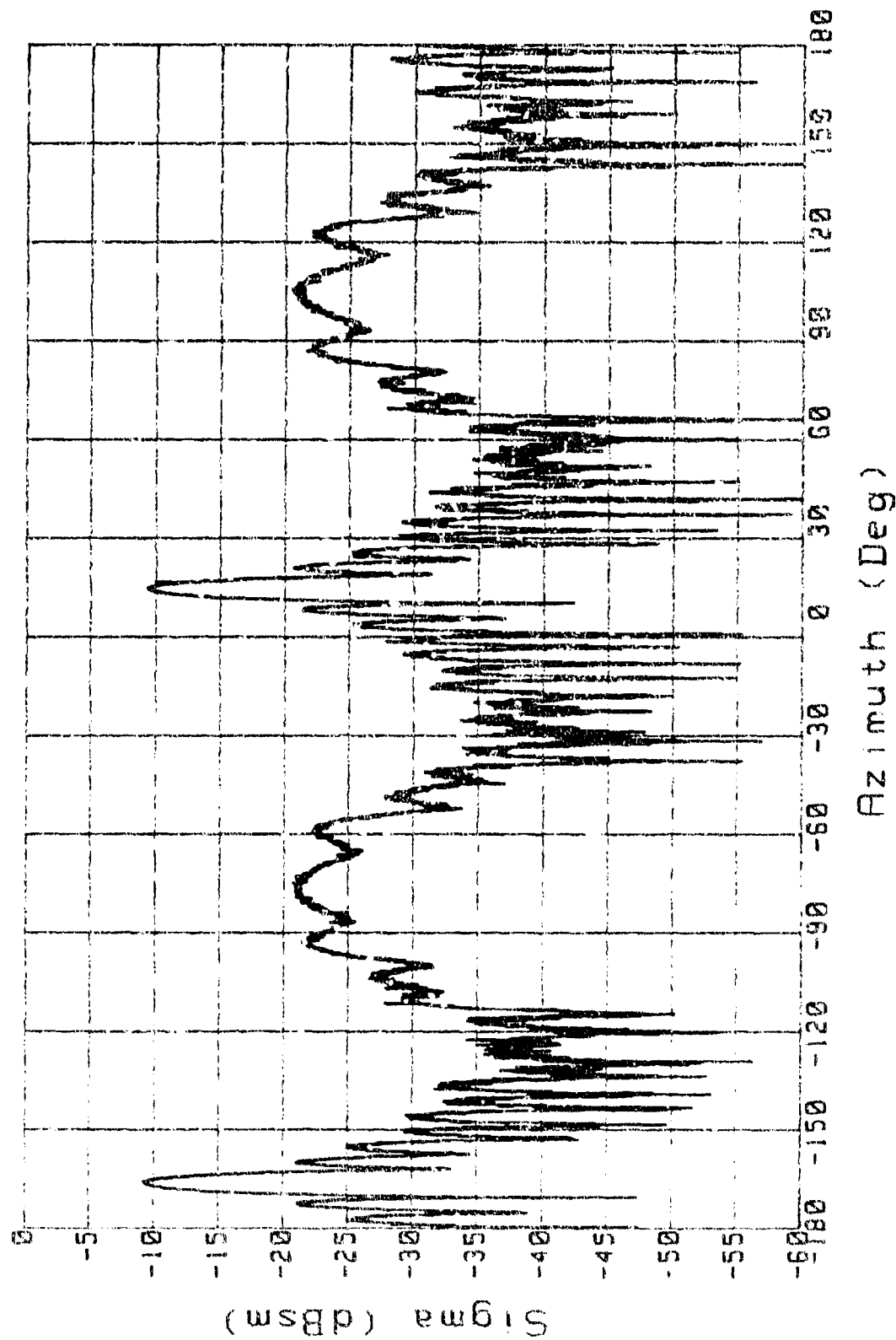
Figure 41B. RCS: Cylinder (8 in), H Pol, BSA=0, Range=15

Figure 42A. RCS: Cylinder (8 in), H Pol, BSA=30, Range=13

110

Figure 42B. RCS: Cylinder (8 in), H Pol, BSA=0, Range=13

111
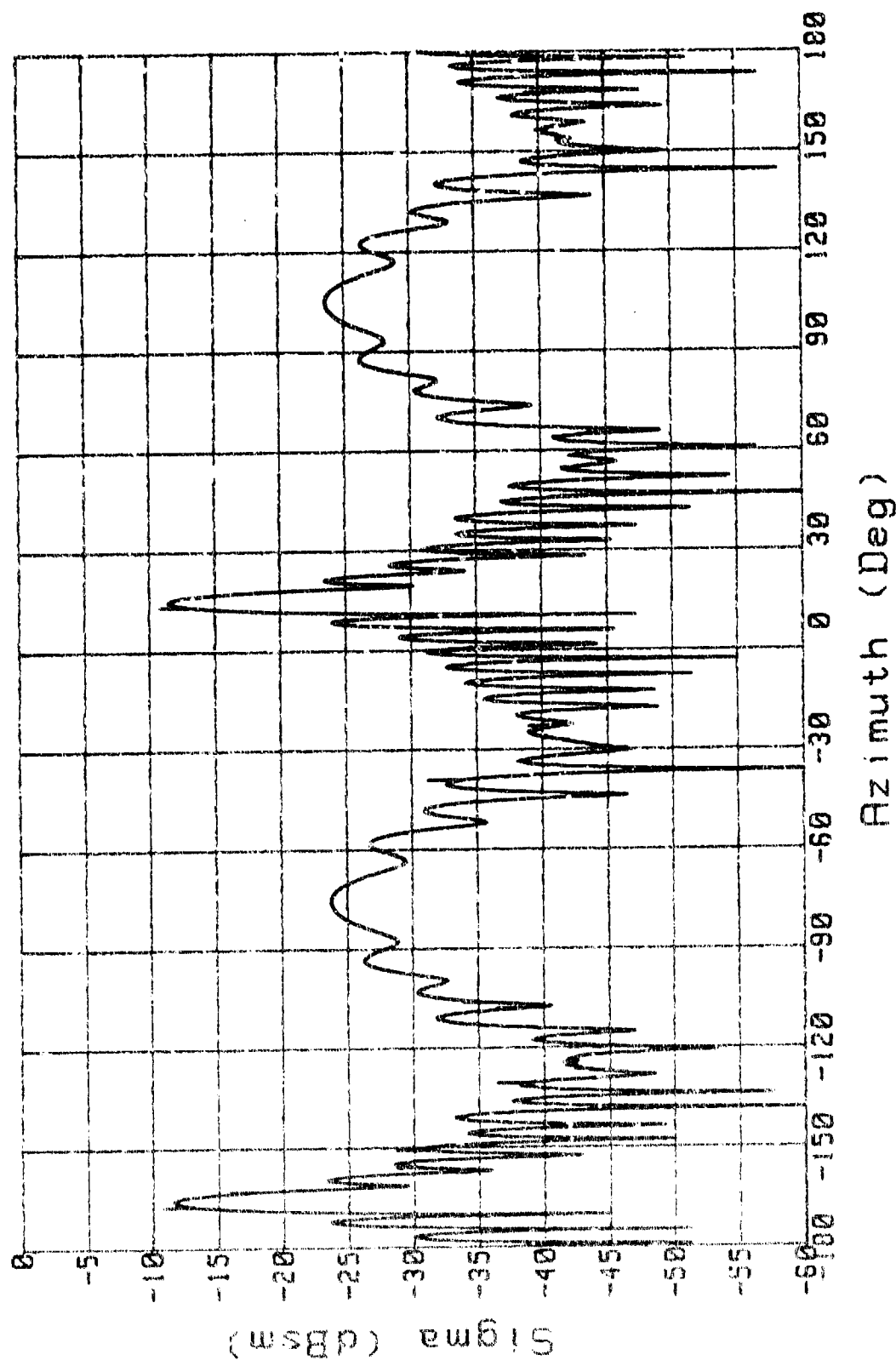
Figure 43A. RCS: Cylinder (8 in), H Pol, BSA=30, Range=10.8

Figure 43B. RCS: Cylinder (8 in), H Pol, BSA=0, Range=10.8

113
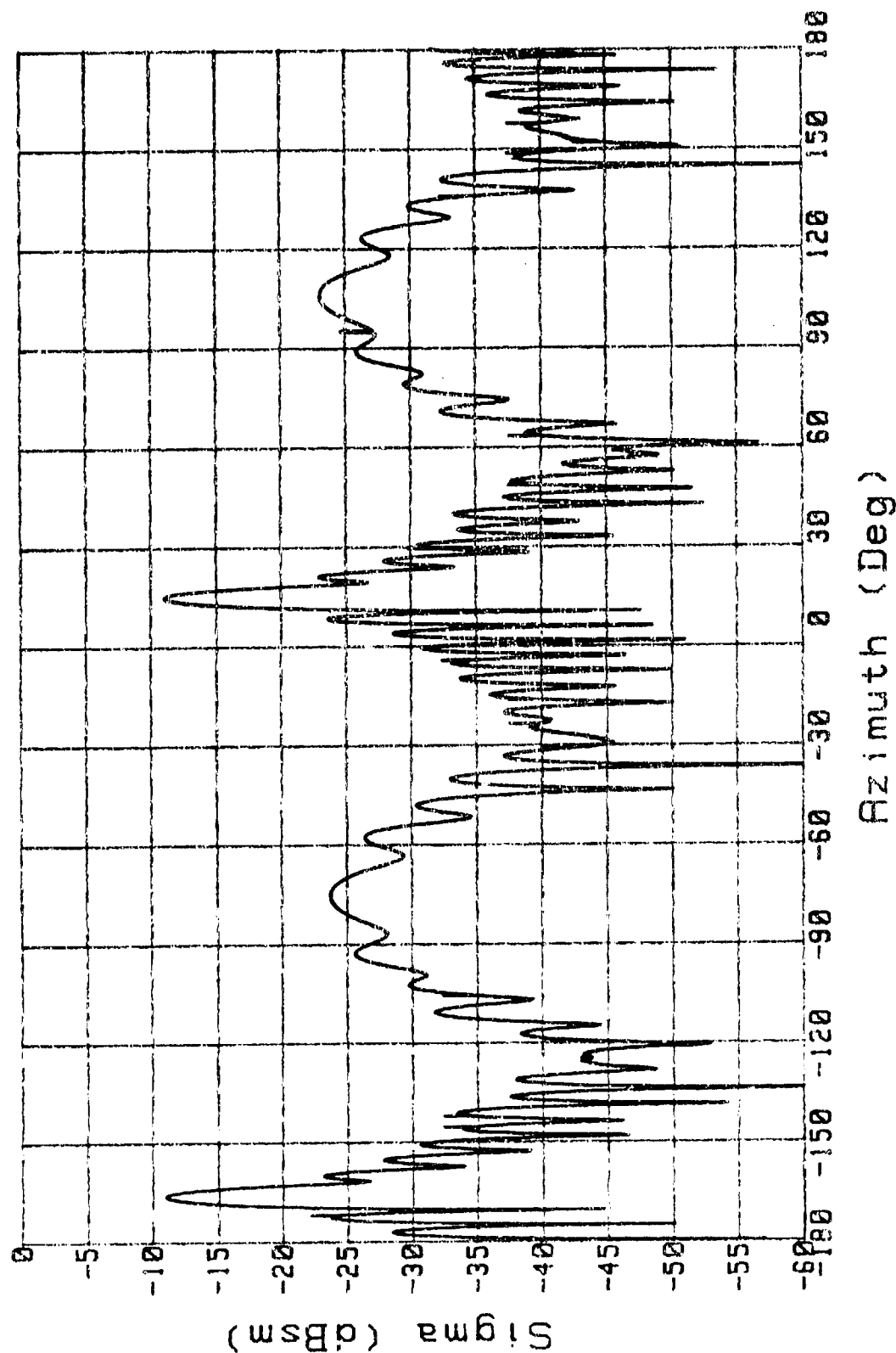
Figure 43C. RCS: Cylinder (8 in), H Pol, BSA=30, Range=7.75

114

Figure 44A. RCS: Cylinder (8 in), H Pol, BSA=30, Range=9

115

Figure 44B. Cylinder (8 in), H Pol, BSA=0, Range=12

Figure 45A. RCS: Cylinder (8 in), H Pol, BSA=30, Range=7
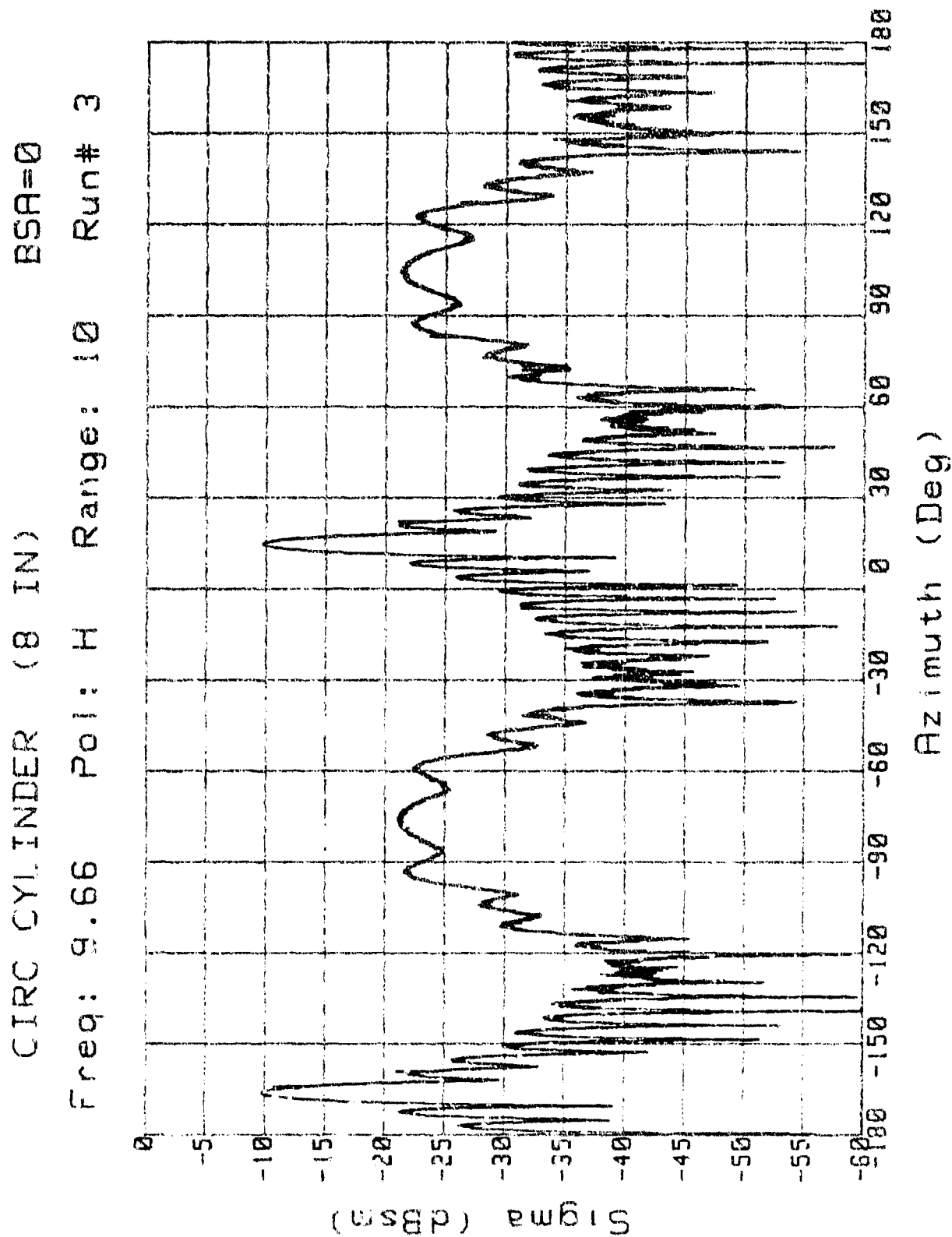
Figure 45B. RCS: Cylinder (8 in), H Pol, BSA=0, Range=10
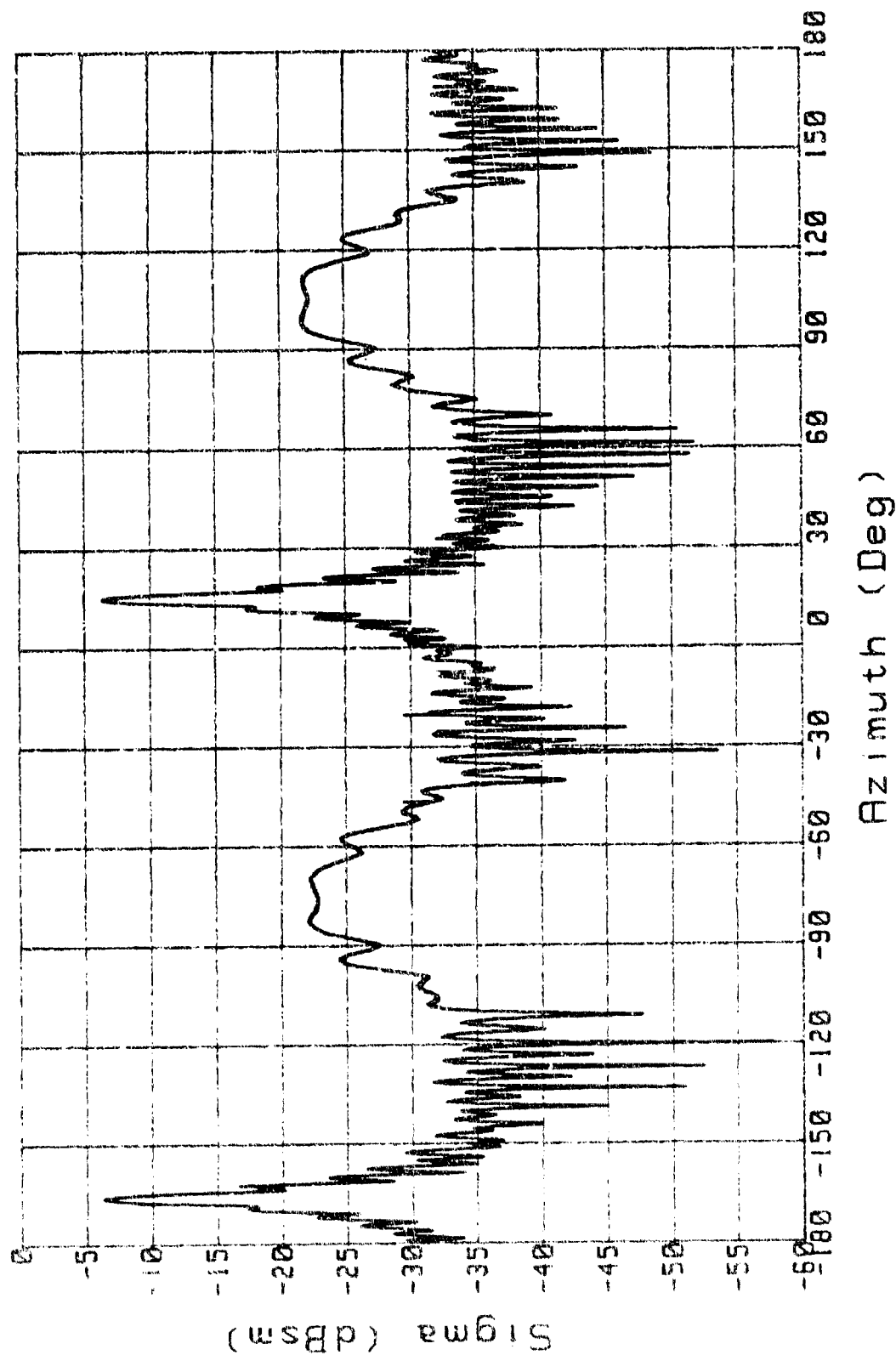
Figure 46A. RCS: Cylinder (14.25 in), V Pol, BSA=30, Range=20

Figure 46B. RCS: Cylinder (14.25 in), V Pol, BSA=0, Range=20
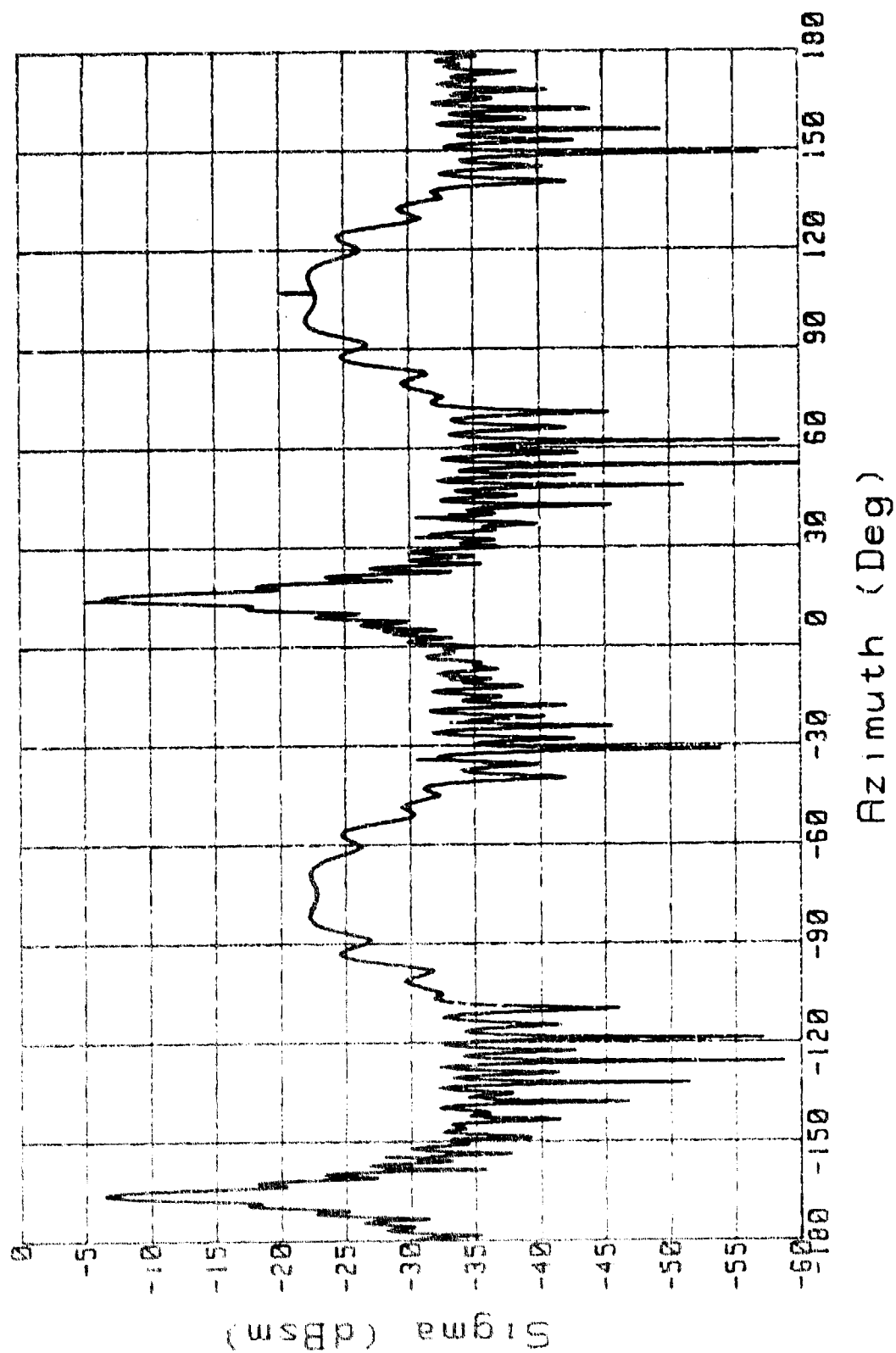
Figure 47A. RCS: Cylinder (14.25 in), V Pol, BSA=30, Range=19

Figure 47B. RCS: Cylinder (14.25 in), V Pol, BSA=0, Range=19
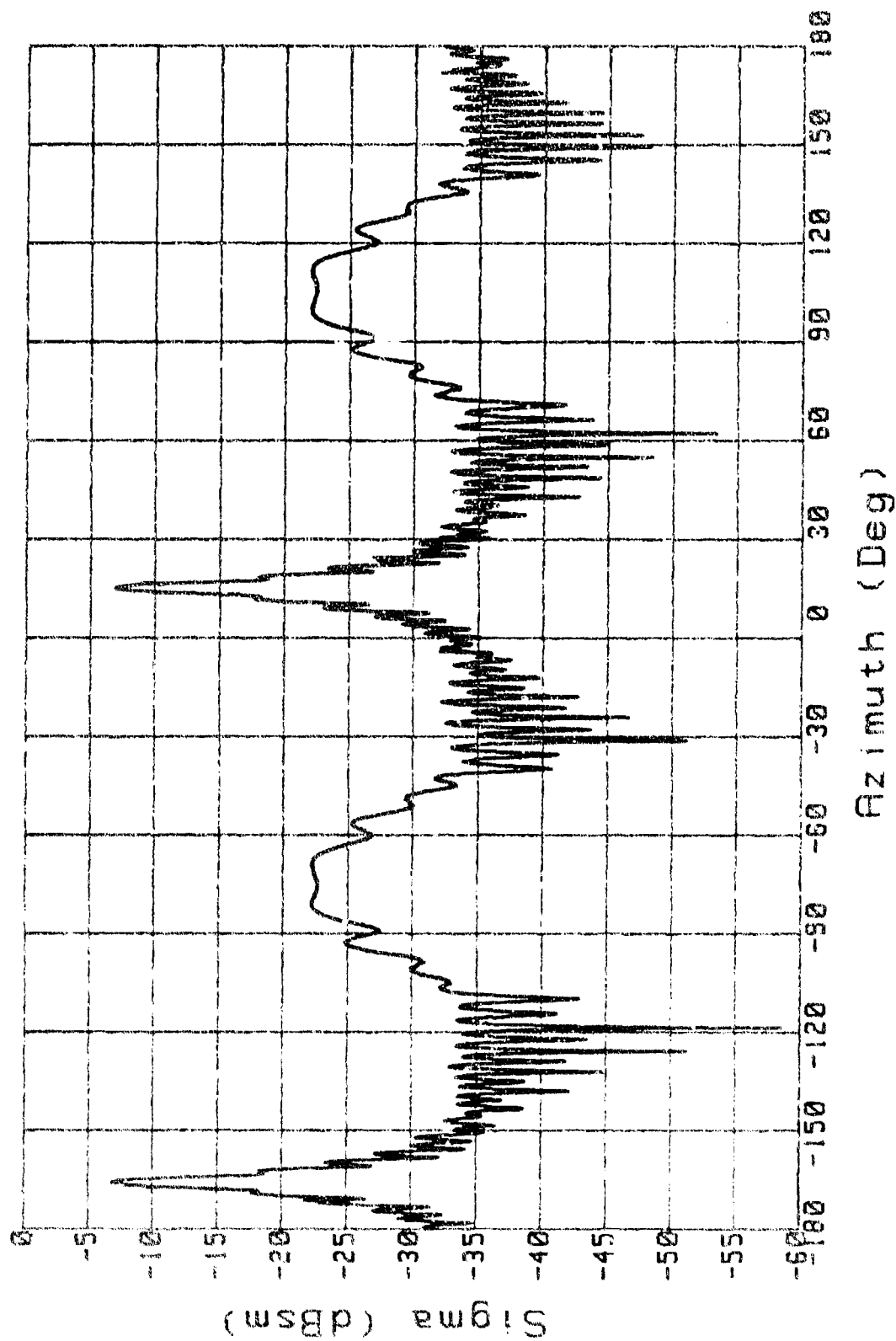
Figure 48A. RCS: Cylinder (14.25 in), V Pol, BSA=30, Range=15

Figure 48R. RCS: Cylinder (14.25 in), V Pol, BSA=0, Range=16.5

124

Figure 49A. RCS: Cylinder (14.25 in), V Pol, BSA=30, Range=11

Figure 49B. RCS: Cylinder (14.25 in), V Pol, BSA=0, Range=13.75

126

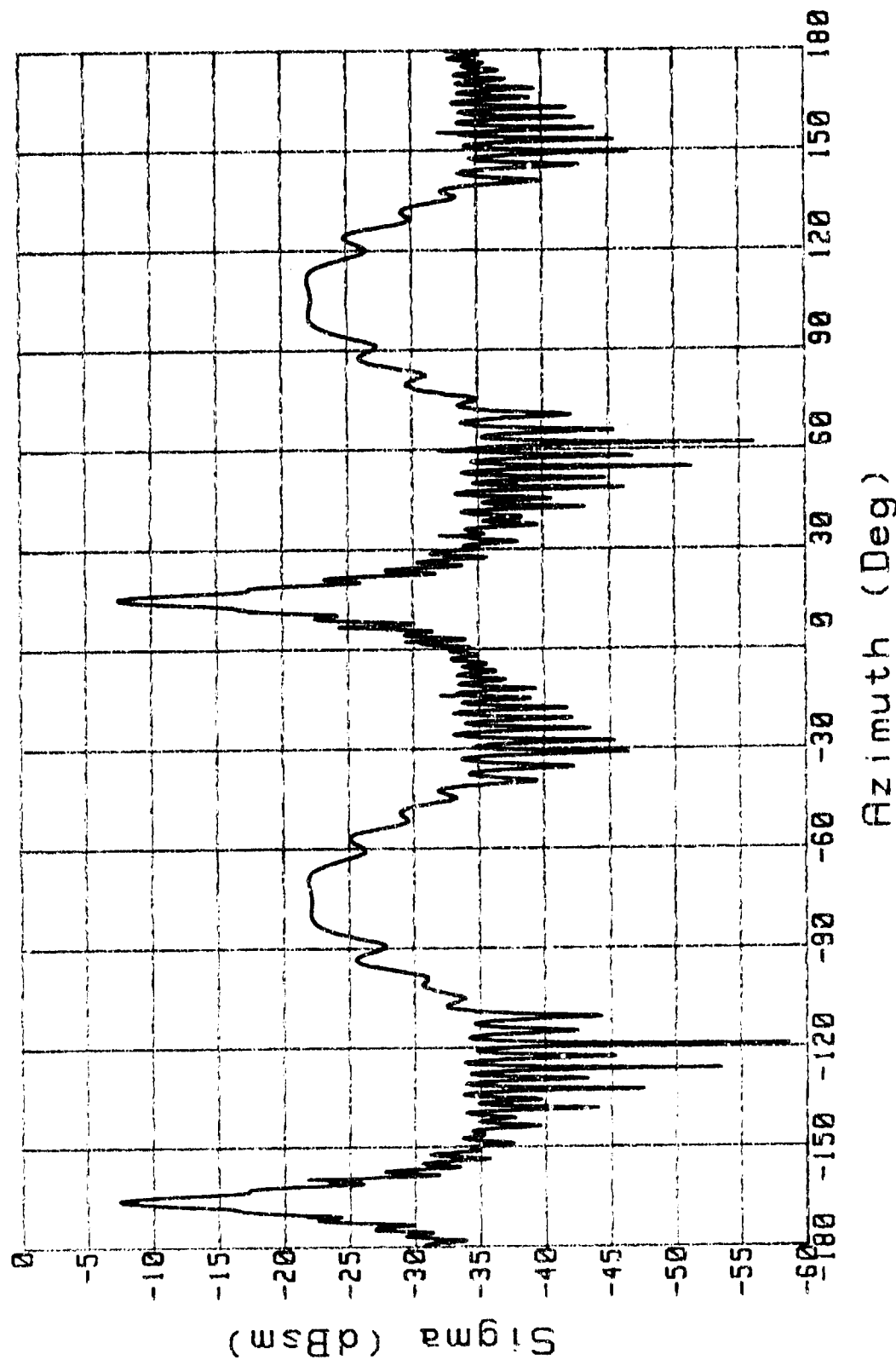Figure 50A.   RCS: Cylinder (14.25 in), V Pol, BSA=30, Range=9
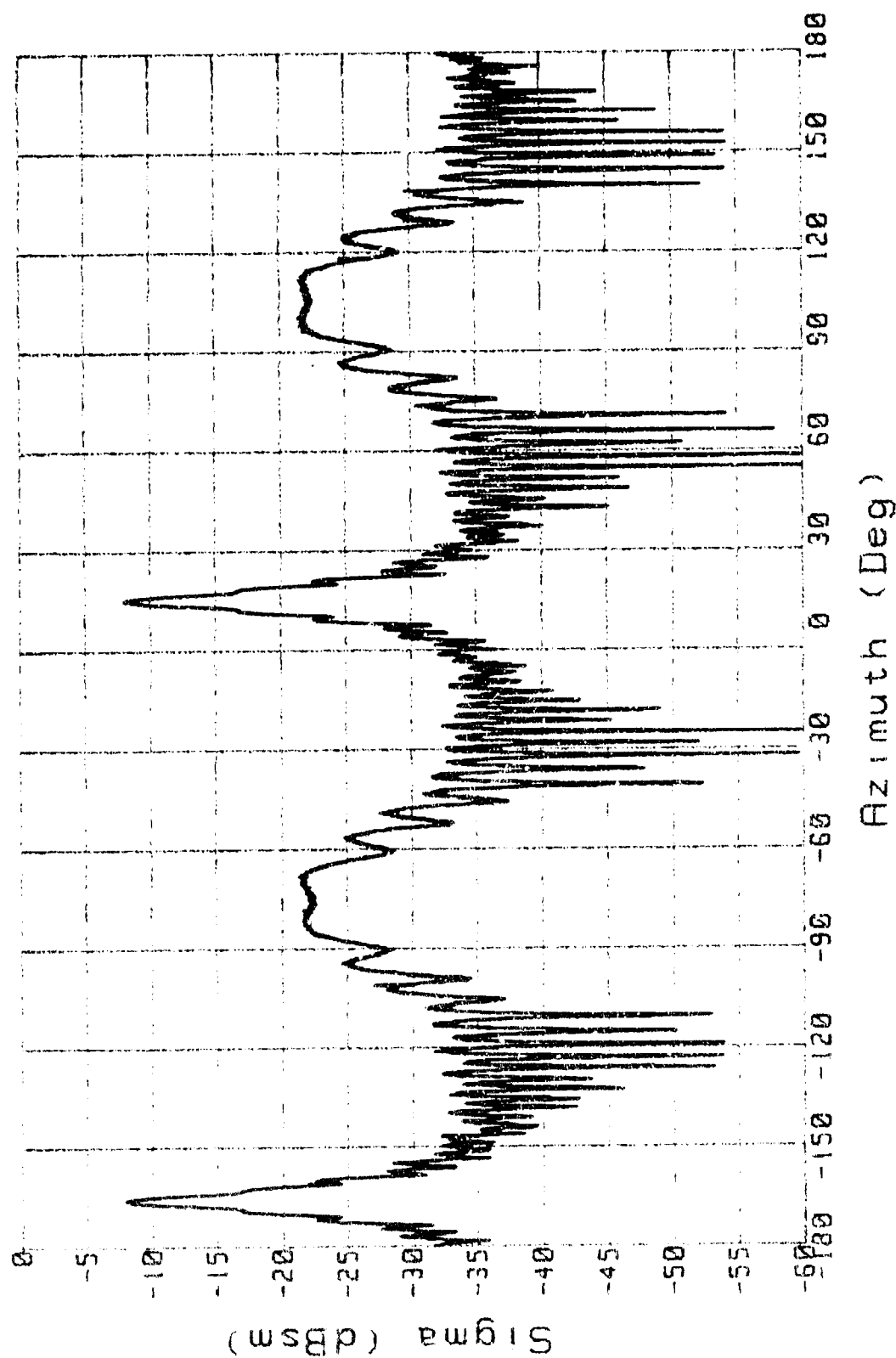
127

Figure 50B. RCS: Cylinder (14.25 in), V Pol, BSA=0, Range=12

128

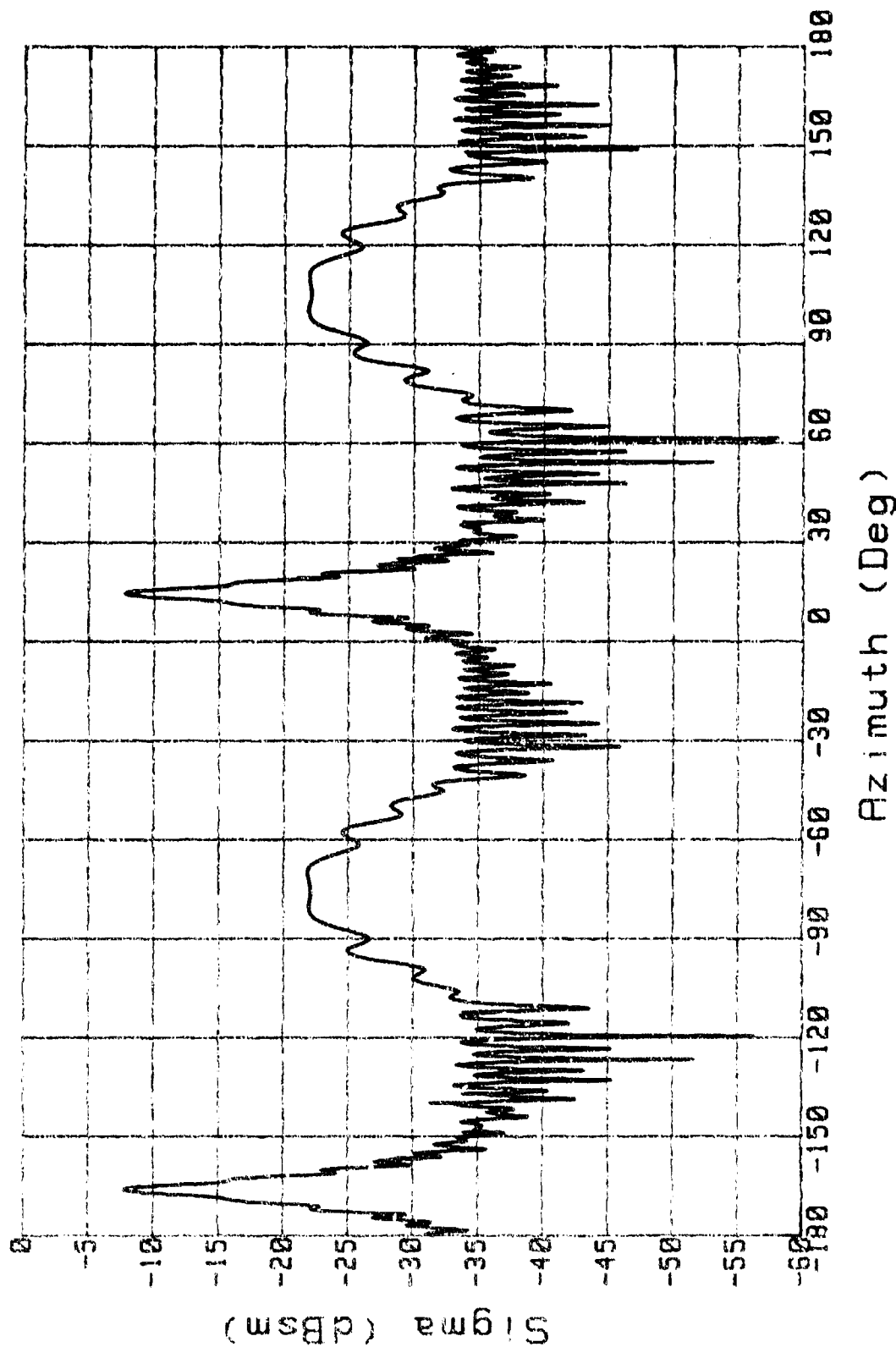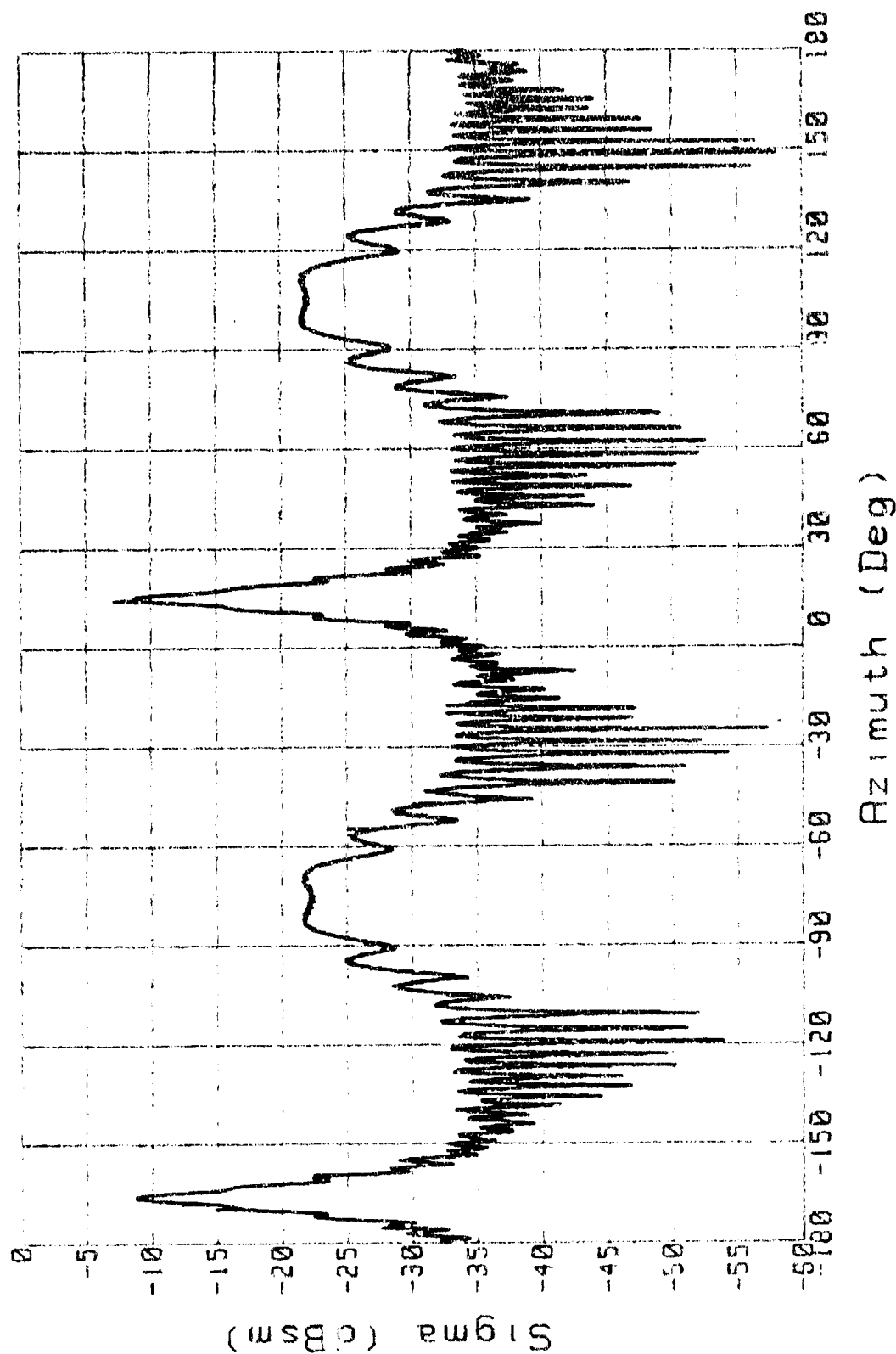CIRC CYLINDER (14.25 IN)   BSA=30

Freq: 10   Pol: V   Range: 7   Run# 2

Figure 51A.   RCS: Cylinder (14.25 in), V Pol, BSA=30, Range=7

Figure 51B. RCS: Cylinder (14.25 in), V Pol, BSA=0, Range=10

130
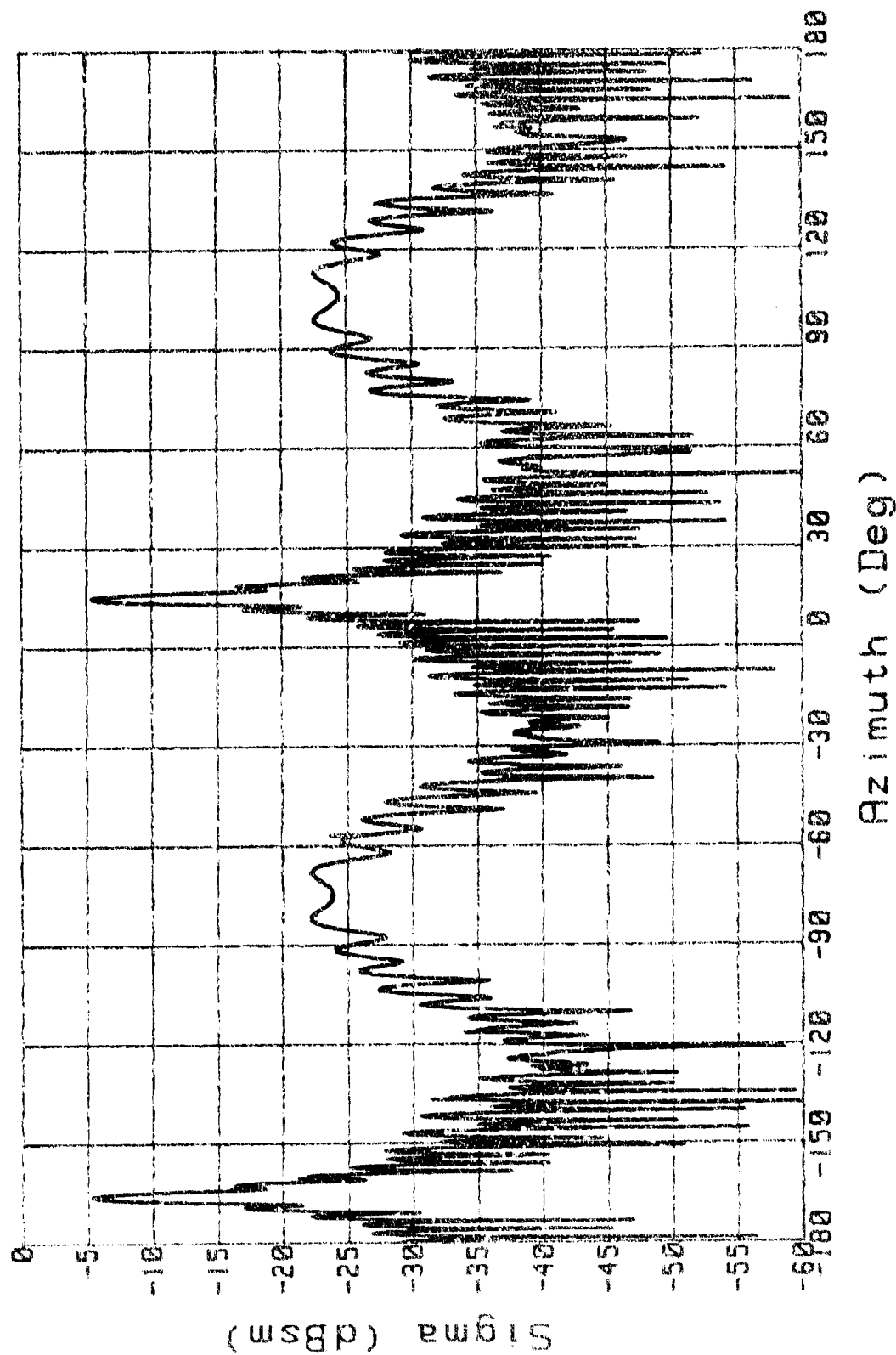
Figure 52A. RCS: Cylinder (14.25 in), H Pol, BSA=30, Range=20

Figure 52B. RCS: Cylinder (14.25 in). H Pol, BSA=0, Range=20

132

Figure 53. RCS: Cylinder (14.25 in), H Pol, BSA=30, Range=19

Figure 54A. RCS: Cylinder (14.25 in), H Pol, BSA=30, Range=15

Figure 54B. RCS: Cylinder (14.25 in), H Pol, BSA=0, Range=16.5

135

Figure 55A. RCS: Cylinder (14.25 in): H Pol, BSA=30, Range=13

Figure 55B. RCS: Cylinder (14.25 in), H Pol, BSA=0, Range=15

CIRC CYLINDER (14.25 IN)   BSA=30

Freq: 10   Pol: H   Range: 11   Run# 2
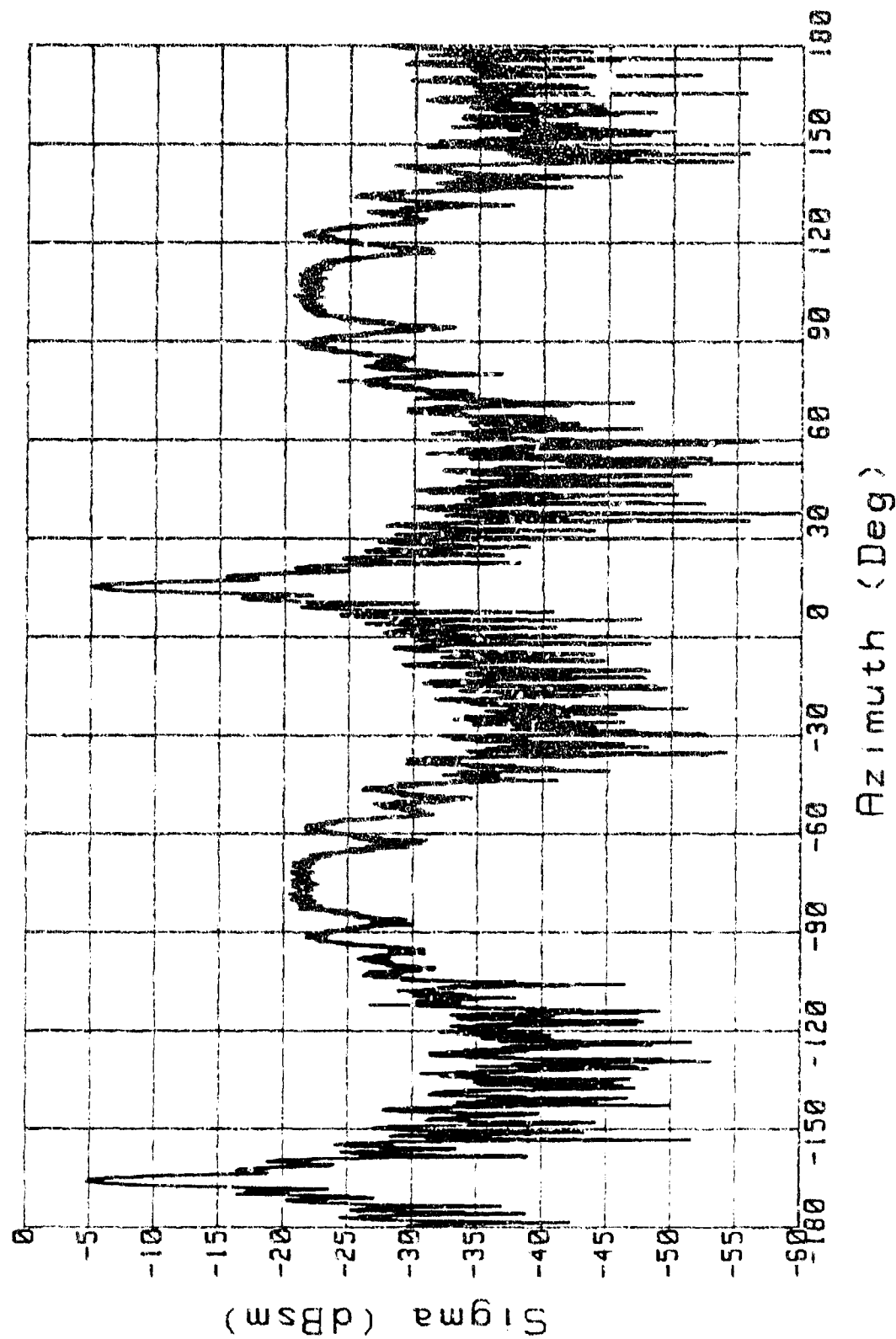
Azimuth (Deg)

Sigma (dBsm)

Figure 56A.   RCS: Cylinder (14.25 in), H Pol, BSA=30, Range=11

138

Figure 56B. RCS: Cylinder (14.25 in), H Pol, BSA=0, Range=13.75

Figure 57A. RCS: Cylinder (14.25 in), H Pol, BSA=30, Range=9

Figure 57B. RCS: Cylinder (14.25 in), H Pol, BSA=0, Range=12

141

Figure 58A. RCS: Cylinder (14.25 in), H Pol, BSA=30, Range=7.75

142

Figure 58B. RCS: Cylinder (14.25 in), H Pol, BSA=0, Range=10.8
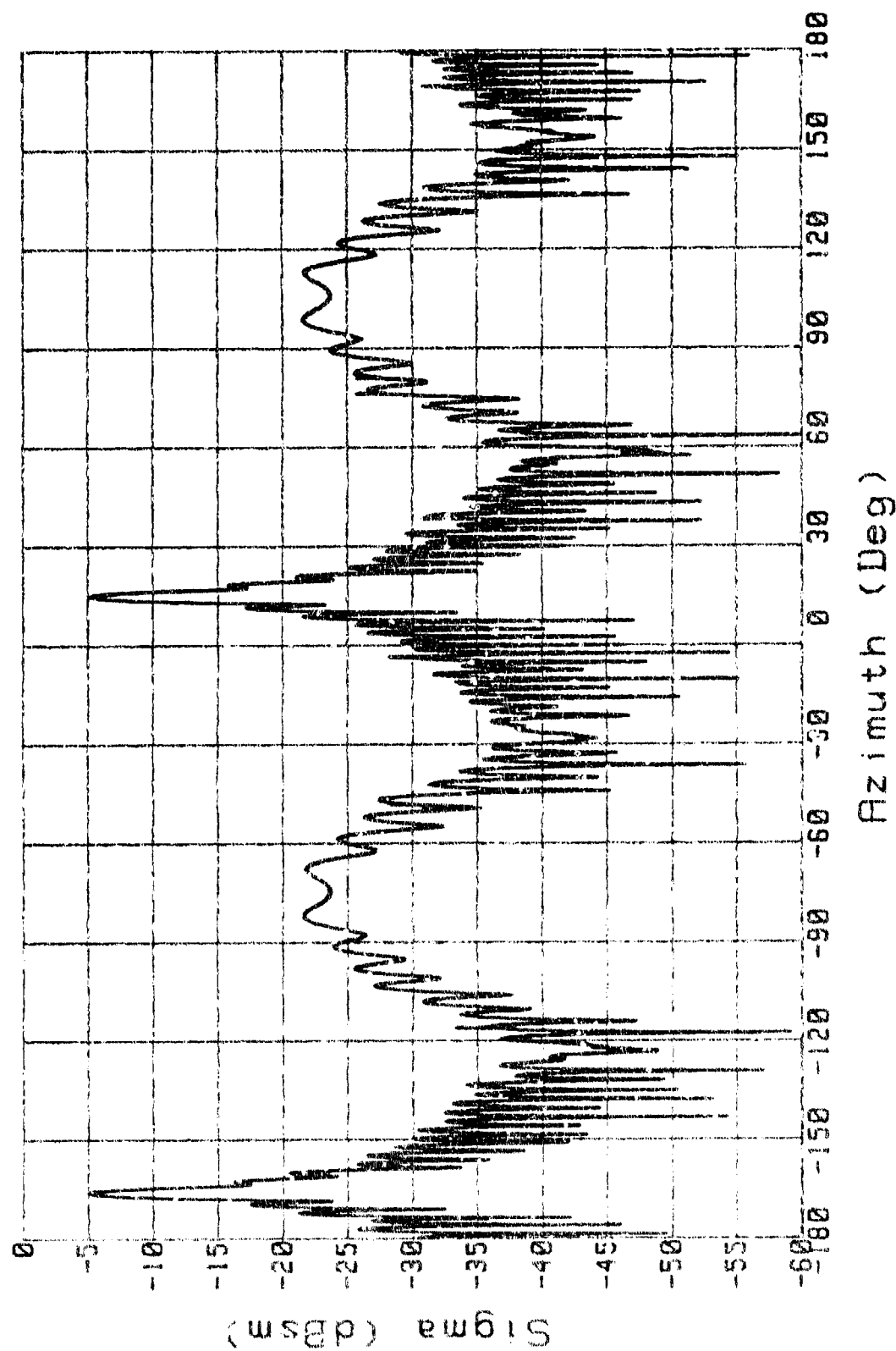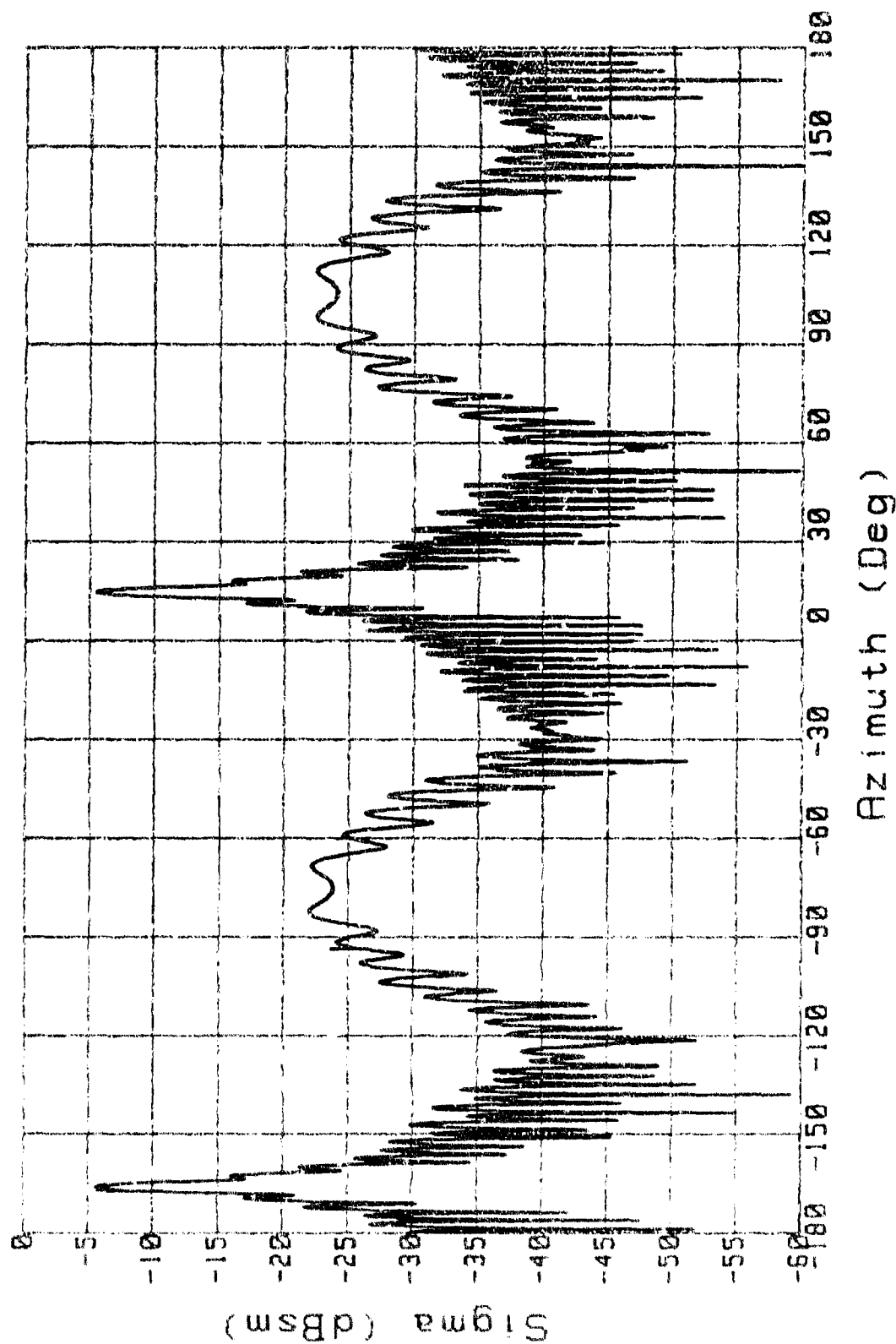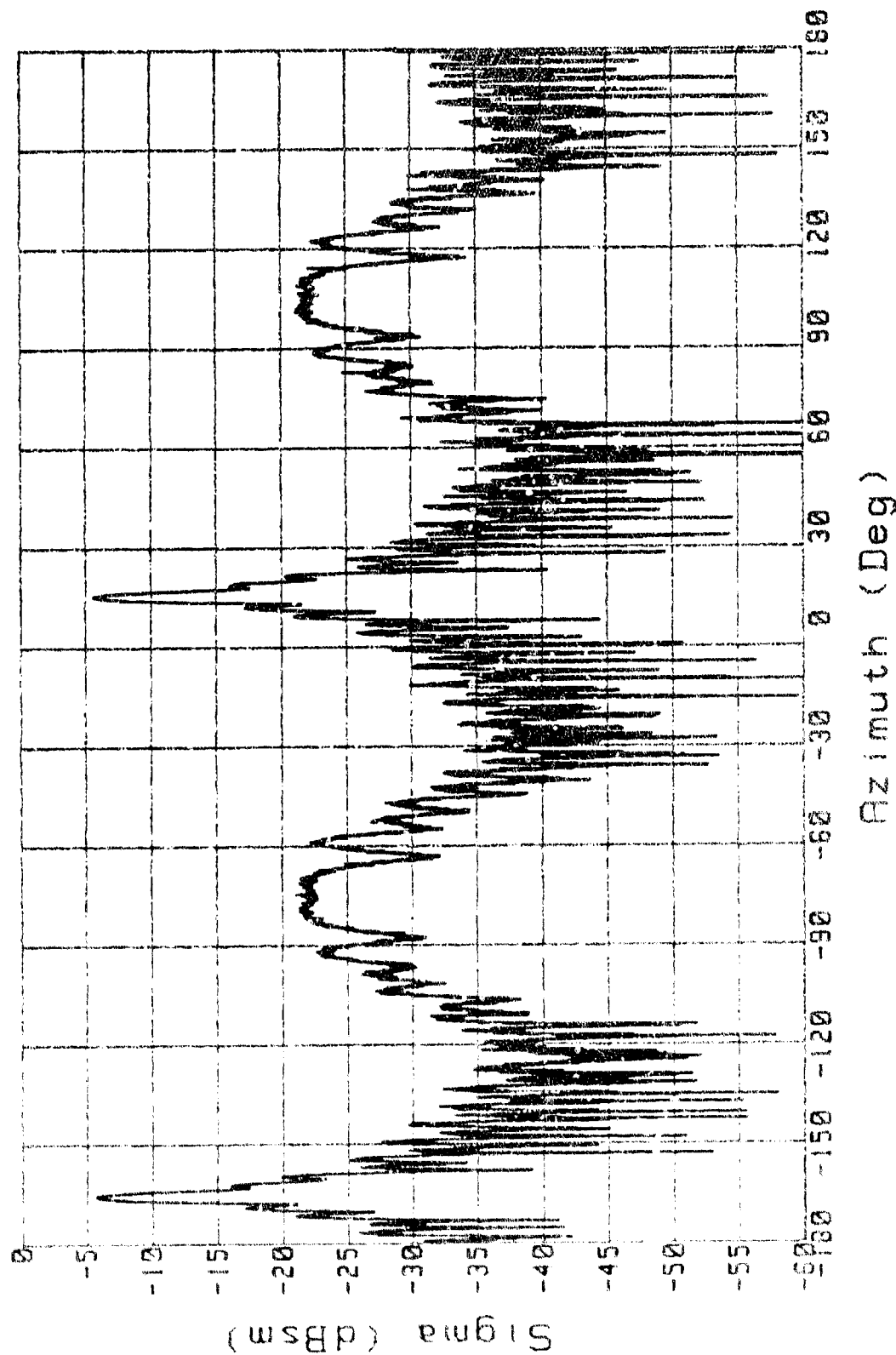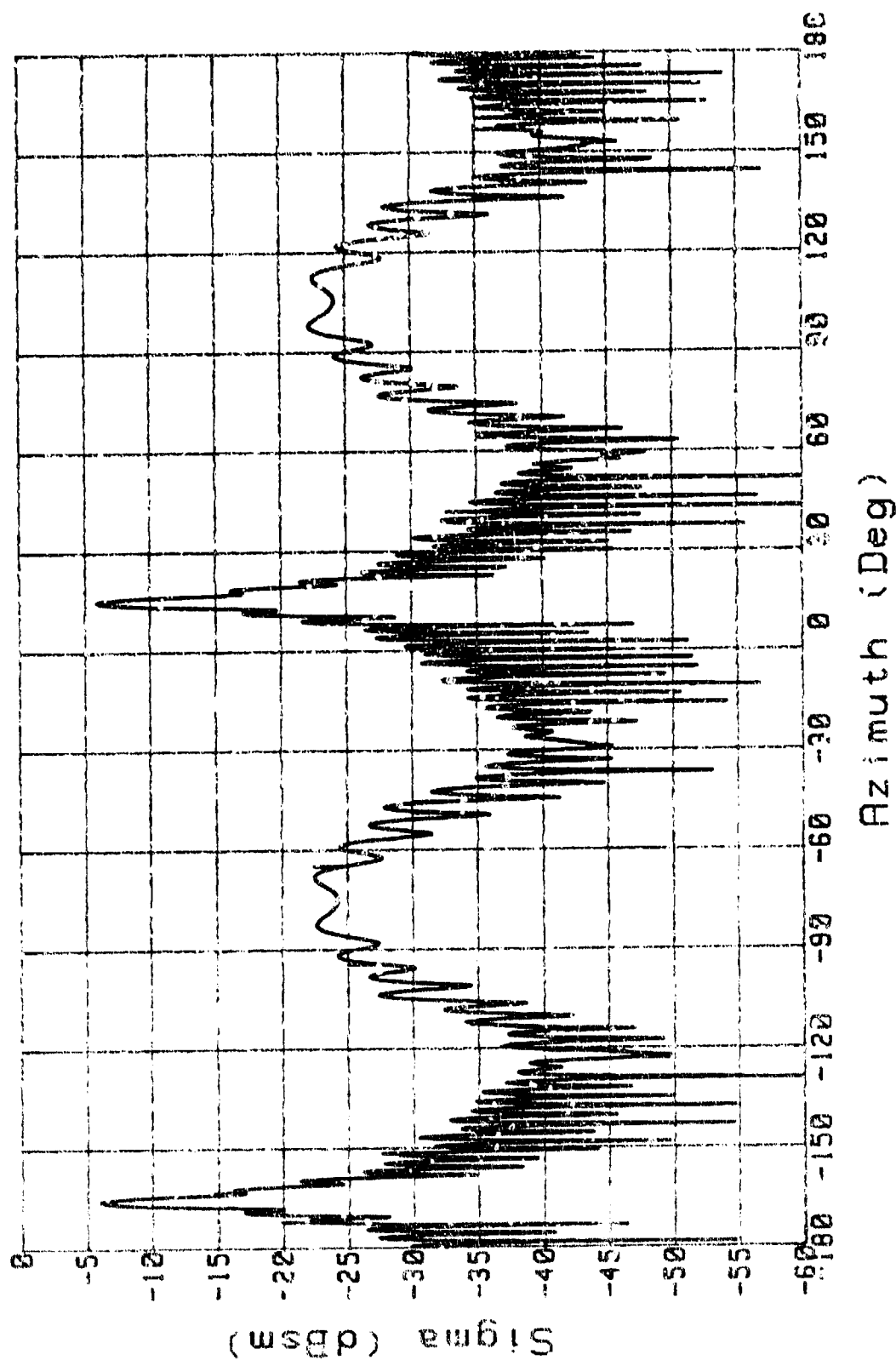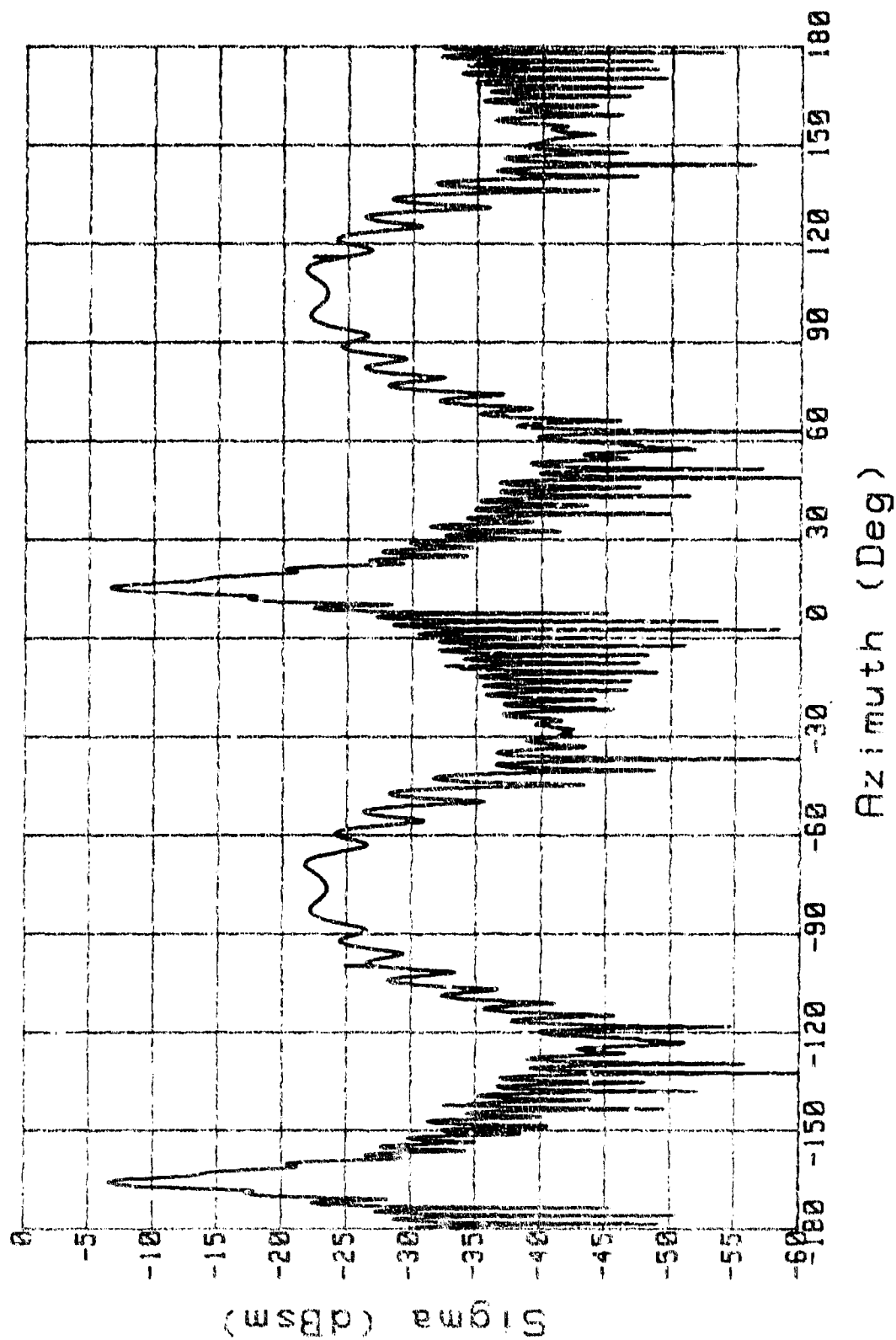
Figure 59A. RCS: Cylinder (14.25 in), H Pol, BSA=30, Range=7

144

CIRC CYLINDER (14.25 IN)   BSA=0
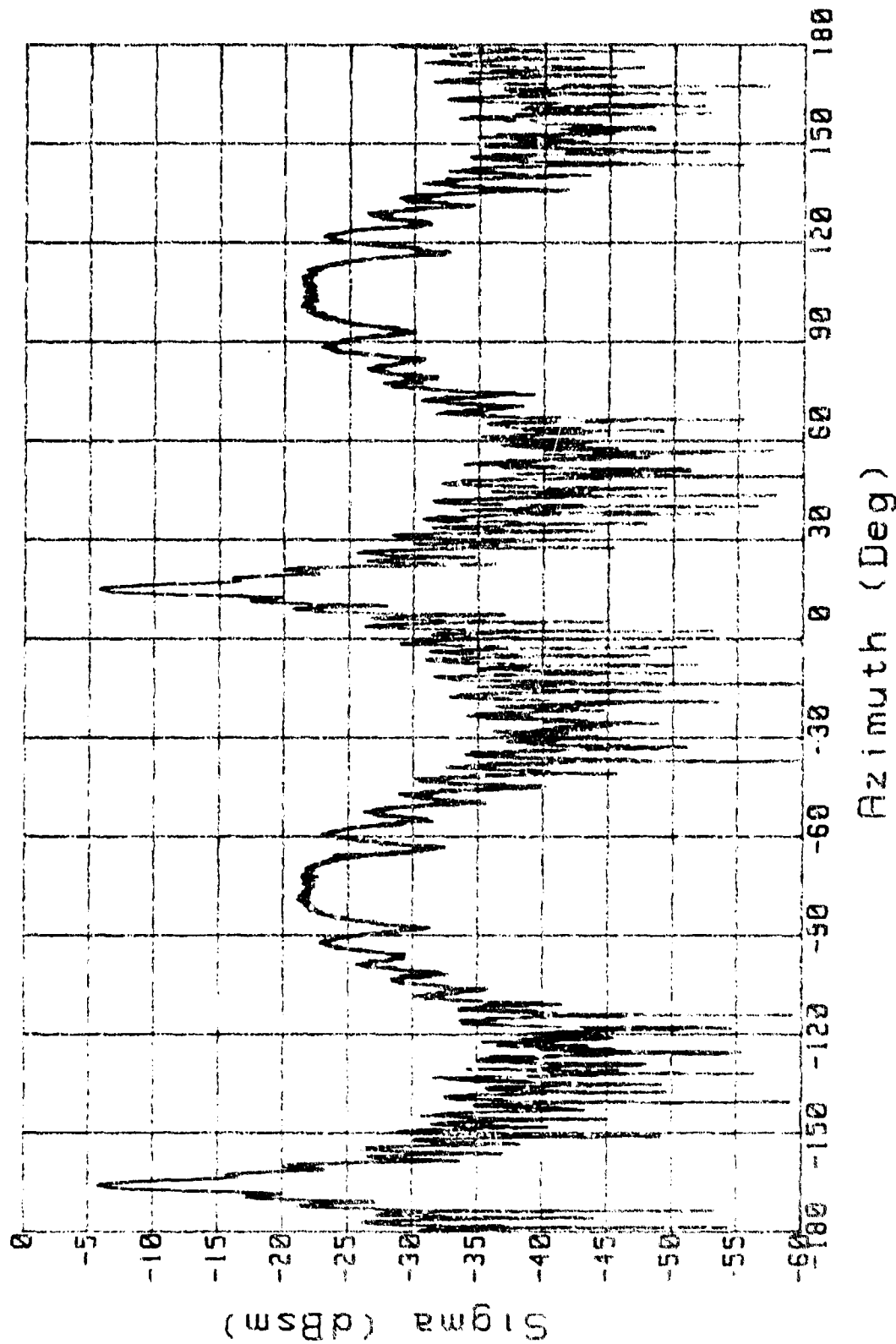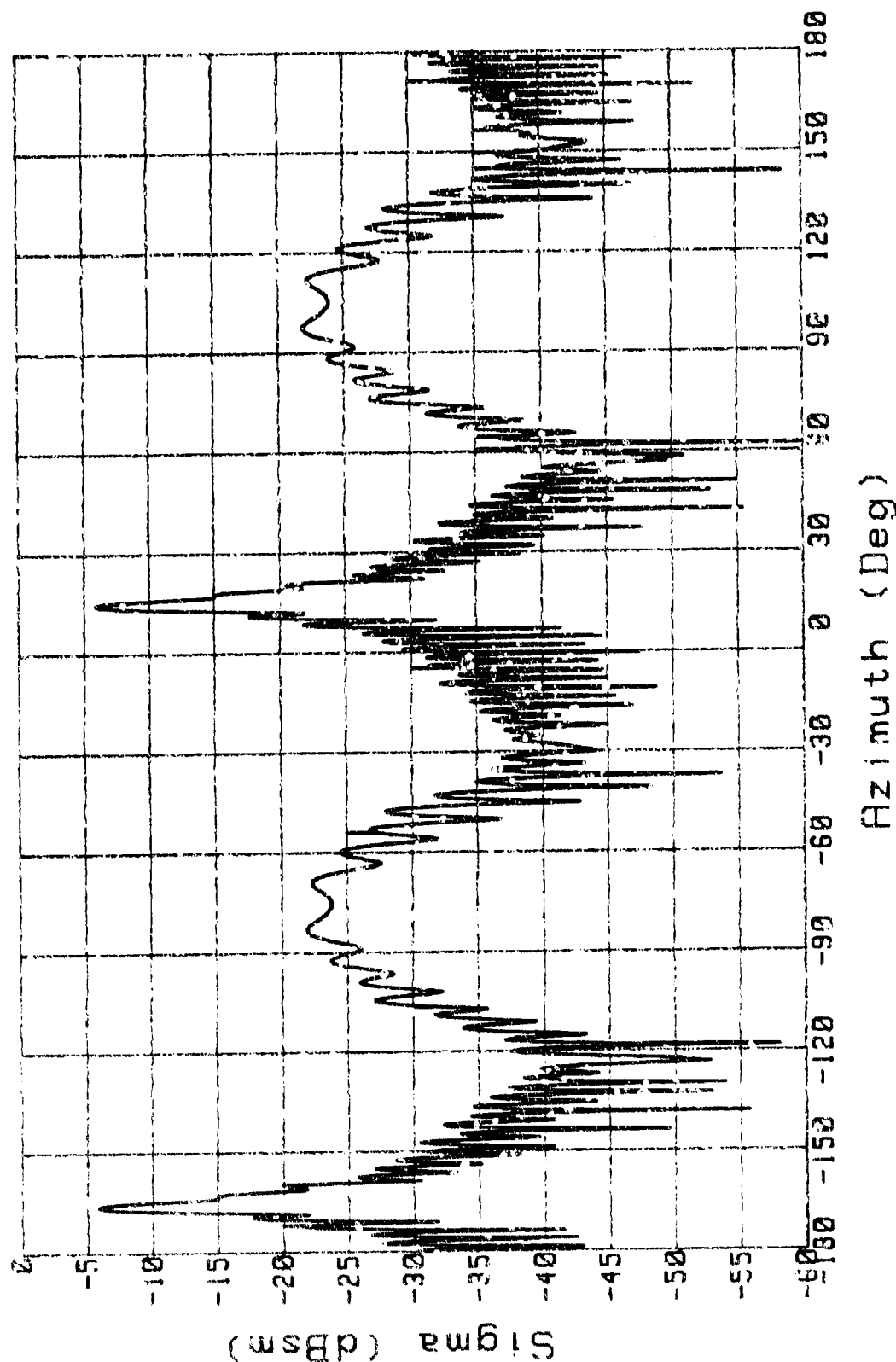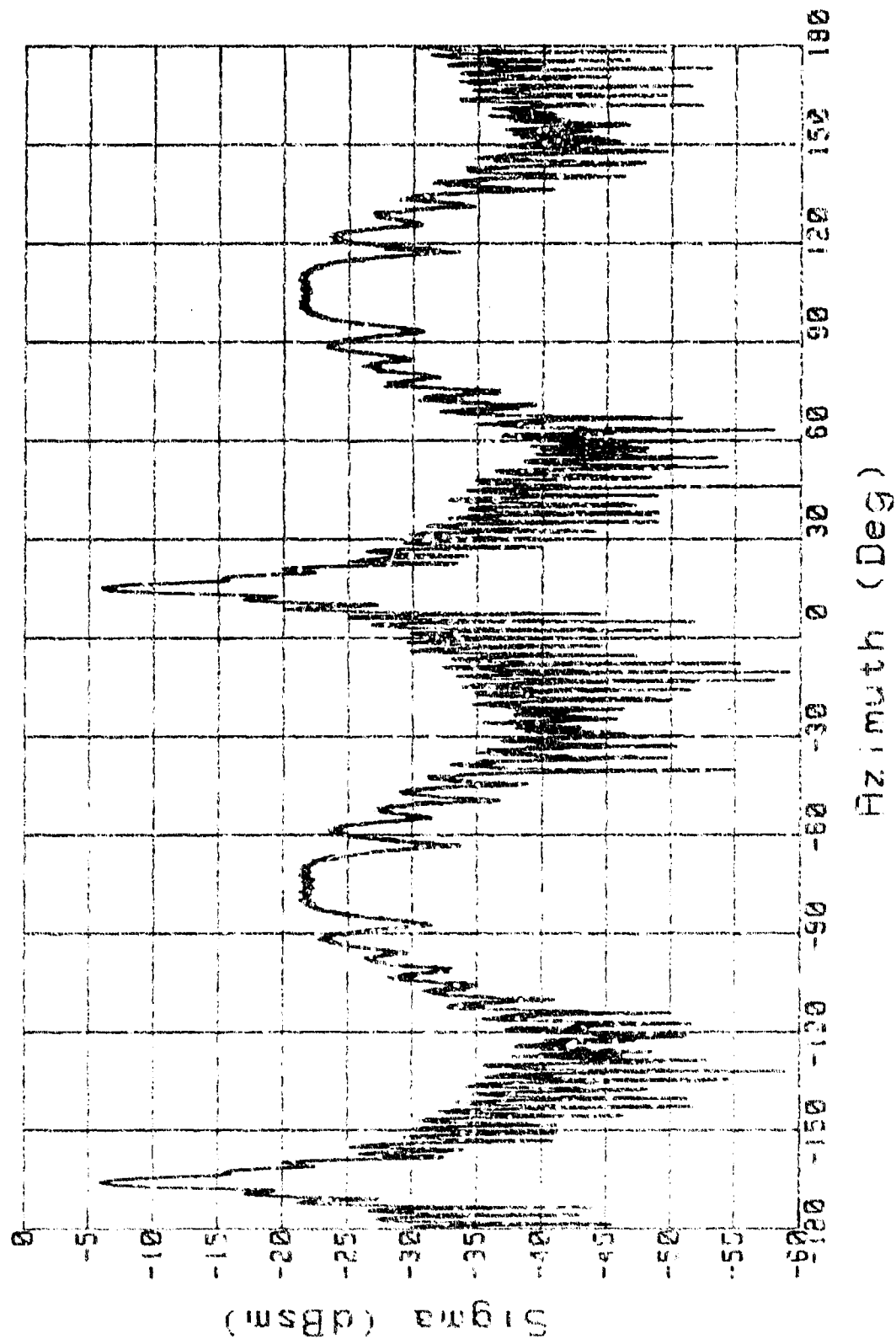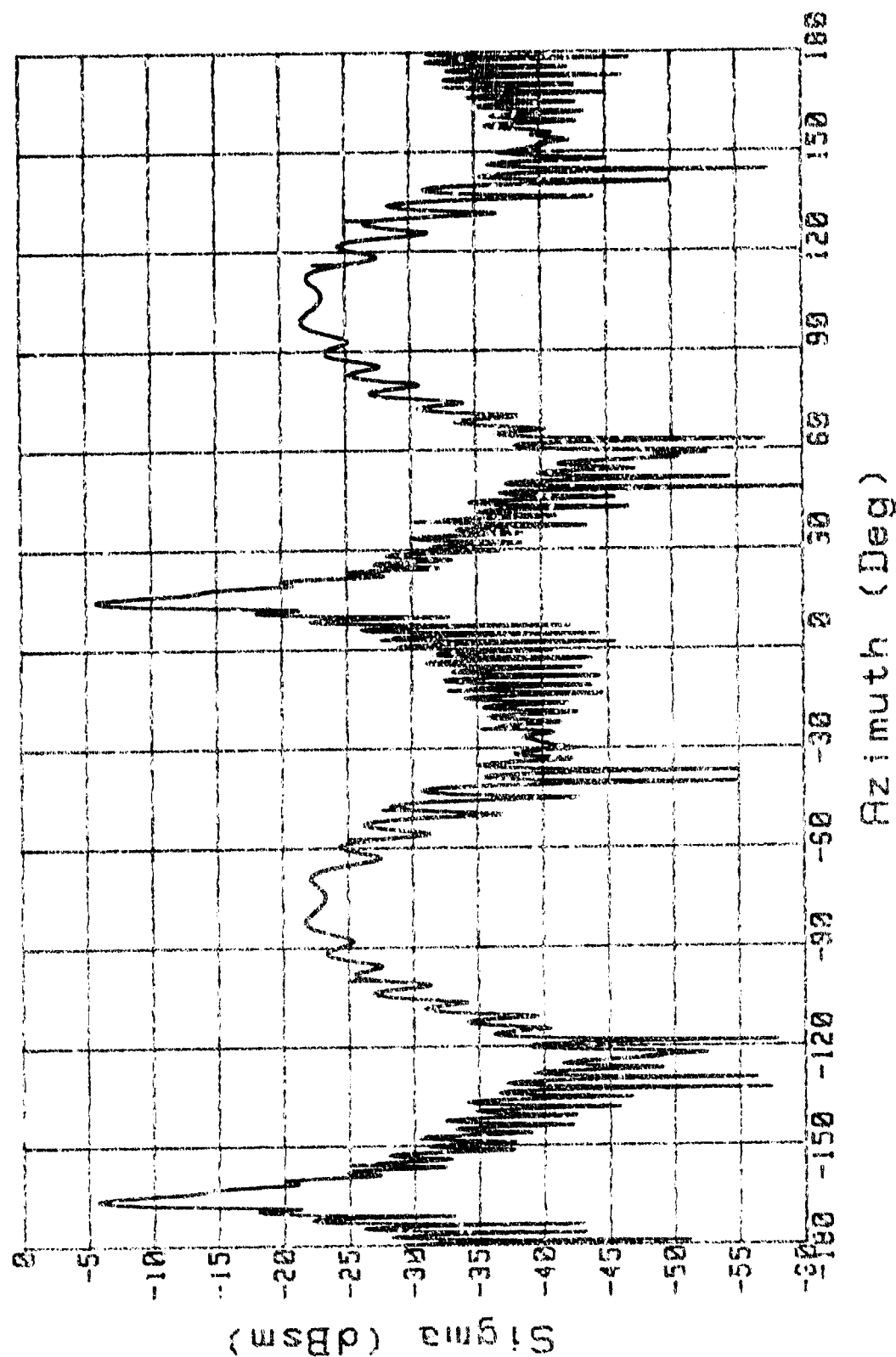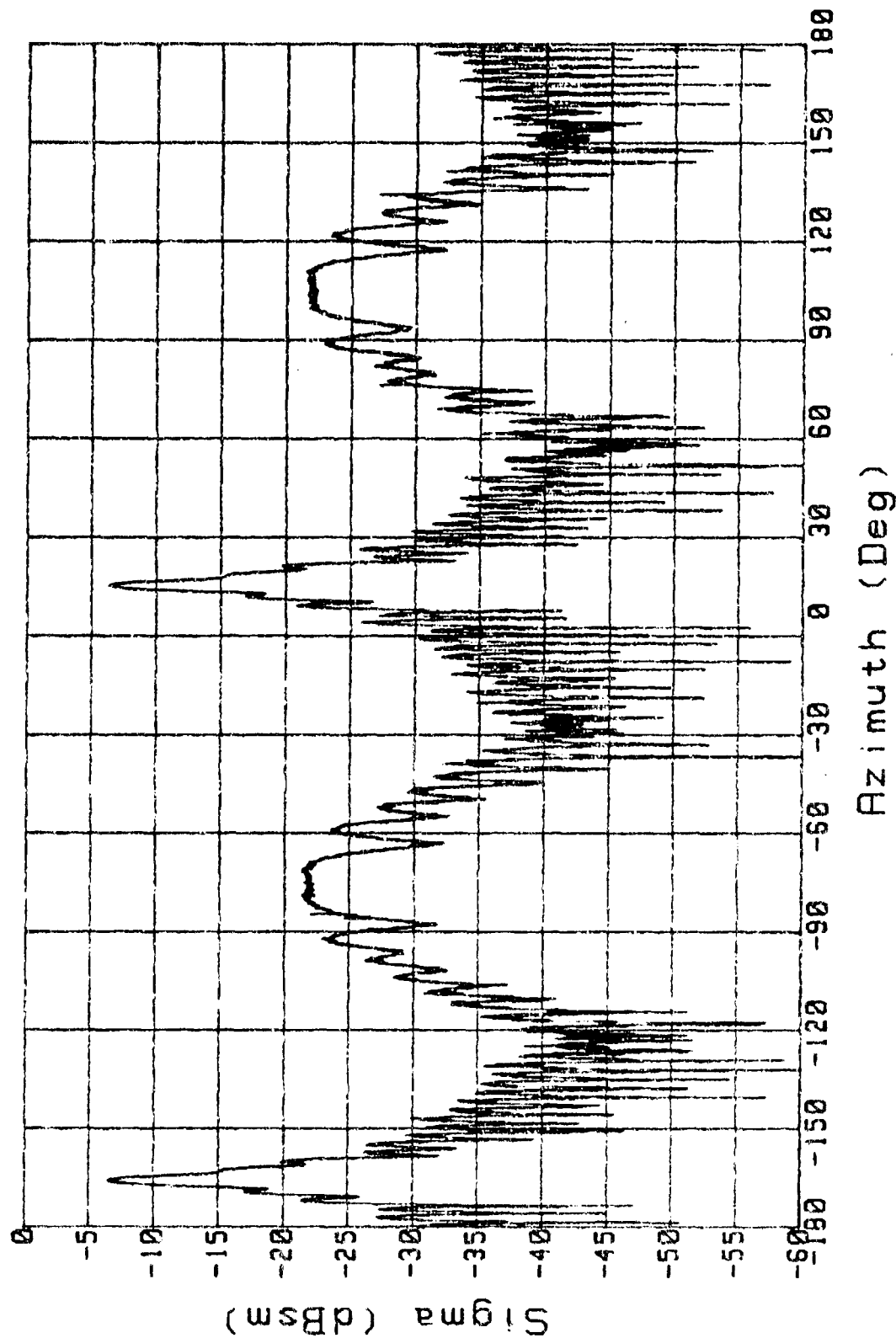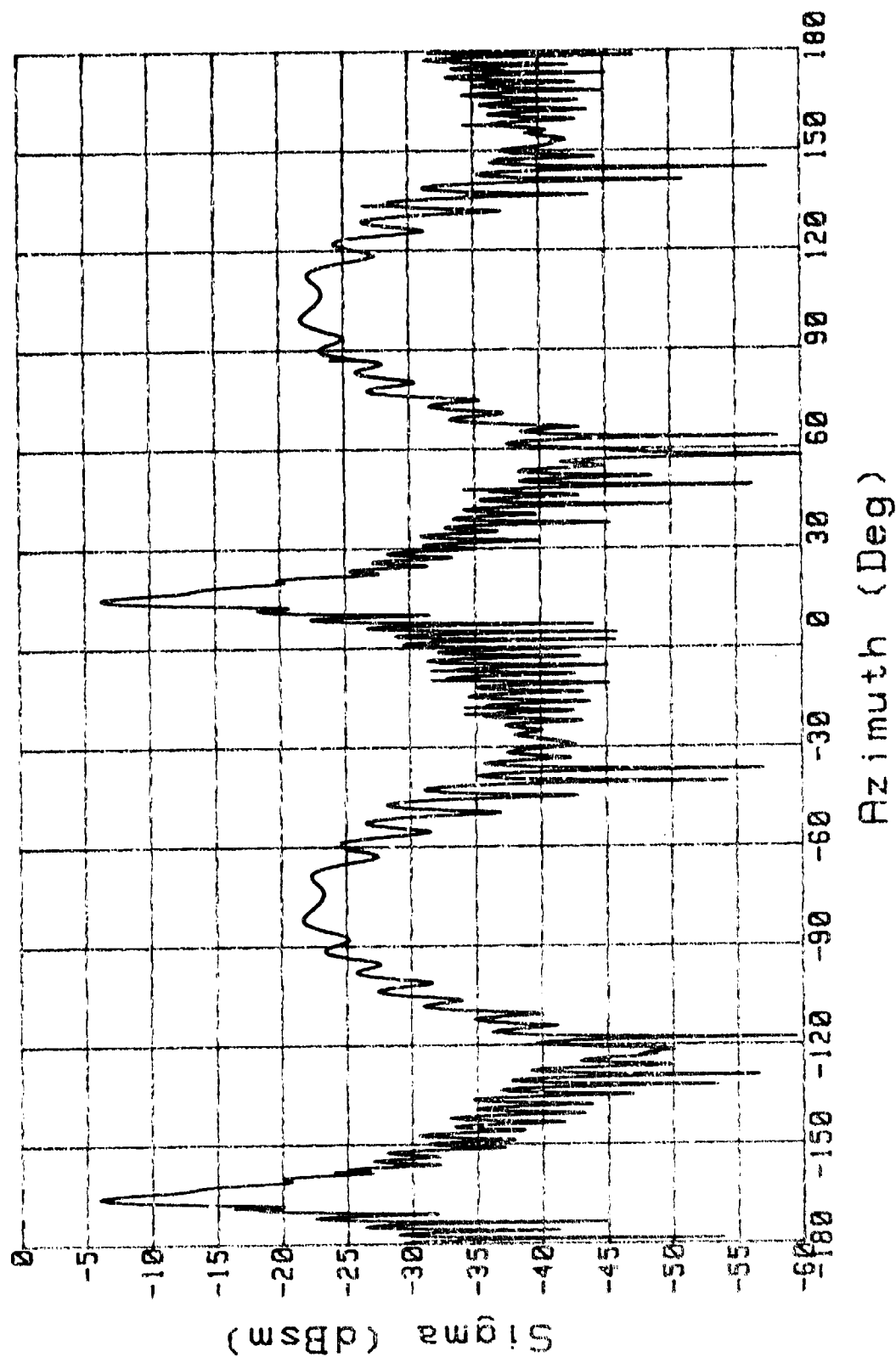
Freq: 9.66   Pol: H   Range: 10   Run# 2

Figure 59B.   RCS: Cylinder (14.25 in), H Pol, BSA=0, Range=10

145
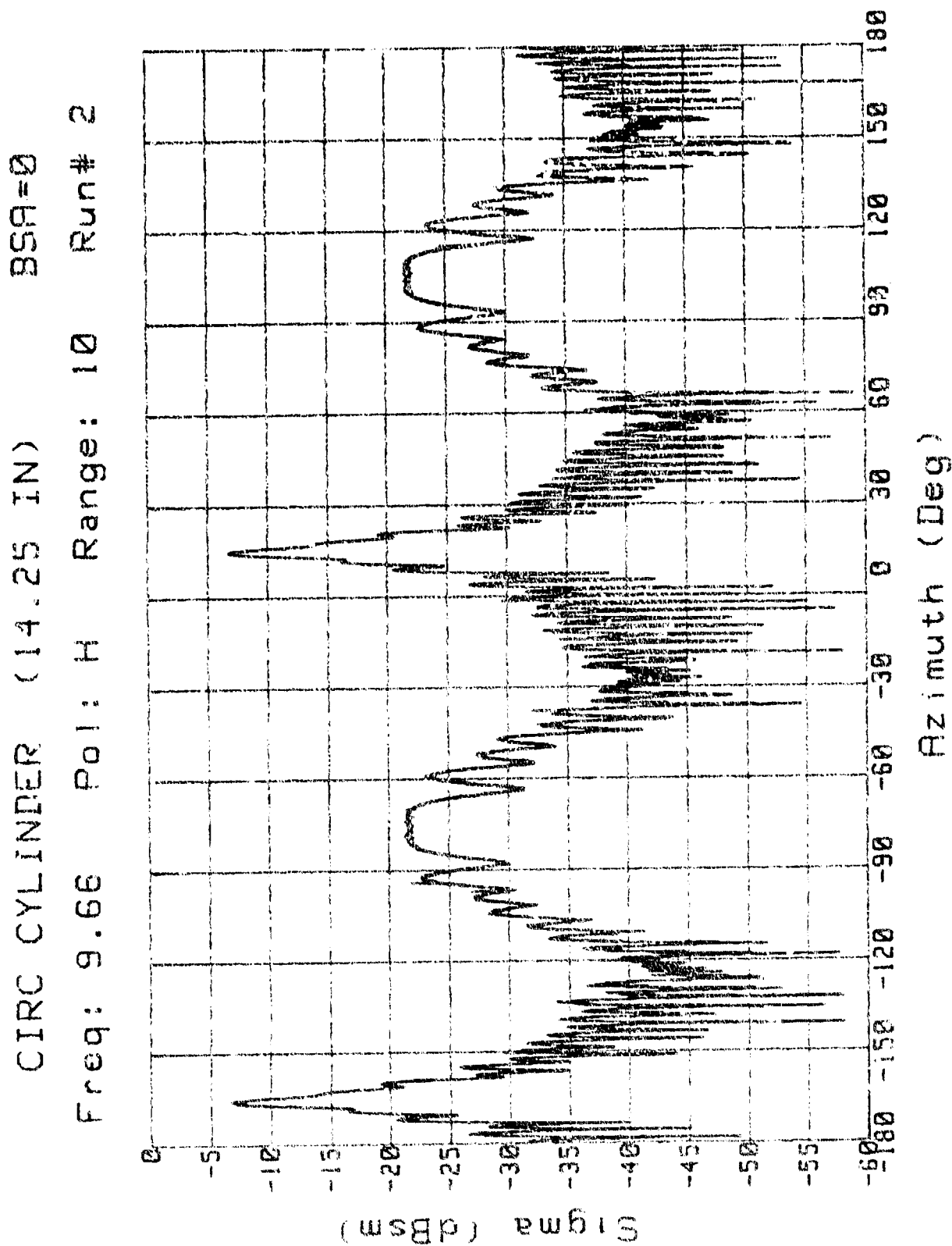
Bibliography

1. Sweetman, Bill. Stealth Aircraft. Osceola, Wisconsin: Motorbooks International Publishers & Wholesalers, Inc., 1986.

2. Blake, Lamont V. Radar Range-Performance Analysis. Norwood, Massachusetts: Artech House, Inc., 1986.

3. Skolnik, Merrill I. Introduction to Radar Systems. New York: McGraw-Hill, Inc., 1980.

4. Adam, John A. "How to Design an Invisible Aircraft," IEEE Spectrum, 25: 26-31 (April 1988).

5. Currie, Nicholas C. Techniques of Radar Reflectivity Measurement. Dedham, Massachusetts: Artech House, Inc., 1984.

6. Air Force Systems Command. Bistatic Radar Cross Section Measurement Considerations. RATSCAT Project No. 87-07. Holloman AFB, New Mexico: 6585th Test Group, September 1988.

7. Georgia Tech Research Institute. Study of Near-Field Measurement Techniques for Large Antennas and Scatterers. White Paper No. EC-EED-C804. Atlanta: Georgia Institute of Technology, 10 August 1987.

8. Joy, E.B. "A Brief History of the Development of the Near-Field Measurement Technique at the Georgia Institute of Technology," IEEE Transactions on Antennas and Propagation, 36: 740-745 (June 1988).

9. Ruck, George T. Radar Cross Section Handbook. New York: Plenum Press, 1970.

10. Crispin, J.W. and K.M. Siegel. Methods of Radar Section Analysis. New York: Academic Press, 1968.

11. Skinner, Capt Paul and Capt Randy Jost. A Short Tutorial on the Methods of Physical Optics for Electromagnetic Scattering. AFWAL/AAWP, Wright-Patterson AFB, OH, February 1988.

12. Kell, Robert E. "On the Derivation of Bistatic RCS from Monostatic Measurements," Proceedings of the IEEE, 53: 983-988 (August 1965).

13. MacLennan, Capt Jeffrey M. Verification and Limitations of the Monostatic-Bistatic Radar Cross Section Derived by Kell. MS Thesis, AFIT/GE/ENG/88D-24. School of Engineering, Air Force Institute of Technology (AU), Wright-Patterson AFB, OH, December 1988.

14. Falconer, David G., Ph.D. "Near-Zone and Time-Harmonic Statements of the Monostatic-Bistatic Theorem" paper prepared for IEEE Transactions on Antennas and Propagation. Menlo Park, California: SRI International, Remote Measurements Laboratory, 1 February 1989.

15. Balanis, Constantine A. Antenna Theory. New York: Harper & Row, Publishers, Inc., 1982.

16. Skolnik, Merrill I. Radar Handbook. New York: McGraw-Hill, Inc., 1970.

17. Utt, Edwin L. Thesis Sponsor. Personal interview. Wright Research and Development Center, Wright-Patterson AFB, OH, 1 May 1989.

18. McCool, Capt Stephen W. Bistatic Resonant Scattering Measurements of Special Shapes. MS Thesis, AFIT/GE/ENG/88D-27. School of Engineering, Air Force Institute of Technology (AU), Wright-Patterson AFB, OH, December 1988.

REPORT DOCUMENTATION PAGE

Form Approved
OMB No. 0704-0188

1a. REPORT SECURITY CLASSIFICATION	1b. RESTRICTIVE MARKINGS
Unclassified	

2a. SECURITY CLASSIFICATION AUTHORITY	3. DISTRIBUTION/AVAILABILITY OF REPORT
2b. DECLASSIFICATION/DOWNGRADING SCHEDULE	Approved for public release; distribution unlimited

4. PERFORMING ORGANIZATION REPORT NUMBER(S)	5. MONITORING ORGANIZATION REPORT NUMBER(S)
AFIT/GE/ENG/89J-1	

6a. NAME OF PERFORMING ORGANIZATION	6b. OFFICE SYMBOL (If applicable)	7a. NAME OF MONITORING ORGANIZATION
School of Engineering	AFIT/ENG	

6c. ADDRESS (City, State, and ZIP Code)	7b. ADDRESS (City, State, and ZIP Code)
Air Force Institute of Technology (AU) Wright-Patterson AFB, Ohio 45433-6583	

8a. NAME OF FUNDING/SPONSORING ORGANIZATION	8b. OFFICE SYMBOL (If applicable)	9. PROCUREMENT INSTRUMENT IDENTIFICATION NUMBER
Wright Research Development Center	SNA	

8c. ADDRESS (City, State, and ZIP Code)	10. SOURCE OF FUNDING NUMBERS			
Wright Patterson AFB, Ohio 45433-6543	PROGRAM ELEMENT NO.	PROJECT NO.	TASK NO.	WORK UNIT ACCESSION NO.
	62204F	7633	13	09

11. TITLE (Include Security Classification)

Evaluation of the Bistatic Equivalence Theorem for the Near and Far-Field Radar Cross Section of Complex Targets (U)

12. PERSONAL AUTHOR(S)
Charles G. Walls, B.S., Maj, USA

13a. TYPE OF REPORT	13b. TIME COVERED	14. DATE OF REPORT (Year, Month, Day)	15. PAGE COUNT
MS Thesis	FROM ___ TO ___	1989 June	163

16. SUPPLEMENTARY NOTATION

17.	COSATI CODES		18. SUBJECT TERMS (Continue on reverse if necessary and identify by block number)
FIELD	GROUP	SUB-GROUP	Near-field, radar cross section, bistatic measurements, monostatic-bistatic theorem
17	09		

19. ABSTRACT (Continue on reverse if necessary and identify by block number)

Thesis Advisor: Dr. Vittal P. Pyati
Assistant Professor of Electrical Engineering

Abstract: See back

20. DISTRIBUTION/AVAILABILITY OF ABSTRACT	21. ABSTRACT SECURITY CLASSIFICATION
☒ UNCLASSIFIED/UNLIMITED ☐ SAME AS RPT ☐ DTIC USERS	Unclassified

22a. NAME OF RESPONSIBLE INDIVIDUAL	22b. TELEPHONE (Include Area Code)	22c. OFFICE SYMBOL
Dr. Vittal P. Pyati	(513) 255-2024	AFIT/ENG

DD Form 1473, JUN 86 — Previous editions are obsolete.

Unclassified

Abstract

This research examined the applicability of the monostatic-bistatic equivalence theorem (MBET) and associated extensions in determining the extent to which correlation exists between monostatic and bistatic data for both the near and far-field. A secondary objective was to determine whether reliable bistatic near-field radar cross section (RCS) data could be collected on a range originally designed to take monostatic far-field measurements.

Dr. David Falconer developed two extensions of the MBET in an effort to estimate the bistatic RCS pattern in both the near and far-field by measuring the monostatic RCS pattern at one-half the bistatic angle, at a reduced frequency, and, for the near-field case, at an adjusted target-to-receiver separation range. The pattern representation and accuracy of these two extensions were examined by measuring the RCS of an ogive, a circular flat plate, and two circular cylinders of different lengths. Target selection allowed for the application of the MBET extensions to targets that provide either a large dynamic range, support travelling and creeping waves, or have large specular returns and independent scattering centers.

The variable parameters for the study included the polarization and target-to-receiver separation range. The transmit frequency and bistatic angle of interest were 10 GHz and 30°, respectively.

Results of this study show that Falconer's MBET extensions have some merit. Application of the far-zone statement and the resultant monostatic data provided good representation of the corresponding bistatic far-field RCS patterns and amplitude levels. Falconer's near-zone version provided fair representation of the bistatic near-field RCS patterns and amplitudes. The accuracy of the RCS amplitude approximations decreased, though, for targets, such as the 8 in cylinder, that had a significant higher order effects contribution.